4-28-2009

Metal-Assisted Hydrolysis of Biological Molecules

Sarah Shealy Cepeda

METAL-ASSISTED HYDROLYSIS OF BIOLOGICAL MOLECULES

by

SARAH SHEALY CEPEDA

Under the Direction of Kathryn B. Grant

ABSTRACT

In Chapter I is a general description of novel metal complexes which hydrolytically cleave peptides, proteins, DNA, and other biological molecules. These reagents are becoming the more important as potential therapeutic agents. A panel of ligands was investigated for coordination to Zr^{IV} and other metals in groups 4, 5, and 6 to effect the greatest degree of hydrolysis. Chapter II describes a Zr^{IV} complex which is capable of hydrolyzing a 30 amino acid peptide, insulin chain B, with amino acid specificity. Oxidized insulin chain B peptide was hydrolyzed after only 4 h of treatment at pH 7.0 and 60 °C using $ZrCl_4$ in the presence of 4,13-diaza-18-crown-6. MALDI-TOF and ESI LC-MS mass spectra indicated that insulin chain B was hydrolyzed by Zr^{IV} at the Gly8-Ser9, Ser9-His10, and Gly20-Glu21 amide bonds within the oligopeptide. To our surprise, the cysteine sulfonic acid sequences Cys(SO_3H)7-Gly8 and Cys(SO_3H)19-Gly20 were also cleaved. To the best of our knowledge, this constitutes the first example of metal-assisted hydrolysis of a Cys(SO_3H)-Xaa amide bond. This is significant in

light of the fact that cysteine sulfonic acid formation in proteins is triggered by oxidative stress and has been associated with amyloid fibril formation, Parkinson's disease, and other deleterious, physiological processes.

Chapter III describes the metal-assisted hydrolysis of sphingomyelin which is a principle phospholipid component of animal cell membranes. The sphingomyelin assays showed evidence of metal-assisted hydrolysis after 20 h of treatment at lysosomal pH 4.8 and cytosolic pH 7.0 at both physiological temperature 37 °C and 60 °C. The metal ion Ce^{IV} was the most reactive, followed by Zr^{IV}, and then Hf^{IV}. The goal of this work is to develop metal-based reagents to reverse the lethal build-up of sphingomyelin that occurs in lysosomes of patients suffering from Niemann-Pick disease.

INDEX WORDS: Cerium(IV), Cleavage, Hydrolysis, Metals, Zirconium(IV), Insulin chain B, MALDI-TOF, ESI-MS, Sphingomyelin, Cholesterol, Vesicle, Micelle, Triton X-100

METAL-ASSISTED HYDROLYSIS OF BIOLOGICAL MOLECULES

by

SARAH SHEALY CEPEDA

A Dissertation Submitted in Partial Fulfillment of Requirements for the Degree of

Doctor of Philosophy

in the College of Arts and Sciences

Georgia State University

2009

METAL-ASSISTED HYDROLYSIS OF BIOLOGICAL MOLECULES

by

SARAH SHEALY CEPEDA

Committee Chair: Kathryn B. Grant

Committee: Dabney W. Dixon
Jerry C. Smith

Electronic Version Approved:

Office of Graduate Studies
College of Arts and Sciences
Georgia State University
May 2009

ACKNOWLEDGMENTS

I am deeply thankful for my mentor Professor Kathryn B. Grant for the freedom to conduct experiments toward exciting medical research goals using inorganic biochemistry and for teaching me to pay critical attention to detail in data, reports, and presentations. I am thankful for the skills of inorganic biochemistry, PCR, and spectrophotometry which I learned in her laboratory. The sweet pictures of her dearest daughter over my desk delighted me everyday. I would also like to thank Dr. Dabney Dixon for her valuable lessons on speaking and presenting myself with clarity and good sense. A special thanks to Dr. Al Baumstark, the director of the Department of Chemistry, who navigated me through some difficult waters. My beloved husband, Pablo Cepeda, has been my support and consolation while reminding me everyday to love God with all my heart, mind, and soul through our Lord Jesus Christ. Te amo más cada día. I would like to thank my mother, Catherine B. Shealy for her lifetime love and encouragement and my brothers Frank and his wife Cynthia, Bill, Merritt, and Mason who brought joy to my life on many celebrations. For the brief time that my late father, H. Franklin Shealy, was able to know that his daughter was working toward a doctorate, may God bless his soul in heaven. I hope that my graduation on his birthday will be a tribute to his parenting. I would like to thank the parishes of Sacred Heart Church and the Shrine of the Immaculate Conception including Fr. T.J. Meehan and Monsignor Henry Gracz for the spiritual support and hospitality. My responsibilities as catechists, altar serving, Eucharistic ministering, and hospitality at Sacred Heart have been a blessing and an offering back to the Lord.

My enrollment at GSU has brought many diverse people into my life, and some have been very helpful in sharing their knowledge including Siming Wang and Professor Jenny Yang. I would like to thank the laboratory coworkers in Dr. Grant's group including David Dukes, Earl

Fields, Miki Kassai, Orapin Kongtragulchone, Rawin Teopithaporn, Carla Terry, and Beth Wilson for their singing, jokes, food, and religious discussions. Also, I would like to thank Hui Zhou of the GSU Atomic Force Microscopy Facility for her friendly AFM service.

This research was supported by a GSU Molecular Basis of Disease Fellowship, A GSU Brains and Behavior Fellowship, and the National Science Foundation grant CHE-0718634.

TABLE OF CONTENTS

LIST OF TABLES

LIST OF FIGURES

LIST OF ABBREVIATIONS

1D or 3D	=	one or three dimensional
Ac	=	acetyl
Ala	=	alanine
AFM	=	atomic force microscopy
Arg	=	arginine
Asp	=	aspartic acid
Asn	=	asparagine
Crown	=	4,13-diaza-18-crown-6
Cys	=	cysteine
Cys_{ox}	=	$Cys(SO_3H)$ = cysteine sulfonic acid
DDA	=	data dependent acquisition
Glu	=	glutamic acid
Gln	=	glutamine
Gly	=	glycine
Gly8-Ser9	=	an example of a dipeptide fragment which originally was from the original intact peptide sequence position numbers 8 and 9 and is a dipeptide of glycine and serine
EDTA	=	ethylenediaminetetraacetate
ESI	=	electrospray ionization

ESI MS/MS	=	tandem mass spectrometry using the electrospray ionization
$t_{1/2}$	=	half-life
HEPES	=	*N*-(2-hydroxyethyl)piperazine-*N'*-2-ethanesulfonic acid
His	=	histidine
HPLC	=	high performance liquid chromatography
HPLC-ESI-MS or HPLC-ESI	=	high performance liquid chromatography electrospray mass spectrometry
HPLC-ESI-MS/MS	=	tanden mass spectrometry using HPLC separation with electrospray ionization
Ile	=	isoleucine
Leu	=	leucine
Lys	=	lysine
LUV	=	large unilamellar vesicles
MALDI-ToF MS or MALDI	=	matrix-assisted laser desorption ionization time-of-flight mass spectrometry
Met	=	methionine
M or M-OH	=	metal and metal-hydroxide
MS	=	mass spectrometry
MS/MS	=	tandem mass spectrometry
NPD	=	Niemann-Pick disease

Phe	=	phenylalanine
Pro	=	proline
pyroGlu	=	pyroglutamate (the dehydrated, cyclized glutamic acid)
Ser	=	serine
SM	=	sphingomyelin
18:0 or 24:1 SM	=	sphingomylein with N-acyl linked stearic or nervonic acid
SUV	=	small unilamellar vesicles
TI	=	tetrahedral intermediate
Thr	=	threonine
Try	=	tryptophan
Tyr	=	tyrosine
Val	=	valine
Xaa	=	any of the 20 natural amino acids
Xaa-Ser	=	a dipeptide with any amino acid in the first sequential position and a defined serine in the second position

CHAPTER I INTRODUCTION: METAL-ASSISTED HYDROLYSIS OF BIOLOGICAL MOLECULES.

Hydrolysis of peptides, proteins, and lipids by metal complexes.

Synthetic metallopeptidases as proteases.

Proteases are a useful tool for protein and peptide research because of their capability to selectively cleave proteins or peptides for sequencing, separation of proteins of interest from fusion protein expression, proteomics, and peptide mapping. The categories of proteases currently used include enzymatic proteases such as trypsin, chymotrypsin, and Lys-C; chemical proteases including cyanogen bromide; and synthetic metalloproteases which are still in the development stage. Synthetic metalloproteases are rapidly emerging as a novel protease category because of the unique physical and chemical properties of each metal complex.[1] Metal-ligand complexes can be designed to hydrolyze the peptide amide bond. Ideally, those complexes will rapidly cleave in high yields under mild conditions of temperature and pH, although many synthetic metalloproteases have been demonstrated to be effective only under extreme conditions. The ability to hydrolyze at specific amino acid residues is a key experimental element in order to produce discrete hydrolytic products that have no oxidative and other post-cleavage modifications.

Synthetic metallophospholipidases as hydrolytic agents.

Studies on the development of metal-assisted hydrolysis of phospholipids are scarce with primary emphasis on lanthanide-assisted hydrolysis of *p*-nitrophenol-activated synthetic phospholipids at the phosphate ester bond. The studies were motivated by metallonucleases which cleave the phosphodiester bonds of RNA and DNA.[2-8] The metal-assisted hydrolysis of

phospholipids is a potential area of therapeutic drug development with the aim of reversing the symptoms of phospholipid accumulation in lysosomal storage diseases such as Niemann-Pick disease and Sandhoff disease where a DNA mutation has caused lowered or negligible levels of phospholipase activity.

Background and significance of phospholipids.

Studies of phospholipid vesicles have provided insight into the cellular membrane environment either as models for membrane fusion or as detergent-solubilized liposomes. The investigations into the size distributions, composition, solubilization, and penetration of small molecules or ions have provided evidence to support a variety of mechanisms and scenarios for diseased states.

One example of membrane composition that involves sphingomyelin is the lipid raft which associates with certain proteins involved in cell signal pathways. Sphingomyelin-cholesterol domains within cellular membranes form localized distributions or cholesterol-enriched microdomains called lipid membrane rafts due to the different miscibilities of phospholipids and cholesterol which together serve as transporters of proteins, lipids, and other second messenger molecules.[9] These rafts are more resistant to Triton X-100 solubilization at 4 °C than 37 °C, and, for the lipids in the fluid state, solubilization at lower temperatures requires less detergent, whereas, for the lipids in the gel state, solubilization at lower temperatures requires more detergent. The rafts exist in a third state called the liquid-ordered phase.[10]

Under non-equilibrium conditions, the bilayers of vesicles in biomembranes have been shown by fluorescence probe systems such as carboxyfluorescein to either leak the inner contents or fuse into aggregates.[11a-e] Sphingomyelin:phosphatidyethanolamine:cholesterol (2:1:1 molar ratio) vesicles were treated with sphingomyelinase enzyme with subsequent ceramide

production which resulted in vesicle leakage of the aqueous contents. When vesicles of the same composition were treated with bacterial phospholipase C to produce a diacylglycerol product, the opposite effect of vesicle fusion and aggregation occurred rather than leakage. The effects of the enzymatic production of ceramide or diacylglyerol gives insight into the bilayer destabilization and fusion caused by these products. Triton X-100 was used to create complete leakage and solubilization of the bilayers.[11b]

The penetration of small molecules into vesicles has been simulated by studies where fluorescent molecules such as carboxyfluorescein, *N*-phenyl-1-naphthylamine (NPN), 1-anilino-8-naphthalene sulphonate (ANS) are entrapped inside the liposomes and therefore emit little fluorescence. As the vesicle is solubilized due to a surfactant such as Triton X-100, the bilayer integrity changes with subsequent release of the vesicle contents of the carboxyfluorescein. As the contents leak out, the fluorescence increase is determined quantitatively. With ANS or NPN probes, the interaction of the fluorescent molecules with the lipids or detergents causes a shift in the λ_{max} to shorter wavelengths, especially with probe-lipid bilayer interactions compared to probe-detergent micelles interactions.[11a-e]

The size and shape of sphingomyelin vesicles have been studied with dynamic light scattering, turbidity measurements, and electron or atomic force microscopy.[12a-b] The size distribution of vesicles is determined because of the different biophysical characteristics that result from the vesicle size categories. The gel to liquid-crystalline phase transition temperature is determined by differential scanning calorimetry. Isothermal titration calorimetry has been the main instrumentation for the study of detergent partitioning into bilayers. Considerable attention has been given to the breakdown of lamellar structures to form lipid-surfactant mixed micelles through the use of detergents such as Triton X-100. Optical measurements of the turbidity

constitute a method to observe changes in vesicle size from aggregation with a turbidity increase or from solubilization followed by decreased turbidity.

Extensive work on the solubilization of vesicles by Triton X-100 has been done to determine the progressively complex structures that form with increasing detergent incorporation. [11a,b,c,e] Since sonicated vesicles with entrapped drug molecules can serve as drug carriers, the Triton X-100 detergent serves to model the changes that occur upon an encounter with physiological amphiphiles that can also solubilize vesicles. Five stages of progressive transformation have been described in the incorporation of Triton X-100 into vesicles to form micelles. [12b]

Background of the therapeutic use of metals.

The use of inorganic complexes in medicinal chemistry for intended biological disease targets is an emerging field.[13] The metal-ligand complexes which demonstrate no cytotoxicity can be delivered to specific tissues, cells, or receptors. Numerous metals under investigation as drugs include Al, Ga, In, Ti, Ru, Pt, Au, and Sn as anticancer drugs; Cu, Zn, Ag, Hg, and Bi as antimicrobial agents; Au as an antiarthritic agent, Li as an antidepressant, Fe and Zn as antihypertensive drugs; Li, Pt, Au, W, and Cu as antiviral drugs; Bi as an antiulcer drug, Al, Na, Mg, and Ca as antacids; and metalloporphyrins for use in photodynamic therapy. The ions of Pt^{II}, Au^{I}, and Bi^{III} are the most prevalent examples with the platinum(II) anticancer agents such as cisplatin and carboplatin; Au^{I} in the form of antiarthritic drugs while Bi^{III} subcitrate and subsalicylate serve as antiulcer drugs. The Pt drugs are known to target DNA while Au^{I} binds DNA very weakly, but binds cysteine-34 of serum albumin very strongly via thiolate exchange reactions. Under oxidative conditions of inflamed joints, Au^{I} is oxidized to Au^{III} in the lysosomes as a result of antigen processing by proteases. Using the Fe^{III} serum transport protein

transferrin with ruthenium and titanium incorporation, the metals are released inside cells especially in the acidic environments such as endosomes. Bismuth^{III} interferes with the uptake and metabolism of Fe^{III} used by bacterium such as *Helicobacter pylori*.[14] By coupling metal properties with natural biodistribution and physiological pathways, a metal complex can be targeted to specific organelles.[15]

Many studies[16-30] have investigated the biological fate of Zr^{IV} in the form of organometallic and inorganic complexes and in radioactive or non-radioactive forms in humans, animals, or cells using several techniques especially positron emission tomography. A few trends have been discerned, e.g., Zr^{IV} complexed with albumin or antibodies is organ-specific and does not accumulate in the bone. Other researchers have noted that zirconium is initially retained in the soft tissue and then slowly accumulates in the bone. The metal is able to cross the blood-brain barrier and the placenta. Inorganic zirconium complexes either accumulate in the bone or are cleared by the kidneys. Zirconium species in deodorants and anti-perspirants produced allergic responses with migration inhibitory factor and lymphocyte production and positive antigenicity. In contrast, Zr salts acted as lymphocyte mitogens and augmented the response of immune cells. Human peri-implant cells including fibroblasts, lymphocytes, osteoblasts-like MG-63 cells were grown with 0.001-10 mM $ZrCl_4$. At concentrations < 0.1 mM $ZrCl_4$, the metal did not reduce proliferation of the cells. Only concentrations > 1.0 mM $ZrCl_4$ produced toxicity to the cells.[16-30]

While Ce^{III} hepatotoxicity injury has been extensively documented[31a-c], a few studies have documented cerium(IV) toxicity mainly via reaction with sulfhydryl-containing compounds such as cysteine amino acids. Cerium^{IV} was shown to generate thiyl free radicals in the cellular systems containing cysteine which caused serious damage in the cell function especially the

muscular protein myosin and the contractile protein actin from rabbit skeletal muscle with conformational changes that affected activity such as the ATPase activity of myosin.[31d] Cerium(IV) sulfate was shown to bind lactoferrin which is a metal-binding protein in the transferrin family. The two Ce^{4+} ions occupied the same position in Ce_2Lactoferrin as the typical in vivo Fe_2Lactoferrin.[31e]

An important development in metal-based drug design are metallocene complexes with transition metals which have demonstrated antitumor effects with antiproliferative properties.[32-35] Metallocenes are neutral complexes of distorted tetrahedral coordination geometry of two η^5-cyclopentadienyl rings between transition metal such as Ti, V, and Zr. Titanocene has been used unsuccessfully in Phase 2 clinical trials. The dichlorides are the most common metallocenes and represented by formula $(Cp)_2MCl_2$ where M is metal and Cp is the cyclopentadienyl group. The metallocenes are ionic and cationic salts without halides. The anion is usually trichloroacetate, picrate, or tetrahalideferrate (III). The largest use of organozirconium compounds is as polymerization catalysts for ethylene polymerization and for transition-metal-catalyzed cross-couplings. A related zirconocene compound is Schwartz Reagent (Cp_2ZrHCl) which has been used for hydrozirconation in the production of antiestrogen drugs.[32-35]

Zirconium is nontoxic, unlike some other transition metals, so its use as a metallocene therapeutic agent merits further exploration. The lack of cytotoxicity of the zirconocene was noted in a study where zirconocene was combined with adriamycin for therapeutic investigations, although, the Zr^{IV}-adriamycin complex was devoid of antitumor activity.[36] The titanium metallocenes have shown strong antiproliferative activity against fluid Ehrlich ascites tumor, solid B16 melanoma, colon 38 adenocircoma, and Lewis lung carcinoma cell lines. The metallocenes (Cp_2MX_2) are generally believed to effect inhibition of nucleic acid metabolism,

mitotic activity, as well as accumulate in the nuclear heterochromatin of the tumor cells.[35,37a-b] In nude mice studies, metallocenes showed antiproliferative effects against implanted human tumors. Comparisons of titanocene dichloride and dibromides to 5-fluorouracil showed similar efficacies. Substitution of the cyclopentadienyl groups reduces tumor inhibition substantially.[32]

Mechanistic studies of peptides.

Transition metal ions and complexes have been investigated for their catalytic ability to hydrolyze the polypeptide backbone under various conditions of temperature and pH. Unlike oxidative cleavage in which the peptide backbone α-carbon hydrogen atoms are abstracted by metal-generated hydroxyl radicals to produce multiple, fragmented peptide products, the hydrolysis of peptides involves addition of water across the amide bond in the backbone followed by release of two hydrolyzed, native peptides with free N-terminal and C-terminal groups as shown in Figure 1.1. The metal-assisted hydrolysis of the peptide would yield products which are comparable to natural metal-activated peptidase reactions.

The proposed role of proteolytic metals ions in promoting hydrolytic reactions in peptides may include molecular scaffolding for proper juxtaposition of a hydroxide nucleophile to the substrate, direct activation of the carbonyl bond by a free metal ion, charge neutralization and stabilization of the negatively-charged tetrahedral intermediate formed by coordination of the metal's electropositive charge to a negatively charged carbonyl oxygen, and/or serve as a metal-hydroxide nucleophile at neutral pH where many metals exist as a hydroxide complex due to the deprotonation of the waters of hydration. Four proposed schemes for mechanisms of the peptide hydrolysis are shown in Figure 1.2. A tetrahedral intermediate is formed in all cases.[1,3] Scheme I shows the direct coordination of the metal to the carbonyl oxygen while a hydroxide nucleophile from the aqueous solution adds to the carbonyl carbon. In Scheme II, a metal-coordinated

hydroxide species which is generated by deprotonation of a metal-bound water of hydration, adds a hydroxide group to the carbonyl. Scheme III involves a multiple coordination of a hydroxide nucleophile and the amide bond's carbonyl oxygen while the attached hydroxide nucleophile adds to the carbonyl carbon. The Zr^{IV} metal used in the studies described in this dissertation is oxophilic and forms complexes with a high coordination numbers such as the coordination of both the amide carbonyl oxygen and the hydroxide group that Scheme III entails. Scheme IV is a variation of Scheme III where the metal-hydroxide species activates the carbonyl oxygen, and the coordinated hydroxide acts as a base toward another acidic water molecule in solution whose deprotonated hydroxide nucleophilic species then attacks the amide carbonyl carbon. The proposed tetrahedral intermediate in schemes I, II, and III forms a metal-coordinated intermediate whose RNH^- M^+ leaving group may not be labile and may form a hydrolytically inactive species. However, Scheme IV involves protonation of the RNH^- group by the metal-bound water of hydration in an acid-base reaction to form a more labile RNH_2 leaving group.

Aqueous speciation of certain metals.

When strong Lewis acid metals are bound by waters of hydration in aqueous solutions, the metals often lower the pK_a of the attached waters from 15.7 to lower, acidic pK_a values. For example, the pK_a of metal-bound water molecules are ≤ 1 for Zr^{IV}, Hf^{IV}, and Ce^{IV} so that the concentration of metal-hydroxide nucleophiles from the deprotonated water bound metal are abundant at neutral and mildly acidic pH values. The precise aqueous speciations of Zr^{IV}, Hf^{IV}, and Ce^{IV} are not known, although Zr^{IV}_{aq} equilibrates at low pH as $[Zr_4(OH)_8(H_20)_{16}Cl_6]^{2+}$ (tetranuclear ion) and $[Zr_8(OH)_{20}(H_2O)_{24}Cl_{12}] + 4H^+ + 4H_2O$ (octanuclear ion). At higher pH values, these Zr^{IV} aqueous complexes speciate to form insoluble gels and precipitates.[37]

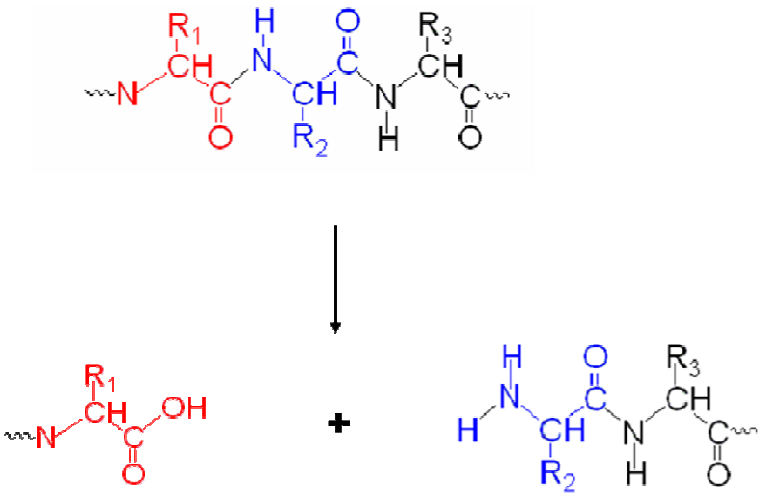

Figure 1.1. The hydrolysis of the peptide bond to yield two intact peptides.[1]

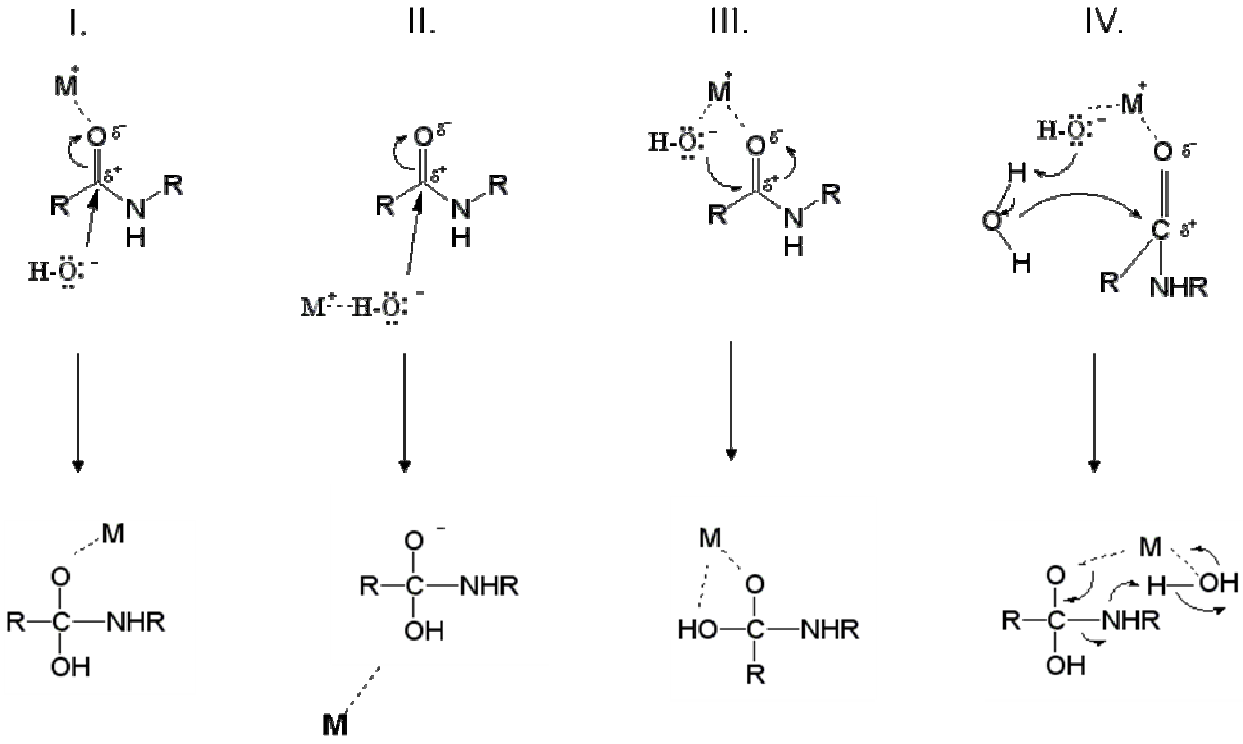

Figure 1.2. Four proposed mechanisms leading to a tetrahedral intermediate in metal-assisted peptide hydrolysis.[1]

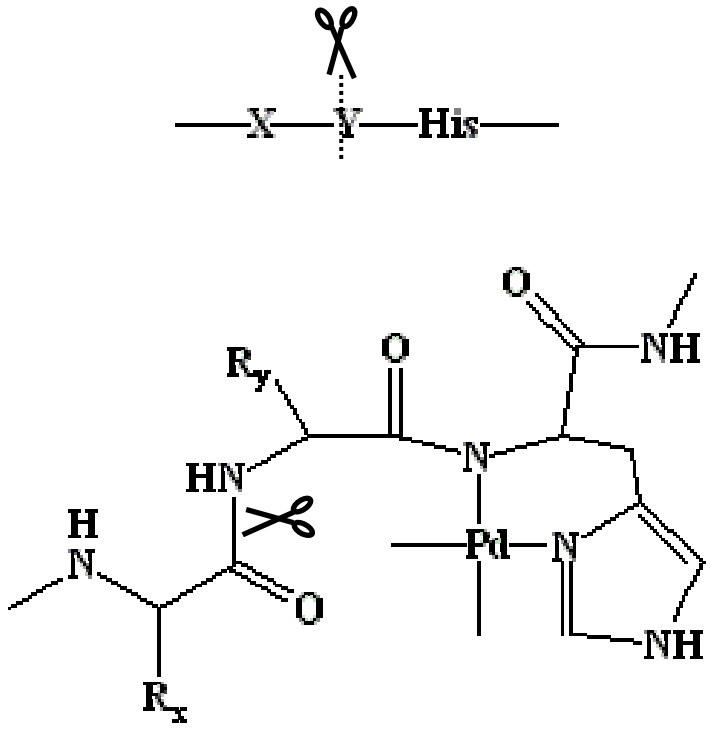

Figure 1.3. The Pd^{II}-assisted coordination with a histidine residue in an X-Y-His peptide sequence. In weakly acidic solutions, the Pd^{II} reagent cleaves the second peptide bond upstream from the anchoring histidine residues.[40h]

The aqueous speciation of Ce^{IV} above pH 4 results in the formation of insoluble Ce^{IV}-hydroxide gels. The dimeric Ce^{IV}-hydroxo species $[Ce^{IV}_2(OH)_4]^{4+}$ is attributed to be the reactive entity in several studies.[4b,39a-]

Background and significance of metal-assisted hydrolysis of peptides.

Transition metals.

Metal ions and complexes of Ce^{IV}, Co^{II}, Ce^{II}, Cu^{II}, Mo^{IV}, Ni^{II}, Pd^{II}, Pt^{II}, Zn^{II}, and Zr^{IV} have been used to hydrolyze peptide bonds.[1,39-43] For Cu^{II}, Co^{III}, Ni^{II}, Pd^{II}, and Pt^{II}, large proteins and peptides have been cleaved. An example is the Pd^{II} hydrolysis of methionine enkephalin at a –G|X-H bond after 1-2 days at 60 °C, and pH 0.5.[40e] Figure 1.3 illustrates the Pd^{II}-assisted coordination with a histidine residue in an X-Y-His peptide sequence. In weakly acidic solutions, the Pd^{II} reagent cleaves the second peptide bond upstream from the anchoring histidine residues.[40h] Another example is the Cu^{II} hydrolysis of insulin chain B at a –G|S-H bond after 4 h at 25 °C, and pH 2.5.[40f] Ni^{II} hydrolyzed a histone peptide at the –E|S-H bond after 134 h at 37 °C, and pH 7.4.[40g] While some metals demonstrate unique specificities and good hydrolytic yields, only a few of the reaction conditions cited in the literature are at non-denaturing pH and temperature. The synthetic metalloprotease preference is for hydrolytic metal complexes with unique specificities toward certain amino acids, that can not only developed as catalytic agents that cleave under physiological conditions, but also as proteolytic tools for protein structural elucidation by mild proteolysis where the tertiary and quaternary protein structures are not disturbed. The $ZrCl_4$ salt in the presence of 4,13-diaza-18-crown-6 was used by our research group to hydrolyze an extensive series of dipeptides to determine the Zr^{IV} specificity toward amino acid residues. Zr^{IV} showed a distinct preference for hydrolysis of dipeptides with negatively charged and oxygen-containing sidechains as determined by LC colorimetric

techniques.[43] Using this information, we then wanted to adapt this same Zr^{IV}/ 4,13-diaza-18-crown-6 complex to hydrolyze larger peptides and proteins and to study the products using mass spectral techniques of matrix-assisted laser desorption ionization (MALDI) and high performance liquid chromatography electrospray mass spectrometry (HPLC-ESI-MS), which allow not only unequivocal determination of molecular weight, but also subsequent confirmation of hydrolysis products by tandem mass spectrometry (MS/MS) analysis.

Zirconium(IV).

As mentioned previously, transition metal complexes that efficiently hydrolyze peptides under non-denaturing conditions of pH and temperature represent an emerging area of research. Zirconium(IV), a transition metal ion with a [Kr] ground state configuration, has been the major emphasis of our metallopeptidase investigations because of its strong Lewis acid strength, fast ligand exchange kinetics, redox inactive state, and its oxophilic characteristics as summarized in Table 1.1. Zirconium(IV) in the presence of 4,13-diaza-18-crown-6 has outstanding proteolytic ability at pH 7.0 and 60 °C with a selectivity toward peptide amide bonds in dipeptides with negatively-charged, oxygen amino acid side chains.[1,43] Consequently, ligands with similar structures to or substructures of the 4,13-diaza-18-crown-6 have been investigated by our laboratory as possible Zr^{IV} complexes. Because of mild experimental conditions of pH and temperature employed, several of the Zr^{IV} complexes showed promise for future use in the study of protein solution structure, the generation of semi-synthetic proteins, the proteolytic cleavage of bioengineered fusion proteins, and therapeutics.

Our first aim in the Zr^{IV}-assisted hydrolysis of peptides was to apply the same Zr^{IV}-4,13-diaza-18-crown-6 complex used in our preliminary dipeptide studies[43] to larger peptides and proteins and to use different detection techniques to study reaction products especially mass

Table 1.1. Properties of zirconium(IV).

Zirconium(IV) Properties
Lowers the pKa of bound water from 15.7 to ≤ 0.6
Redox inactive (d_o electron configuration)
Stable +4 oxidation state
Complexes have high coordination number
Oxophilic
Hydrolyzes phosphodiester bonds
Strong Lewis acids

spectrometry ionization techniques. An initial study of metal-assisted hydrolysis of oxidized insulin chain B, from the biologically active insulin peptide hormone that regulates the cellular uptake, utilization, and storage of glucose, amino acids, and fatty acids, was undertaken.

As described in Chapter II, our data demonstrates that Zr^{IV} is capable of hydrolyzing insulin chain B in a sequence specific fashion after only 4 h of treatment at 60 °C and pH 7.

Background and significance of metal-assisted hydrolysis of phospholipids.

Under normal conditions, most phospholipids are metabolized in the acidic lysosomes of cells that contain lipases and other hydrolytic enzymes.[45-46] Many inherited phospholipid-related disorders are the result of the accumulation of specific unmetabolized phospholipids with manifestation of clinical symptoms due to decreased activity of a defective hydrolytic enzyme. The disorders associated with defective lysosomal enzymes are categorized as lysosomal storage diseases or LSDs and include more than forty diseases resulting from chromosomal mutations. Examples include Niemann-Pick disease types A and B where defective acid sphingomyelinase causes sphingomyelin and associated cholesterol accumulation in lysosomes. In Gaucher's disease, glucocerobroside accumulates from the lack of metabolism due to a defective glucocerobrosidase enzyme. Fabry's disease results from a deficiency of the enzyme alpha galactosidase A which normally metabolizes a glycosphingolipid known as globotriaosylceramide or Gb3.[47]

Mechanistic studies of metal-assisted phosphate ester bond hydrolysis.

Mechanistic studies on phosphate ester hydrolysis of phospholipids are scarce. The Lewis acids of Zr^{IV}, Hf^{IV}, and Ce^{IV} are classified as hard acids and oxophilic so that the metals are capable of activating a phosphate ester bond towards nucleophilic attack by charge neutralization and the provision of metal-bound hydroxides due to their ability to lower the pKa of the bound

waters of hydration.[48-49] Metal-assisted catalysis of the activated phosphate ester bond in bis(*p*-nitrophenyl)-phosphate or BNPP which is a model for DNA phosphodiester linkage has been studied to compare the rates of hydrolysis by various metals of which the lanthanide metals, especially the highly reactive Ce^{IV}, have the highest rates.[6] The Ce^{IV} ion, as cerium(IV) ammonium nitrate was fifty times more reactive than other lanthanides such as Eu^{III}, La^{III}, or Pr^{III} in a Brij-induced micellar preparation of BNPP.[6] Other applications of metal-assisted catalysis have been applied as nucleases toward phosphate ester hydrolysis with RNA more susceptible to hydrolysis than DNA. Zr^{IV} was shown to hydrolyze bis(*p*-nitrophenyl)phosphate in a pH dependent fashion as well as Ce^{IV} with maximum reactivity at pH 4. In the same study, Zr^{IV} (5 mM) salt hydrolyzed the phosphodiester linkage in the DNA dinucleotide thymidylyl (3′→5′) thymidine in the presence of 10 mM Tris at pH 5.5 and 20 °C at a rate with a half-life of 28 days.[2]

Summary of mechanisms.

The general agreement about the mechanism of metal-assisted cleavage of the phosphate ester bonds in lipids is that the positively-charged metal binds and partially neutralizes the negatively-charged $P\text{-}O^-$ oxygen while activating and polarizing the substrate for nucleophilic attack by the metal's attached hydroxyl nucleophile (M-OH) which attacks the phosphate group of the P=O functional group. Figure 1.4 shows an example of this mechanism with the Cu([9]aneN_3)Cl_2-assisted hydrolysis of an activated phosphate ester. The transition state and intermediates show the intramolecular nucleophilic attack by the metal-bound hydroxide.[50]

Lanthanide ions La^{III}, Eu^{III}, and Lu^{III} were used in modeling RNA cleavage and catalysis via phosphate diester transesterification by studying the amount of released 4-nitrophenol from 4-nitrophenolphosphate esters of propylene glycol following lanthanide- assisted hydrolysis. The

pH-rate profiles showed that the lanthanide hydroxide species [$Ln(OH)^{2+}$] is the active catalyst and serves as a general base where two coordination sites are required for binding of both a hydroxide and a phosphate ester. The pseudo-first-order rate constants showed a pH dependence of increasing k_{obs} with increasing pH and a maximum rate in the pH range 8.5-9.[51]

Figure 1.5 shows a proposed schematic of the Zr^{IV} hydrolysis of the sphingomyelin phospholipid with a Zr-OH bound transition state to release choline and a phosphoceramide. The release of choline is one of two possible pathways of Zr^{IV} hydrolysis. The release of phosphocholine is the physiological pathway.

Significance of metal-assisted hydrolysis of sphingomyelin.

Niemann-Pick disease is an incurable, autosomal recessive, lysosomal storage disorder with two phenotypes A and B.[52] Type A primarily affects Ashkenazic Jews with infant mortality while type B affects other diverse ethnic groups with middle age mortality. The defective enzyme acid sphingomyelinase has only 1-3% normal activity in type A while type B has 10 - 60% of normal enzyme activity resulting in fatal accumulation of sphingomyelin in the lysosomes. The affected organs in type A are the spleen, lymph nodes' monocyte-macrophage system, liver, kidneys, brain, and lung, while type B has similar patterns except for no accumulation in the brain. Cholesterol also builds up in the lysosomes, most probably due to the interdispersion of cholesterol with sphingomyelin in the periplasmic membrane. Enzyme replacement and chemical chaperones have had limited therapeutic success in Niemann-Pick patients. A novel therapeutic cure based on Zr^{IV}-assisted phospholipid hydrolysis is a developing concept in our laboratory to decrease this fatal accumulation of the sphingomyelin. Since Zr^{IV} is redox-inactive and possesses low cellular toxicity, a Zr^{IV} complex which efficiently hydrolyzessphingomyelin at the same hydrolytic bonds as the acid sphingomyelinase enzyme

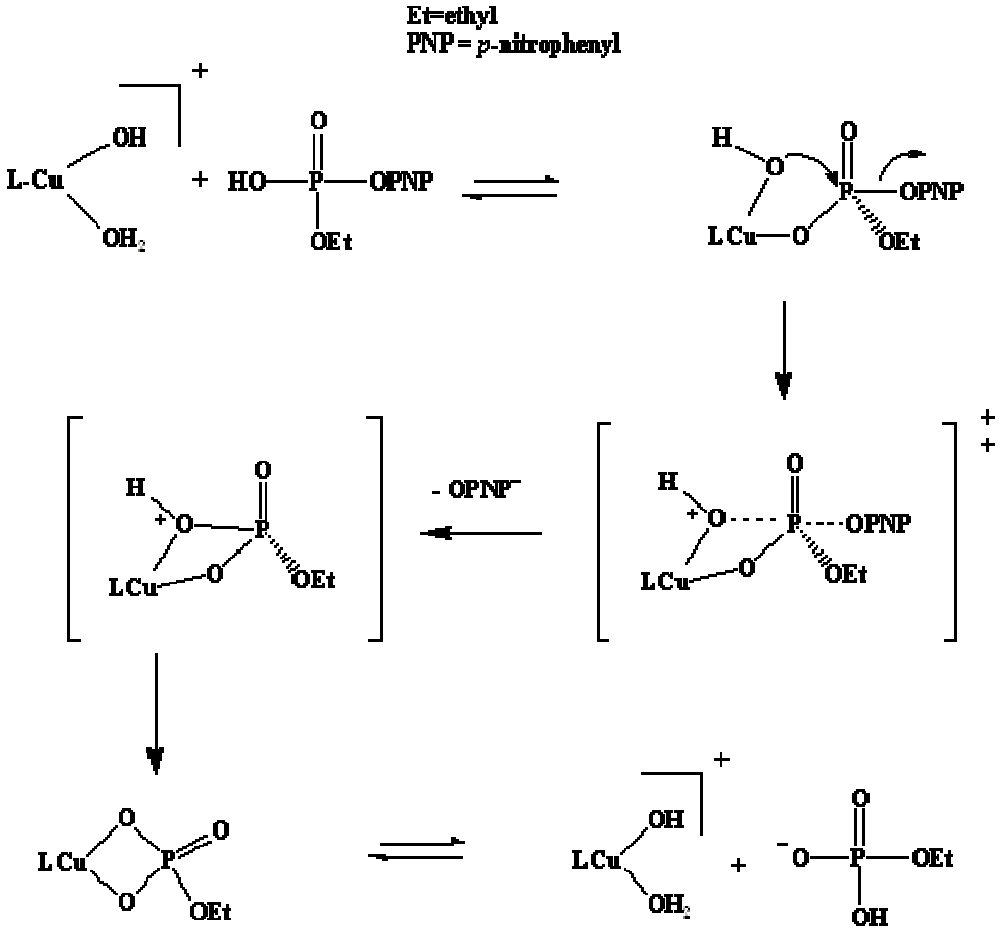

Figure 1.4. Proposed mechanism of the Cu([9]aneN_3)Cl_2-assisted hydrolysis of an activated phosphate ester showing the transition state and intermediates.[50]

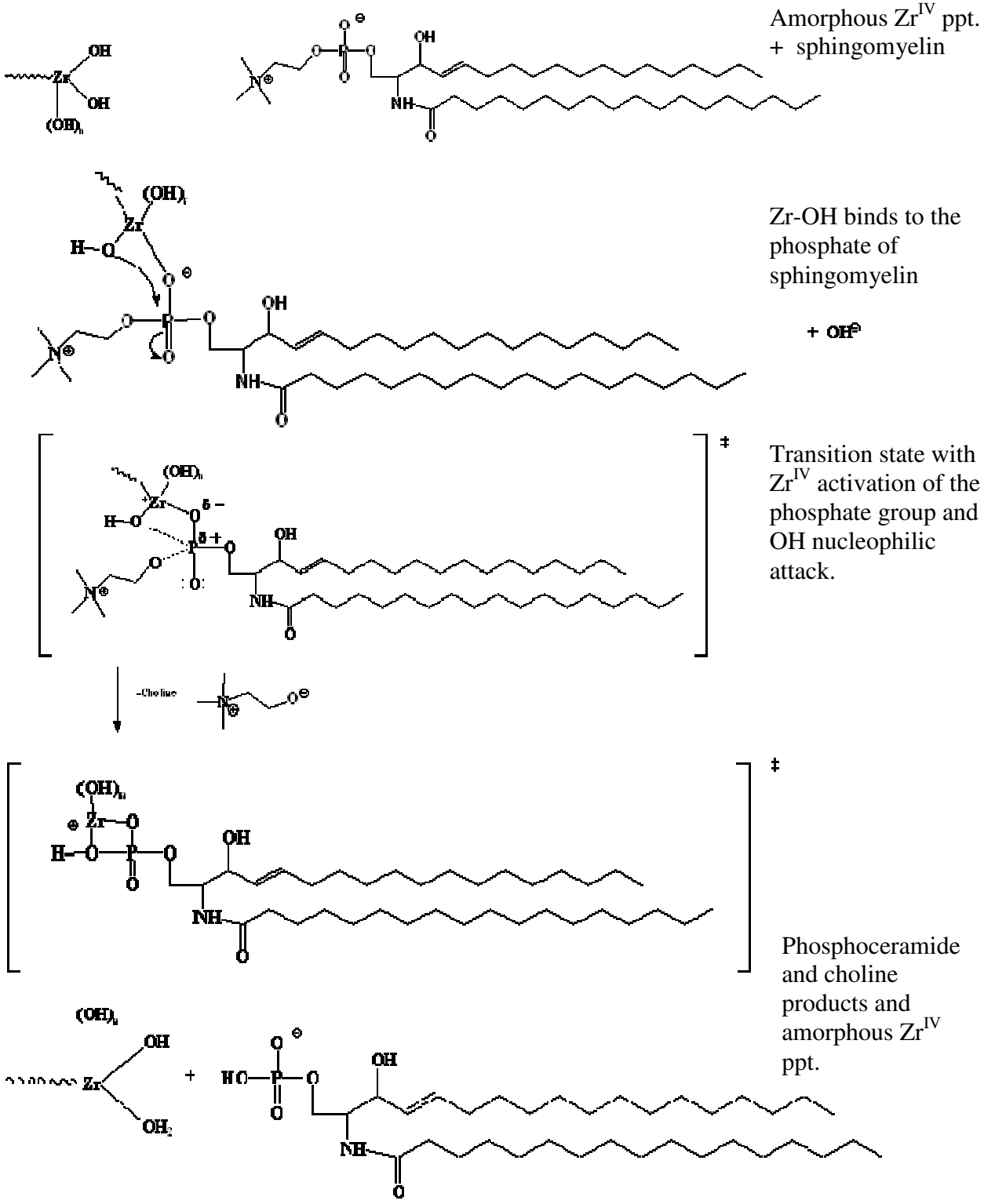

Figure 1.5. Proposed schematic of the Zr^{IV} hydrolysis of sphingomyelin with a Zr-OH bound transition state to release choline and a phosphoceramide.

may function as an enzymatic mimic. It is worthwhile to investigate the pH-dependent reactivities of metals to determine the increase in metal-assisted hydrolytic cleavage in the lysosomes compared to cytosol. Several rat studies have shown that zirconium(IV) is localized in the lysosomes upon ingestion which suggests a possible therapeutic ability to target the diseased organelle. Electron probe x-ray microanalysis of thin tissue sections from rat have shown that ingested Zr^{IV} plus Hf^{IV} and Ce^{IV} accumulates in the lysosomes as a phosphorus complex probably due to the activity of acid phosphatase.[54a] Zirconium(IV), injected as zirconium sulfate, localized in the lysosomes of the lymph node macrophages as a phosphorus complex.[54b] The optimal hydrolysis of DNA and acetylated peptides by Zr^{IV} has been shown to be higher at (lysosomal) pH 4.8 than (cytosol) pH 7.0.[2,53] A proposed mechanism for the Zr^{IV}-assisted hydrolysis of sphingomyelin to release choline and a phosphoceramide is shown in Figure 1.5. Hydrolysis could likely occur on the other side of the phosphate ester bond to release phosphocholine and ceramide which is similar to the *in vivo* enzymatic reaction. The presence of the Triton X-100 compound, used in our studies for solubilization purposes, has been applied therapeutically to the encapsulation of biodegradable nanoparticles with drugs since the surfactact stabilizes the polymer particles during the microencapsulation process.[55a-b]

Research objectives.

In Chapter II of this dissertation, our research goals were to design and evaluate Zr^{IV} complexes which hydrolyze the amide bond of peptides and proteins with amino acid residue specificity. We have demonstrated the proteomic capabilities of the Zr^{IV}-assisted hydrolysis of larger biological proteins by mass spectral data and determined post-reaction side modifications to the protein or its products. We found that the Zr^{IV} in the presence of 4,13 diaza-18-crown-6 hydrolyzes not only a Gly-Glu amide bond, but also the oxidized cysteine sulfonic acid residues

in the insulin chain B protein. Clinically, these oxophilic Zr^{IV} complexes can perhaps be developed to target specific disease-related proteins that have irreversible oxidation especially cysteine oxidation in order to prevent cellular accumulation.

In Chapter III of this dissertation, our aim was to expand the studies of Zr^{IV} complexes with comparison to other metals to observe the hydrolysis of an unexplored class of molecules of phospholipids, namely sphingomyelin. To the best of our knowledge, we are the first to present the metal-assisted hydrolysis of sphingomyelin. The impact of this research is the development of therapeutic applications to Niemann-Pick diseases type A and B which exhibits fatal symptoms due to the accumulation of sphingomyelin in the lysosomes. We found that the tetravalent metals Zr^{IV}, Ce^{IV}, and Hf^{IV} efficiently hydrolyzed sphingomyelin in good yields as quantified by an Amplex® Red and inorganic phosphate assays. The effects of Triton X-100 and cholesterol on the hydrolysis of sphingomyelin were investigated.

The conclusions of the contributions of the metal-assisted hydrolysis of two classes of biological molecules including proteins and phospholipids are presented in Chapter IV. The specific hydrolytic capabilities of certain metals to mimic enzymatic reactions that are defective in diseased states represents progress in an emerging research area.

References.

1 K.B. Grant, M. Kássai, *Curr. Org. Chem.*, 2006, 10, 1035.

2 R. Ott, R. Kramer, *Angew. Chem. Int. Edit.*, 1998, 37, 1957.

3 L.M. Sayre, *J. Am. Chem. Soc.,* 1986**,** 108*,* 1632.

4 (a) R.A. Moss, W. Jiang, *Langmuir*, 2000, 16, 49;

(b) R.A. Moss, H. Morales-Rojas, *J.Am. Chem. Soc.*, 2001, 123, 7457.

5 R.A. Moss, B.D. Park, P. Scrimin, G. Ghirlanda, *J. Chem. Soc., Chem. Commun*., 1995, 1627.

6 K. Bracken, R.A. Moss, K.G. Ragunathan, *J.Am. Chem. Soc.*, 1997, 119, 9323.

7 R.A.Moss, J. Zhang, K. G. Ragunathan, *Tetrahedron Lett.*, 1998, 39, 1529.

8 P.Scrimin, S. Caruso, N. Paggiarin, P. Tecilla, *Langmuir*, 2000, 16, 203.

9 A. Rietveld, K. Simons, *Biochim. Biophys. Acta*, 1998, 1376, 467.

10 C. Amulphi, J. Sot, M. García-Pacios, J.-L. R. Arrondo, A. Alonso, F. M. Goñi, *Biophys. J.*, 93, 2007, 3504.

11 (a) A. Alonso, R. Saez, F.M.Goñi, *FEBS Lett.*, 1982, 137, 141;

(b) M.B. Ruiz-Argűello, F.M. Goñi, A. Alonso, *J. Biol. Chem*, 1998, 272, 22977;

(c) M.B. Ruiz-Argűello, G. Basáñez, F.M. Goñi, A. Alonso, *J. Biol. Chem.*, 1996, 271, 26616;

(d) K. Matsuzaki, O. Murase, K. Sugishita, S. Yoneyama, K. Akada, M. Ueha, A. Nakamura, S. Kobayashi, *Biochim. Biophys. Acta*, 2000, 1467, 219;

(e) J.-L. Nieva, F. M. Goñi, and A. Alonso, *Biochemistry*, 1989, 28, 7364.

12 (a) A. de la Maza, J.L. Parra, *Biochem. J*., 1994, 303, 907;

(b) O. López, A. de la Maza, L. Coderch, C. López-Iglesias, E. Wehrli, J. L. Parra, *FEBS Lett.*, 1998, 426, 314.

13 Metal-based Drugs: http://wwwtw.vub.ac.be/aosc/mbd/mbd.htm

14 Edward R.T. Tiekink, Edward R.T., *Crit. Rev. Oncol. Hemat.*, 2002, 42, 217.

15 Peter J. Sadler, Zijian Guo, *Pure Appl. Chem.,* 1998, 70, 863.

16 W. E. Meijs, H. J. Haisma, R. P. Klok, F. B. Van Gog, E. Kievit, H. M. Pinedo, J. D.M. Herschied, *J. Nucl. Med.*, 1997, 38, 112.

17 W. E. Meijs, H. J. Haisma, R. Van Der Schors, R. Wijbrandts, K. Van Den Oever, R. P. Klok, H. M. Pinedo, J. D.M. Herscheid, *Nucl. Med. Biol.*, 1996, 23, 439.

18 R. Amano, S. Oishi, S. Enomoto, F. Ambe, *Riken Rev.,* 1996, 13, 25.

19 A. Ando, I. Ando, S. Sanada, T. Hiraki, T. Takeuchi, K. Hisada, N. Tonami, *Ann. Nucl. Med.*, 1999, 13, 83.

20 L. R. Perk, O. J. Visser, M. Stigter-Van Walsum, M. Vosjan, G.W.M.Visser, J. M. Zijlstra, P. C. Huijgens, G. Dongen, *Eur. J. Nucl. Med. Mol. Imaging*, 2006, 33, 1337.

21 K. Yo, J.E. Salvaggio, *Igaku no Ayumi*, 1976, 98, 665.

22 K.-Y. Kang, D. Bice, E. Hoffmann, R. D'Amato, J. Salvaggio, *J. Allergy Clin. Immun.*, 1977, 59, 425.

23 R. J. Price, D. N. Skilleter, *Toxicol. Lett.*, 1986, 30, 89.

24 Y. Ukai, S. Shima, T. Yoshida, H. Kurita, K. Nagai, N. Mori, Y. Murai, F. Narusawa, Y. Yamamoto, K. Morita, *Nippon Eiseigaku Zasshi*, 1990, 45, 648.

25 N. Mori, S. Shima, K. Morita, H. Kurita, T. Yoshida, T. Arakawa, H. Taniwaki, *Rodo Kagaku*,1990, 66, 493.

26 N. J. Hallab, S. Anderson, M. Caicedo, J. J. Jacobs, *J ASTM Int*, 2006, 3.

27 N. J. Hallab, S. Anderson, M. Caiceo, J. J. Jacobs, *ASTM Spec. Tech. Pub. , Titanium, Niobium, Zirconium, and Tantalum for Medical and Surgical Applications*, 2006, STP 1471, 248.

28 M.G. Tikhaya, *Meditsinskaya Radiologiya*, 1959, 4, 62.

29 A.D. Montemarano, P. Sau, F.B. Johnson, W.D. James, *J. Am. Acad. Dermatol*, 1997, 37, 496.

30 B. Liu, S. Enomoto, S. Ambe, R. G. Weginwar, F. Ambe, *Riken Review*, 1996, 13, 35.

31 (a) M. Salas, B. Tuchweber, K. Kovacs, B.D. Garg, *Beitr. Path. Bd.*, 1976, 157, 23.

(b) B.Tuchweber, M. Salas, *Arch. Toxicol.,* 1978, 41, 223.

(c) M. Salas, B. Tuchweber, *Arch. Toxicol. (Berl.)*, 1976, 35, 115.

(d) M. Kiss, F. Konczol, N.Farkas, D. Lorinczy, J. Belagyi, J. Therm. Anal. Calorim., 2001, 65, 627.

(e) H. M. Baker, C. J. Baker, C. A. Smith, E. N. Baker, J. Biol. Inorg. Chem. (2000) 5: 692-698.

32 P. Kopt-Maier, H. Kopf, *Chem. Rev.*, 1987, 87, 1137.

33 A. M. Rouhi, *Chem. and Eng. News*, 2004, 82, 36.

34 P. Wipt, C. M. Coleman, J. M. Janjic, P. S. Iyer, M. D. Fodor, Y. A. Shafer, C. R.J. Stephenson, C. Kendall, B. W. Day, *J. Comb. Chem.*, 2005, 7, 322.

35 J. H. Toney, T. J. Marks, *J.Am. Chem. Soc.*,1985, 107, 947.

36 A. Moustatih, M.M.L. Fiallo, A. Garnier-Suillerot, *J. Med. Chem.*, 1989, 32, 336.

37 (a) J. H. Murray, M. M. Harding, *J. Med. Chem.,* 1994, 37, 1936;

(b) M. M. Harding, G. Mokdsi, *Curr. Med. Chem.*, 2000, 7, 1289.

38 R.C. Fay in *Comprehensive Coordination Chemistry*, Pergamum Press, G. Wilkinson et al., *editor*, 1987, 3, 364.

39 (a) T. Takarada, M. Yashiro, M. Komiyama, *Chem. Eur. J.,* 2000, 6, 3906;

(b) M. Komiyama, *Met. Ions Biol. Syst*., 2001, 38, 25;

(c) M. Komiyama, T. Takarada, *Met. Ions Biol. Syst*., 2003, 40, 355.

40 (a) I.E. Burgeson, N.M. Kostić, *Inorg. Chem.,*1991, 30, 4299;

(b) L. Zhu, N.M. Kostić, *Inorg. Chem.*,1992, 31, 3994;

(c) N.M.Milović, L.-M. Dutca, N.M. Kostić, *Chem. Eur. J.,* 2003, 9, 5097;

(d) X. Sun, C. Jin, Y. Mei, G. Yang, Z. Guo, L. Zhu, *Inorg. Chem.,* 2004, 43, 290;

(e) N.M. Milović, N.M. Kostić, *J. Am. Chem. Soc.*, 2002, 124, 4759;

(f) X.M. Luo, W.J. He, Y. Zhang, Z.J. Guo, L.G. Zhu, *Chin. Chem. Lett.*, 2000,11, 951;

(g) W. Bal, J. Lukszo, K. Bialkowski, and K.S. Kasprzak, *Chem. Res. Toxicol.*, 1998, 11, 1014;

(h) N.M. Milovic and N.M. Kostić, *J. Am. Chem. Soc*., 2003, 125, 781.

41 M. Yashiro, Y. Sonobe, A. Yamamura, T. Takarada, M. Komiyama, Y. Fuji, *Org. Biomol. Chem.*, 2003, 1, 629.

42 (a) E. Bamann, A. Rother, H. Trapmann, *Naturwiss.*, 1956, 43, 326;

(b) E. Bamann, H. Trapmann, A. Rother, *Chem. Ber*., 1958, 91, 1744.

43 M. Kassai, R.G. Ravi, S.J. Shealy, K.B. Grant, *Inorg. Chem*., 2004, 43, 6130.

44 J. Brodbelt, E. Kempen, and M. Reyzer, *Struct. Chem.*, 1999, 10, 213.

45 N.J. Weinreb, R.O. Brady, A.L. Tappel, *Biochim. Biophys. Acta*, 1968, 159, 141.

46 B. Ramstedt, J.P.Slotte, *FEBS Lett.*, 2002, 531, 33.

47 E.F. Neufeld, *Ann. Rev. Biochemistry*, 1991, 60, 257.

48 J. F. Pankow, *Aquatic Chemistry Concepts*, Lewis Publishers: Chelsea, Michigan. 1991.

49 D. Langmuir, *Aqueous Environmental Chemistry*, Prentice-Hall, Inc.: Upper Saddle River, N. J., 1997.

50 E.L. Hegg, J.N. Burstyn, *Coordin. Chem. Rev.*, 1998, 173, 133.

51 K.O.A. Chin, J.R. Morrow, *Inorg. Chem.*, 1994, 33, 5036.

52 http://en.wikipedia.org/wiki/Niemann-Pick_disease

53 Unpublished data by R.G. Ravi, M.Kassai, and K.B. Grant.

54 (a) J.P. Berry, *Cell Mol. Biol.*, 1996, 42, 395.

(b) J.P. Berry, *Toxicol.*, 1990, 62, 239.

55 (a) W. Yin, Z. Dong, X.Chen, N. Finn, M.Z. Yates, *J. Supercrit. Fluids*, 2007, 41, 293.

(b) H. Liu, M.Z. Yates, *Langmuir*, 2003, 19, 1106.

CHAPTER II HYDROLYSIS OF INSULIN CHAIN B USING ZIRCONIUM(IV) AT NEUTRAL PH.

(This chapter is taken verbatim from an article by Sarah S. Cepeda and Kathryn B. Grant, *New Journal of Chemistry*, **2008**, *32*, 388-391. Sarah S. Cepeda conducted the experiments and contributed to the writing of the article. The final version of the manuscript was written by Prof. Kathryn B. Grant. Following the chapter is an unpublished epilogue showing additional data)

Abstract.

Zirconium(IV) hydrolyzes the 30-mer oligopeptide oxidized bovine insulin chain B after 4 h to 8 h of treatment at pH 7.0 and 60 °C: MALDI-TOF and HPLC-ESI-MS and MS/MS data show significant levels of cleavage at Gly8-Ser9, Gly20-Glu21, Ser9-His10, Cys(SO_3H)7-Gly8, and Cys(SO_3H)19-Gly20 amide bonds within the oligopeptide.

Introduction.

There has been widespread interest in the development of metal complexes that hydrolyze peptide amide bonds under mild conditions of pH and temperature.[1] These compounds are of great importance due to their potential applications in the analysis of protein solution structure, in protein engineering, and in therapeutics.[1d,f,h,2] Our own research efforts have primarily focused on zirconium (IV). Because of its enhanced Lewis acid strength, oxophilicity,[3] tendency to form complexes with high coordination numbers,[3] and rapid ligand-exchange kinetics,[4] this metal center should be able to catalyze peptide hydrolysis by activating an amide carbonyl carbon in the peptide backbone while delivering a hydroxide nucleophile to the scissile amide bond.[1f] Recent efforts in our laboratory have demonstrated that Zr^{IV} in the presence 4,13-diaza-18-crown-6 has excellent reactivity: $t_{1/2}$ values are 5.3 ± 0.1 h and 36.6 ± 2.7 h for Zr^{IV}-assisted hydrolysis of the dipeptide Gly-Glu at pH 7.1/60°C and at pH 7.3/37°C.[1f]

(These half-lives represent significant rate enhancements compared to the $t_{1/2}$ of ~250 years for spontaneous hydrolysis of unactivated peptide amide bonds at pH 7.0 and 37°C).[5] The formation of insoluble Zr^{IV} precipitates during the cleavage reactions led us to speculated that hydrolysis of peptides by Zr^{IV}/4,13-diaza-18-crown-6 might have a heterogeneous component similar to peptide hydrolysis by lanthanide hydroxide gels.[6] Yet, in spite of the attributes of Zr^{IV}, the largest peptide to have been hydrolyzed by this metal center was Ala-Gly-Asp-Val.[1f] To address this size limitation, herein we report efficient, Zr^{IV}-assisted hydrolysis of the 30-mer oligopeptides oxidized bovine insulin chain B.

Results and discussion.

In a typical cleavage reaction, 500 uM to 1 mM of oxidized bovine insulin chain B was added to 20 mM of 4,13-diaza-18-crown-6[7] in the presence or absence of 10 mM of $ZrCl_4$. Hydrolysis reactions were allowed to proceed at pH 6.9-7.2 and 60°C. Aliquots were removed at ~t = 0 h, 4 h, and 8 h time points, quenched with the strong chelating agent EDTA, and then analyzed by HPLC-electrospray ionization mass spectrometry (ESI-MS) or by matrix-assisted laser desorption ionization time-of-flight (MALDI-TOF) MS. Mass spectral peak assignments of peptide hydrolysis products were made using FindPept software and ESI tandem mass spectrometry (MS/MS) (Figure 2.1(a) and (b)). Each of the peptide fragments produced by Zr^{IV}/4,13-diaza-18-crown-6 was defined as either an apparent major, intermediate, or trace product depending on its percent relative abundance in the HPLC-ESI chromatograms and MALDI-TOF mass spectra. In Figure 2.1(c) is the primary amino acid sequence of insulin chain B showing the positions of peptide amide bond hydrolysis indicated by the MS data. In addition to percent relative abundance, Tables 2.1 and 2.2 summarize observed vs. calculated *m/z* values.

The HPLC-ESI chromatograms and MALDI-TOF mass spectra in Figure 2.2 and Figure 2.3 reveal the time-dependent appearance of prominent insulin chain B peptide hydrolysis products B, C, D, E, F, G, I, K, K‡, L, W, and X. It is evident that shorter peptide fragments B, D, F, I, K, K‡, L, W, and X become more dominant as the reaction proceeds from t = 4 h to t = 8 h, while the larger fragments C, E, G are prominent only at t = 4 h (Figure 2.2).

The cleavage yields corresponding to the HPLC-ESI chromatograms shown in Figure 2.2 were estimated by taking the sum of the peak areas of all the peptide hydrolysis products, dividing this sum by the total peak areas of the peptide hydrolysis products added to the peak area of any remaining unhydrolyzed peptide, and then multiplying the quotient by 100: hydrolysis yield = [sum of all peptide hydrolysis product peak areas / (sum of all peptide hydrolysis product peak areas + unhydrolyzed insulin chain B peak area)] x 100. In the presence of Zr^{IV}/4,13-diaza-18-crown-6, these values were 0% at t = 0 h, 15 % at t=4 h and 51 % at t = 8 h (pH 7.0 and 60 °C). In parallel control reactions in which $ZrCl_4$ was substituted by equivalent volumes of water, corresponding values were minimal (0 % at t=0 h, 0 % at t=4 h and 3 % at t= 8 h).

As expected, a larger number of peptide fragments was detected by HPLC-ESI-MS in comparison to MALDI-TOF MS. (In complex mixtures of analytes, competition for charge can lead to ion suppression. As a result, pre-separation is often needed to enhance sensitivity).[8] Notwithstanding, the MALDI and HPLC-ESI experiments are in good general agreement (Figure 2.1, 2.2, 2.3). The data collectively indicate that Zr^{IV}/4,13-diaza-18-crown-6 produces major amounts of hydrolysis at the following five amide bonds: Gly8-Ser9, Gly20-Glu21, Ser9-His10, Cys(SO_3H)7-Gly8, and Cys(SO_3H)19-Gly20. With respect to Gly8-Ser9, cleavage of Xaa-Ser(Thr) in peptides and proteins containing the sequence Xaa-Ser(Thr)-His has been extensively

documented for Cu^{II},[2b,9a,b,e,f] Ni^{II},[1b] and Pd^{II}, [9b-d] and is thought to involve an N→O acyl rearrangement promoted by the hydroxyl group side chains of serine or threonine.[1b,9a,d] We also expected to observe significant levels of hydrolysis at Gly20-Glu21 and at Ser9-His10. In a previously published report, we demonstrated that Zr^{IV}/4,13-diaza-18-crown-6 displays a clear preference for hydrolysis of neutral and negatively charged peptides containing glycine or amino acids with oxygen-rich side chains.[1f] (In fact, Gly-Glu was the most reactive of the 16 dipeptides studied.) The oxophilicity of Zr^{IV} combined with electrostatic interactions between this positively charged metal center and negatively charged Cys(SO_3^-) could account for the efficient hydrolysis of the Cys(SO_3H)7-Gly8 and Cys(SO_3H)19-Gly20 amide bonds in bovine insulin chain B. In addition to the five major products, Zr^{IV}/4,13-diaza-18-crown-6 produced apparent intermediate amounts of hydrolysis at: Leu6-Cys(SO_3H)7, Arg22-Gly23, and Gly23-Phe24. This pattern again may reflect the preference of Zr^{IV} for hydrolysis of peptides with glycine or oxygen-rich side chains. As shown in Figure 2.1 and Tables 2.1 (in ESI), trace amounts of hydrolysis were seen at five sites within the oligopeptides.

Up until now, hydrolysis of oxidized insulin chain B has been studied using salts and/or complexes of Cu^{II},[9b,g] Pd^{II},[9b,c] Pt^{II},[9g] and Zn^{II} [9h]. These experiments were conducted under acidic conditions (pH 2.0 to 2.5) at temperatures ranging from 40 °C to 60 °C. Hydrolysis reactions were studied by ESI-MS,[9b,g,h] HPLC-ESI-MS,[9g] MS/MS,[9g,h] and MALDI-TOF MS.[9c] The data showed that metal binding sites included the N-terminal amino group of Phe1 (Cu^{II}, Pd^{II}, and Pt^{II}),[9b,c,g] the imidazole side chains of His5 and His10 (Cu^{II}, Pd^{II}, Pt^{II}, and Zn^{II}), [9b,c,g,h] and Arg22 (Zn^{II}).[9h] If the metal-peptide complexes formed were hydrolytically active, then amide bond hydrolysis occurred in close proximity to the anchoring amino acid residue. Thus, the following insulin chain B peptide amide bonds were hydrolyzed: Phe1-Val2 (Cu^{II}),[9g] Asn3-Gln4 (Cu^{II}, Pd^{II},

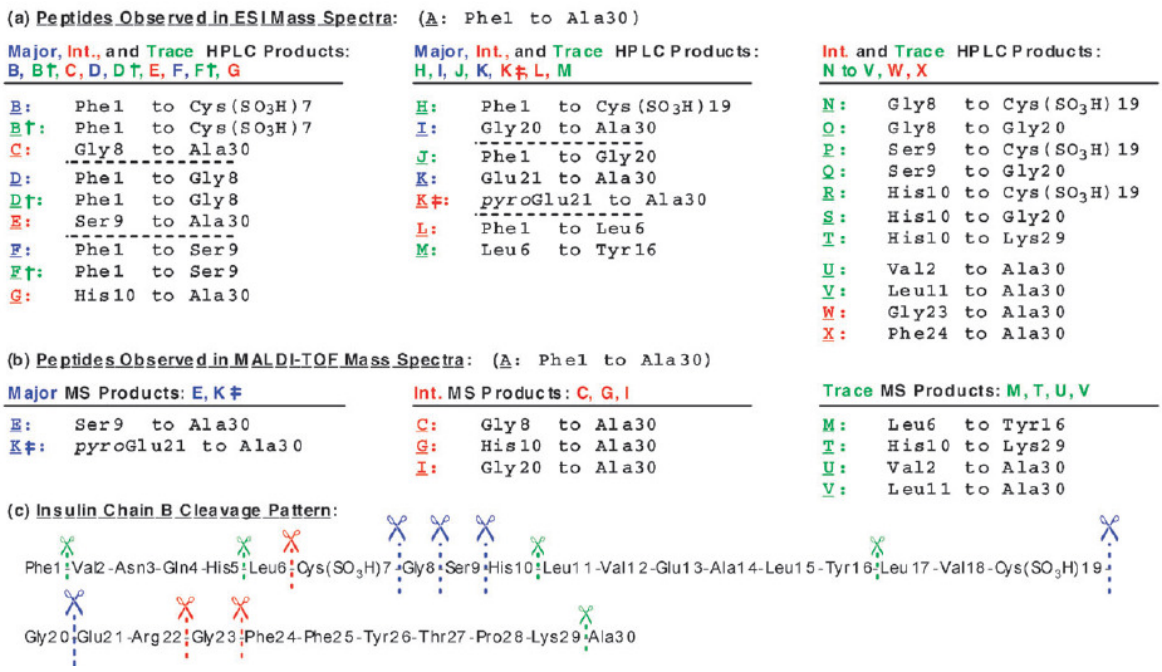

Figure 2.1. Peptides detected in (a) HPLC-ESI and (b) MALDI-TOF mass spectra. The colors blue, red, and green identify apparent major, intermediate, and trace hydrolysis products, respectively. "†" = deamidation of Asn3 to Asp3, and/or Gln4 to Glu4. "‡" = lactamization of Glu21 to *pyro*glutamate21 (*pyro*Glu21). (c) Corresponding Zr^{IV}/4,13-diaza-18-crown-6 cleavage sites superimposed on the amino acid sequence of oxidized bovine insulin chain B.

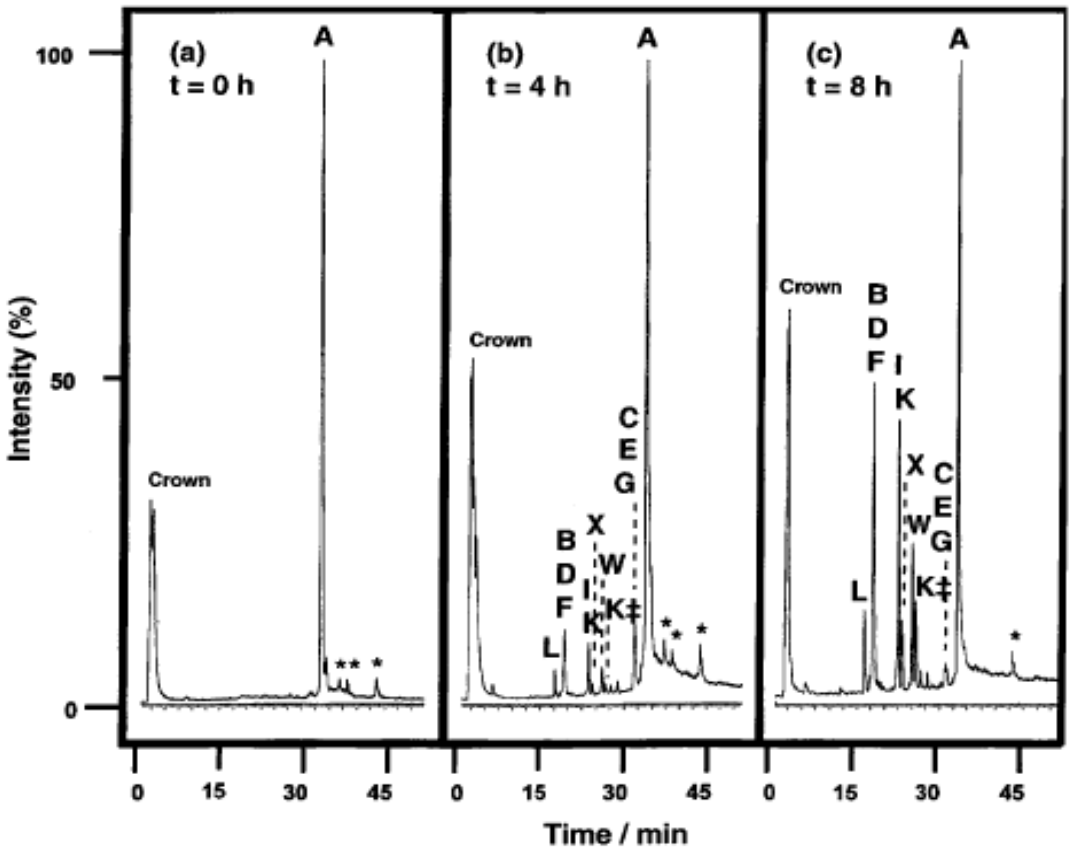

Figure 2.2. HPLC chromatograms of 500 μM of insulin chain B treated with 10 mM $ZrCl_4$ in 20 mM 4,13-diaza-18-crown-6 for t = (a) 0 h, (b) 4 h, and (c) 8 h (pH 7.0 and 60 °C). Peak A is unhydrolyzed insulin chain B. Peaks B, D, F, I, K, and peaks L, X, W, K‡, C, E, G correspond to apparent major and intermediate peptide hydrolysis products, respectively. Trace hydrolysis products are in Table 2.1 (in ESI). Representative ESI mass spectra are in Figure 2.4 to 2.6 "Crown" identifies the azacrown ether. "*" identifies Na-adducted monomer and Na-adducted cluster dimers of peak A.

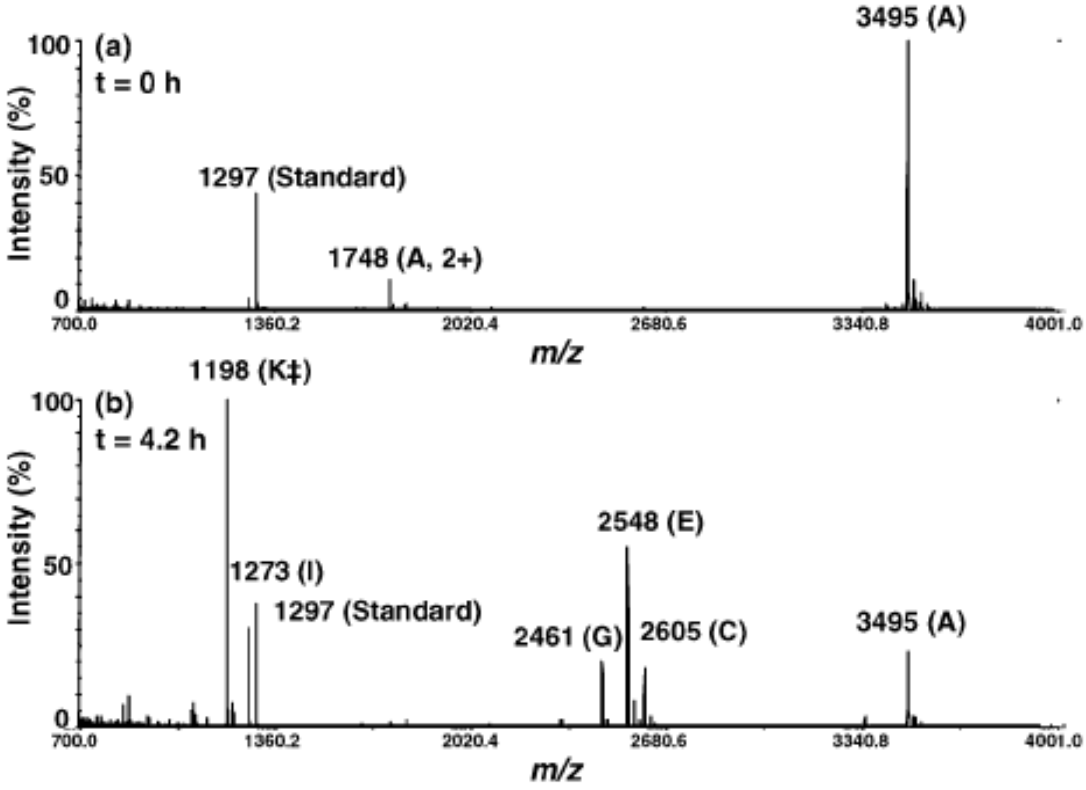

Figure 2.3. Representative MALDI-TOF mass spectra for hydrolysis of 1 mM of insulin chain B at (a) t = 0 h and (b) t = 4.2 h. Reactions were run in 10 mM $ZrCl_4$ and 20 mM 4,13-diaza-18-crown-6 at pH 7.2 and 60 °C. Peak A is unhydrolyzed insulin chain B. Peaks K‡ and E and peaks I, G, and C correspond to apparent major and intermediate peptide hydrolysis products, respectively. Trace hydrolysis products are listed in Table 2.2 (in MALDI). Human angiotensin I is the internal standard. All masses are singly charged unless otherwise indicated.

Zn^{II}),[9c,g,h] His5-Leu6 (Zn^{II}),[9h] Gly8-Ser9 (Cu^{II}, Pd^{II}, Zn^{II}),[9c,g,h] His10-Leu11 (Pt^{II}),[9g] and Glu21-Arg22 (Zn^{II}).[9h] In urea-denatured oxidized hog insulin chain B, Pd^{II} produced cleavage at Leu6-Cys(SO_3H)7 and at Gly8-Ser9.[9b,10] Because no other cleavage sites were observed in any of the MS studies,[9b,c,g,h] the hydrolysis of Cys(SO_3H)7-Gly8 and Cys(SO_3H)19-Gly20 amide bonds by Zr^{IV}-4,13-diaza-18-crown-6 points to unprecedented cleavage of insulin chain B at approximately neutral pH.

Metal salts of Ce^{III}, Ce^{IV}, La^{III}, Th^{IV}, and Zr^{IV} accelerate the lactamization of glutamate (Glu) to pyroglutamate (pyroGlu) at 70 °C over a weakly acidic to weakly alkaline pH range.[11] As shown in Figure 2.2 and Figure 2.3, Zr^{IV}-assisted hydrolysis of oxidized bovine insulin chain B produces peptide fragment K (Glu21 to Ala30, m/z 1216) and a second prominent peptide K‡ (*pyro*Glu21 to Ala30, m/z 1198). We attributed the appearance of the latter fragment to loss of water through lactamization of the N-terminal glutamate residue in peptide K. Pyroglutamate formation was confirmed by ESI-MS/MS of K‡ which produced a *pyro*Glu immonium ion at *m/z* 84.2. In addition to lactamization of glutamate, Ce^{III}, Ce^{IV}, La^{III}, Th^{IV}, and Zr^{IV} ions accelerate the hydrolytic deamidation of glutamine and asparagines residues.[12] In our experiments, HPLC-ESI analyses of the Zr^{IV} reactions detected the production of apparent trace quantities of the following three sets of insulin chain B peptides: B†(1) and B†(2); D†(1) and D†(2); and F†(1) and F†(2) (Table 2.1. in ESI). We then employed ESI-MS/MS sequencing to show that these fragments were produced by deamidation of parent peptides B, D, and F; in B†(1), D†(1), and F†(1), Gln4 in the corresponding parent was converted to Glu4; in B†(2), D†(2), and F†(2), Asn3 and Gln4 were deamidated to Asp3 and Glu4 (Figure 2.7). Interestingly, deamidation of glutaminyl and asparaginyl residues occurs *in vivo*. Because a correlation exits between protein

lifetime and total amide content, it has been suggested that deamidation may play a physiological role in triggering protein degradation.[13]

Up until now, the largest peptide to have been hydrolyzed by zirconium(IV) consisted of only four amino acid residues.[1f] We have successfully addressed this apparent limitation in the present study. By using HPLC-ESI-MS and MS/MS, and MALDI-TOF MS, we have demonstrated that Zr^{IV}/4,13-diaza-18-crown-6 facilitates hydrolysis of the 30-mer oligopeptides oxidized bovine insulin chain B at pH 7.0 and 60 °C. Apparent major levels of cleavage were produced at Gly8-Ser9, Gly20-Glu21, Ser9-His10, Cys(SO_3H)7-Gly8 and Cys(SO_3H)19-Gly20 sequences, while intermediate amounts of hydrolysis were at Leu6-Cys(SO_3H)7, Arg22-Gly23, and Gly23-Phe24, Zr^{IV}/4,13-diaza-18-crown-6 was also shown to promote lactamization of *N*-terminal Glu21 and deamidation of Asn3 and Gln4. To the best of our knowledge, this paper presents the first example of metal-assisted hydrolysis of a Cys(SO_3H)-Xaa peptide amide bond. This is significant in light of the fact that the formation of cysteine sulfonic acid in proteins is triggered by oxidative stress and has been associated with amyloid fibril formation, Parkinson's disease, and physiological processes involving oxidative stress response proteins.[14] Our current work is focused on mechanistic studies that should enable us to design new zirconium ligands that optimize sequence specificity and increase the hydrolytic efficiency of Zr^{IV}.

We thank the National Science Foundation for financial support under grant CHE-0718634.

Experimental.

Peptide hydrolysis reactions. A total of 500 μM to 1 mM of oxidized bovine insulin chain B (freshly dissolved in doubly distilled H_2O) was added to 20 mM of 4,13-diaza-18-crown-6 in the presence or absence of 10 mM of $ZrCl_4$ (400 μL total volume). The pH value of

the zirconium solution was adjusted at 25 °C to 6.9-7.2 by addition of the azacrown ether.[7] (Alternatively, in the absence of $ZrCl_4$, pH was adjusted with HCl.) Hydrolysis reactions wre then allowed to proceed at 60 °C and aliquots were removed at ~ t = 0 h, 4 h, and 8 h time points. Pre- and post-reaction pH measurements varied by only ± 0.12 units. The aliquots were quenched at 4 °C with 1/10 volume of 0.5 M EDTA pH 8, and then analyzed by HPLC-ESI-MS or by MALDI-TOF MS. Each of the peptide fragments produced by Zr^{IV}/4,13-diaza-18-crown-6 was arbitrarily defined as either an apparent major, intermediate, or trace product depending on its percent relative abundance in the HPLC-ESI chromatograms recorded at t = 4 h or t = 8 h (Table 2.1 in ESI) and in MALDI-TOF mass spectra recorded at t = 4.2 h (Table 2.2): 44 % to 100 % for apparent major hydrolysis products, 12 % to 30 % for apparent intermediate hydrolysis products, 1 % to 5 % for apparent trace hydrolysis products.

Mass spectrometry.

HPLC-ESI-MS and HPLC-ESI-MS/MS. HPLC-ESI chromatograms and corresponding mass spectra were acquired over a scanning mass range of *m/z* 100 to 3000 on a Micromass Q-Tof Micro mass spectrometer equipped with a Waters 2695 HPLC. Hydrolysis reactions were diluted 10-fold with doubly distilled H_2O. A 20 µL amount of each diluted solution was injected into a Waters Atlantis™ dC_{18} 3 um, 100Å, 2.1 mm x 150 mm reversed-phase HPLC column. Separations were conducted over 109 min at 20 °C with a flow rate of 0.2 mL min^{-1} and a mobile phase gradient elution scheme consisting of 2 % to 98 % of acetonitrile in 0.1 % formic acid. The ESI instrument settings were: electrospray needle voltage, + 3.0 kV; N_2 cone gas flow, 60 L h^{-1}; N_2 desolvation gas flow, 450 L h^{-1}; capillary desolvation temperature, 200 °C. Spectra were acquired in positive ion mode (Figure 2.4, 2.5, 2.6, 2.7,) or in negative ion mode (Figure 2.8) with a scan time of 1.0 s.

HPLC-ESI-MS/MS sequencing of peptide fragments was done on the Micromass Q-Tof Micro mass spectrometer with data-directed acquisition (DDA). The MS to MS/MS switch criteria allowed a precursor selection of a maximum of 4 concurrent ions when the ion intensity was above a threshold of 10 ion counts per second. To induce collisional activation, the collision energy was set at 25 V and argon was used as a collision gas at a pressure of 28 psi.

MALDI-TOF MS. To prepare the CHCA matrix, a total of 10 mg of α-cyano-4-hydroxycinnamic acid was dissolved in 1 mL of water-acetonitrile (50 : 50, v/v) containing 0.1% trifluoroacetic acid. A total of 5 μL of the matrix was mixed with 5 μL of a ten-fold dilution of the peptide hydrolysis reaction and with 1 μL of an internal standard (1.5 uM human synthetic angiotensin I). A total of 1 μL of the resulting solution was transferred to a MALDI sample stage and air-dried. Positive ion MALDI-TOF mass spectra were then acquired using an Applied Biosystems Voyager-DE PRO Biospectrometry instrument in reflectron mode. Following time-delayed extraction, ions were accelerated to 20 kV. A total of 500 laser shots was averaged for each mass spectrum. The nitrogen laser source parameters included a grid voltage of 68.2%, a guide wire voltage of 0.001%, and a delay time of 50 ns. The average difference between calculated and observed mass values was *m/z* 0.044 ± 0.061.

Software. All mass spectral peptide hydrolysis product peak assignments were made using FindPept software (The Swiss Institute of Bioinformatics; http://ca.expasy.org/tools/findpept.html). The majority of the peak assignments was subsequently confirmed by HPLC-ESI-MS/MS sequencing (Tables 2.1 and 2.2). Isotope distribution patterns were predicted using the "Isotope Distribution Calculator and Mass Spec Plotter" (Scientific Instrument Services, Inc.; http://www2.sisweb.com/mstools/isotope.htm).

MS/MS fragmentation patterns were predicted with MassLynx/Biolynx software, version 4.0 (Micromass).

References.

1 (a) K.W. Bentley and E.H. Creaser, *Biochem J*., 1973, 135, 507;

(b) W. Bal, J.Lukszo, K. Bialkowski, and K.S. Kasprzak, *Chem. Res. Toxicol.*, 1998, 11, 1014;

(c) C.V. Kumar, A. Buranaprapuk, A. Cho and A. Chaudhari, *Chem. Commun.*, 2000, 597;

(d) J.W. Jeon, S.J. Son, C.E. Yoo, I.S. Hong and J. Suh, *Bioorg. Med. Chem.*, 2003, 11, 2901;

(e) N.M. Milovic and N.M. Kostić, *J. Am. Chem. Soc.*, 2003, 125, 781;

(f) M. Kassai, R.G. Ravi, S.J. Shealy, and K.B. Grant, *Inorg. Chem.*, 2004, 43, 6130;

(g) S. Manka, F. Becker, O.Hohage and W.S. Sheldrick, *J. Inorg. Biochem*., 2004, 98, 1947;

(h) P.S. Chae, M.-S. Kim, C.-S. Jeung, S.D. Lee, H. Park, S. Lee, and J. Suh, *J. Am. Chem. Soc.* , 2005, 127, 2396;

(i) A. Erxleben, *Inorg. Chem.*, 2005, 44, 1082;

(j) K.B. Grant and M. Kassai, *Curr. Org. Chem.*, 2006, 10, 1035.

2 (a) C.J.A. Wallace, in *Protein Engineering by Semisynthesis*, CRC: Boca Raton, Florida, 2000;

(b) D.P. Humphreys, L.M. King, S.M. West, A.P. Chapman, M. Sehdev, M.W. Redden, D.J. Glover, B.J. Smith, and P.E. Stephens, *Protein Eng*., 2000, 13, 201;

(c) Q. Pan, W. Jiang, Z. Liao, T. Zhang and C. Liu, *Inorg. Chem*., 2006, 45, 490.

3 R.C. Fay, in *Comprehensive Coordination Chemistry*, ed. G. Wilkinson, R.D. Gillard and J.A. McCleverty, Pergamon, Oxford, 1987, vol. 3, pp. 364.

4 A. Singhal, L.M. Toth, J.S. Lin and K. Affholter, *J. Am. Chem. Soc.*, 1996, 118, 11529.

5 R. Smith and D.E. Hansen, *J. Am. Chem. Soc.*, 1998, 120, 8910.

6 M. Yashiro, T. Takarada, S. Miyama and M. Komiyama, *J. Chem. Soc., Chem. Commun.,* 1994, 1757.

7 Because the pKa_1 of 4,13-diaza-18-crown-6 is 7.94 at 25 °C, the azacrown ether was used to effectively buffer reaction pH[1f].

8. V.C. Chen, K. Cheng, W. Ens, K.G. Standing, J.I. Nagy and H. Perreault, *Anal. Chem.,* 2004, 76, 1189.

9 (a) G. Allen and R.O. Campbell, *Int. J. Pept. Protein Res.*, 1996, 48, 265;

(b) X.-M. Luo, W.-J. He, Y.Zhang, Z.-J. Guo and L. Zhu, *Chin. J. Chem.,* 2000, 18, 855;

(c) N.M. Milovic and N.M. Kostić, *Inorg. Chem.,* 2002, 41, 7053;

(d) L. Zhu and N.M. Kostić, *Inorg. Chim. Acta*, 2002, 339, 104;

(e) L. Zhang, Y. Mei, Y. Zhang, S. Li, X. Sun and L. Zhu, *Inorg. Chem*., 2003, 42, 492;

(f) S.H. Yoo, B.J. Lee, H. Kim and J. Suh, *J. Am. Chem. Soc*., 2005, 127, 9593;

(g) J. Hong, R. Miao, C. Zhao, J. Jiang, H. Tang, Z. Guo and L. Zhu, *J. Mass Spectrom*., 2006, 41, 1061;

(h) J. Jiang, Y.-H. Mei, W.-J. Wang, Q.-J. Wu and L. Zhu, *Wuji Huaxue Xuebao*, 2007, 23, 948.

10 Because no cleavage was observed when urea was omitted from this reaction[9b], it can be inferred that the interaction of oxidized insulin chain B with metals is dependent on protein secondary structure. Thus, in our experiments, the failure of oxophilic Zr^{IV} to

produce hydrolysis adjacent to Glu13, Tyr27, and Thr28 may have been due to steric hindrance associated with secondary structure.

11 E. Bamann and H. Muenstermann, *Arch. Pharm.,* 1965, 298, 750

12 E. Bamann, H. Trapmann and H. Muenstermann, *Arch. Pharm*., 1963, 296, 47

13 (a) A.B. Robinson, *Proc. Natl. Acad. Sci. U.S.A.,* 1974, 71, 885

(b) N.E. Robinson and A.B. Robinson, *Proc. Natl. Acad. Sci.,U.S.A*., 2001, 98, 4367.

14 (a) M. Chevallet, E. Wagner, S. Luche, A. van Dorsselaer, E. Leize-Wagner and T. Rabilloud, *J. Biol. Chem.*, 2003, 278, 37146;

(b) A. Lim, T. Prokaeva, M.E. McComb, L.H. Connors, M. Skinner and C.E. Costello, *Protein Sci.*, 2003, 12, 1775;

(c) T. Kinumi, J. Kimata, T. Taira, H. Ariga and E. Niki, *Biochem. Biophys. Res. Commun*., 2004, 317, 722.

Supporting information.

Additional experimental details.

Materials. Distilled, deionized water was utilized in the preparation of all buffers and all aqueous reactions. Chemicals were of the highest available purity and were used without further purification. L-glutamic acid, α-cyano-4-hydroxycinnamic acid (CHCA), human synthetic angiotensin I, and oxidized bovine insulin chain B were purchased from Sigma. Ethylenediaminetetraacetic acid disodium salt (EDTA) was from Fisher Scientific and HPLC grade acetonitrile was from Burdick & Jackson. All other reagents including 4,13-diaza-18-crown-6 (1,4,10,13-tetraoxa-7,16 diazacyclooctadecane), formic acid, and $ZrCl_4$ (purity >99.99 %) were obtained from the Aldrich Chemical Company.

Representative HPLC-ESI mass spectra. As described in the accompanying manuscript, a total of 500 μM of oxidized bovine insulin chain B was treated with 10 mM $ZrCl_4$ in 20 mM 4,13-diaza-18-cown-6 from t = 4 h to t = 8 h at pH 7.0 and 60 °C. Peptide hydrolysis products were then identified by HPLC-electrospray ionization mass spectrometry (HPLC-ESI MS). Shown in Figures 2.4, 2.5, 2.6 are representative ESI mass spectra at HPLC elution times of 18.36 min, 23.54 min, and 31.70 min, respectively.

Zirconium(IV)-assisted deamidation and lactamization reactions.

Zirconium(IV)-assisted deamidation. HPLC-ESI analyses of the Zr^{IV} hydrolysis reactions detected the production of apparent trace quantities of the following three sets of chromatographically separable insulin chain B peptide fragments: B†(1) and B†(2); D†(1) and D†(2); and F†(1) and F†(2) (Table 2.1.). Fragments B†(1) at *m/z* 909.3, D†(1) at *m/z* 966.4, and F†(1) at *m/z* 1053.5 were all observed to have masses that were approximately one mass unit higher than the parent peptides B (Phe1 to Cys(SO_3H)7, at *m/z* 908.3), D (Phe1 to Gly8, at *m/z* 965.5), F (Phe1 to Ser9, at *m/z* 1052.5; Table 2.1.). This result indicated that B†(1), D†(1), and F†(1) could be deamidated forms of the starting material with either Asn3 or Gln4 being converted to α-Asp3, α-Glu4, or to the geometric isomers β-Asp and γ-Glu.[1] Fragment B†(2) at *m/z* 910.3, D†(2) at *m/z* 967.4, and F†(2) at *m/z* 1054.4, were all approximately two mass units higher that the parent peptides B, D, and F. Therefore, B†(2), D†(2), and F†(2) were proposed to be doubly deamidated. We then employed ESI-MS/MS sequencing to demonstrate that the three sets of fragments were indeed produced by deamidation of parent peptides B, D, and F: in B†(1), D†(1), and F†(1), Gln4 in the corresponding parent was converted to Glu4; in B†(2), D†(2), and F†(2), Asn3 and Gln4 were deamidated to Asp3 and Glu4.

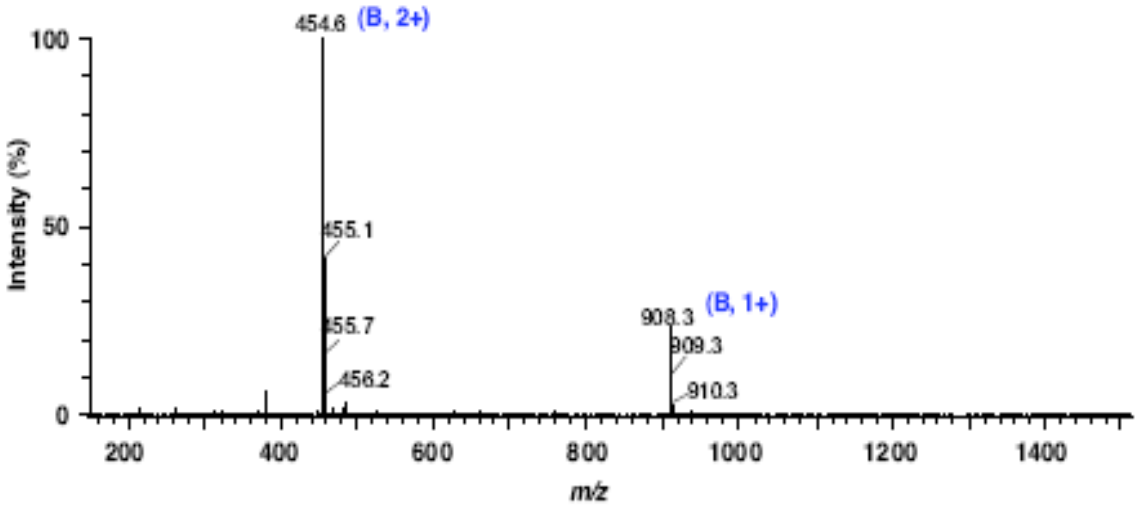

Figure 2.4. HPLC-ESI mass spectrum at an HPLC elution time of 18.36 min. Oxidized bovine insulin chain B was treated with Zr^{IV}/4,13-diaza-18-crown-6 for t=8 h. In the spectrum are the singly and doubly charged observed masses corresponding to insulin chain B hydrolysis fragment Phe1 to Cys(SO_3H)7 (fragment B, Table 2.1.). The spectrum was acquired in positive ion mode.

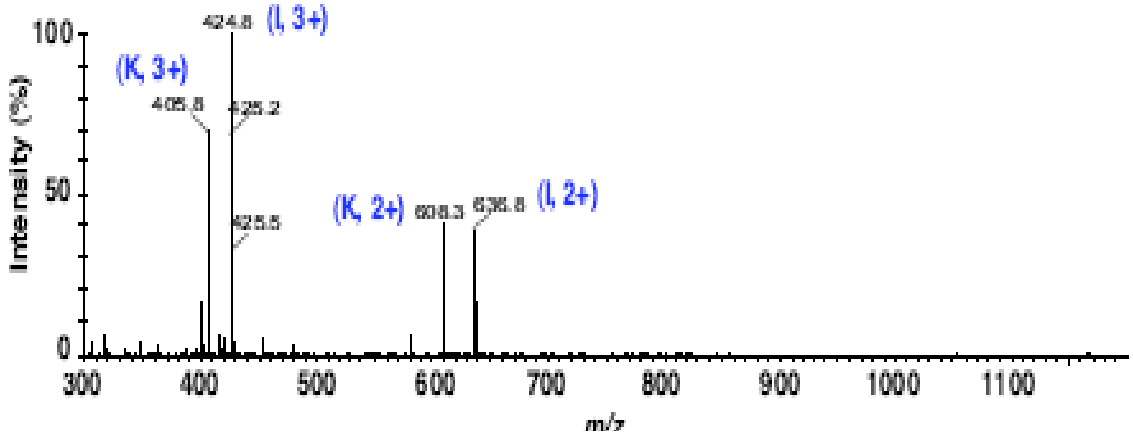

Figure 2.5. HPLC-ESI mass spectrum at an HPLC elution time of 23.54 min. Oxidized bovine insulin chain B was treated with Zr^{IV}/4,13-diaza-18-crown-6 for t = 4. In the spectrum are the doubly and triply charged observed masses corresponding to insulin chain B hydrolysis fragments Gly20 to Ala30 (fragment I, Table 2.1.) and Glu21 to Ala30 (fragment K, Table 2.1.). The spectrum was acquired in positive ion mode.

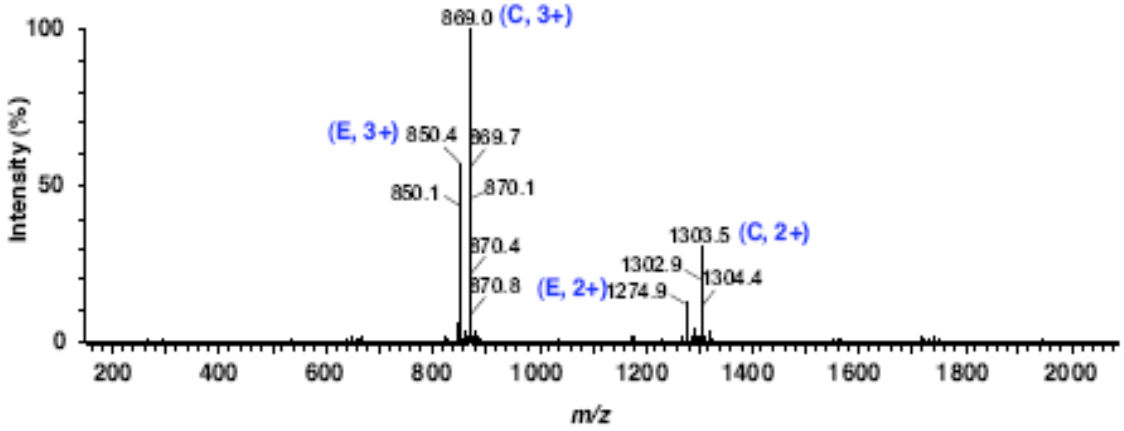

Figure 2.6. Representative HPLC-ESI mass spectrum at an HPLC elution time of 31.70 min. Oxidized bovine insulin chain B was treated with Zr^{IV}/4,13-diaza-18-crown-6 for t = 4 h. In the spectrum are the doubly and triply charged observed masses corresponding to insulin B chain hydrolysis fragments Gly8 to Ala30 (fragment C, Table 2.1.) and Ser9 to Ala30 (fragment E, Table 2.1.). The spectrum was acquired in positive ion mode.

Figures 2.4, 2.5, and 2.6 show representative ESI spectra with singly- and doubly-charged spectra of the major products. Shown in Figure 2.7 are representative HPLC-ESI-MS/MS spectra acquired from precursor ions at *m/z* 965.5 (Fragment D, HPLC elution time 18.50 min), at *m/z* 966.4 (Fragment D†(1), HPLC elution time 19.82 min), and at *m/z* 967.4 (Fragment D†(2), HPLC elution time 20.54 min). A side by side comparison of successive *N*-terminal fragment ions b_3 to b_5 and of successive *C*-terminal fragment ions y_4 to y_6 confirms the deamidation patterns described above. Because peptide deamidation at neutral pH is associated with the formation of α-Asp and β-Asp in a 1:3 ratio and α-Glu and γ-Glu in a 1:1.7 ratio,[1a-b] we propose that insulin chain B fragments B†(1) and (2), D†(1) and (2), and F†(1) and (2) are likely to consist of mixtures of geometric isomers. With respect to parent fragments B, D, and F, the MS/MS data consistently revealed preferential deamidation of Gln4 over Asn3. This result was initially unexpected, in light of the fact that the majority of literature reports have maintained that asparaginyl residues are more susceptible to hydrolytic deamidation under neutral conditions.[2] Notwithstanding, deamidation rates are influenced by primary, secondary, tertiary, and quaternary protein structures.[3] Consistent with our results, glutamine deamidation has been shown to be accelerated by flanking carboxyl side histidine residues (i.e., His5 in oxidized bovine insulin chain B).[4]

Zirconium(IV)-assisted lactamization. In order to further substantiate that Zr^{IV} is capable of promoting lactamization in the presence of 4,13-diaza-18-crown-6, a total of 2 mM of glutamate was reacted in the presence of 20 mM of the azacrown ether, with and without 10 mM of $ZrCl_4$. After 24 h of treatment at pH 7.0 and 60 °C, significant conversion of Glu (*m/z* 146.4) to *pyro*Glu (*m/z* 128.5) was observed in the reaction containing Zr^{IV}/4,13-diaza-18-crown-6, and not in the reaction in which Zr^{IV} was substituted by an equivalent volume of water (Figure 2.8.).

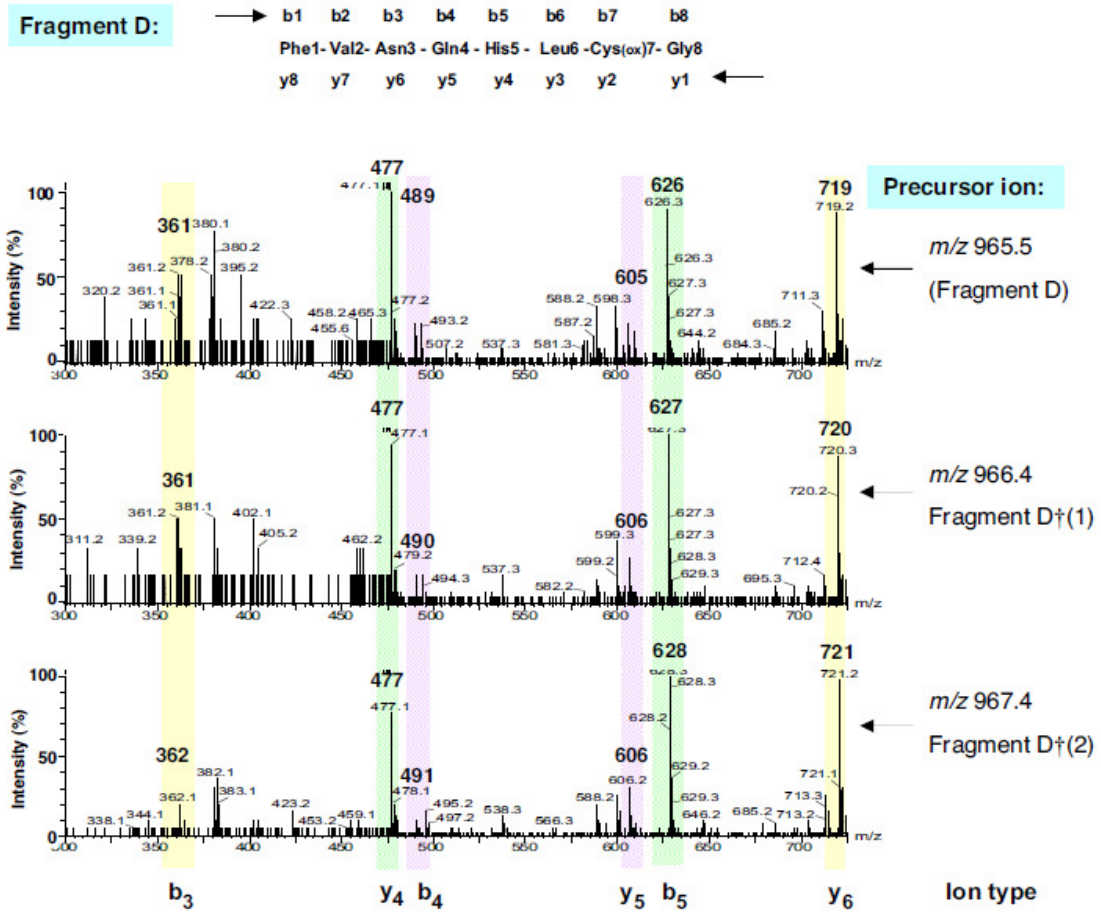

Figure 2.7. Comparison of MS/MS spectra for Fragment D: Phe1-Gly8 and deamidation products. A total of 500 µM of oxidized bovine insulin chain B was treated with 10 mM $ZrCl_4$ in 20 mM 4,13-diaza-18-crown-6 for t = 8 h at pH 7.0 and 60 °C. The MS/MS spectra show N-terminal b-ions and C-terminal y-ions generated from *m/z* 965.5 (Fragment D: Phe1-Gly8), from m/z 966.4 (Fragment D‡(1): Gln4 in D converted to Glu4) and from *m/z* 967.4 (Fragment D‡(2): Asn3 and Gln4 in D converted to Asp3 and Glu4). The *m/z* values in bold are rounded to the nearest Da. The spectra were acquired in positive ion mode.

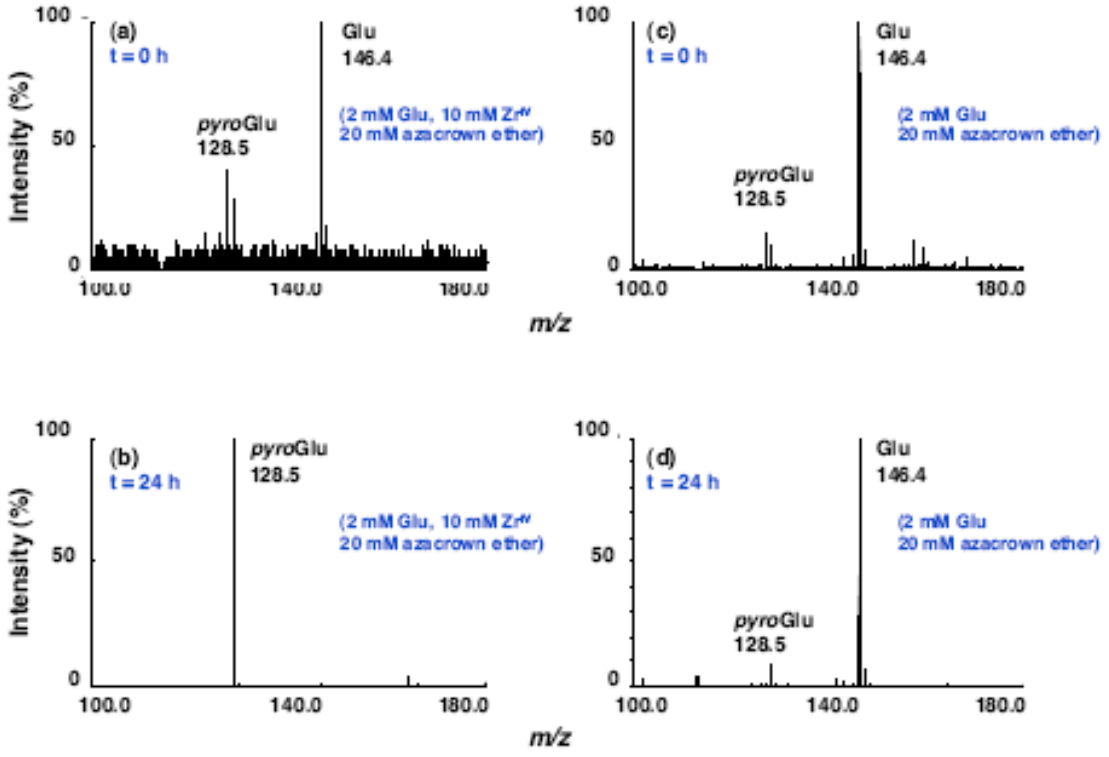

Figure 2.8. ESI mass spectra of glutamate treated at pH 7.0 and 60 °C. (a) & (b): A total of 2 mM of Glu was reacted with 10 mM of $ZrCl_4$ in the presence of 20 mM 4,13-diaza-18-crown-6 for 0 h and 24 h, respectively. (c) & (d): A total of 2 mM of Glu in 20 mM 4,13-diaza-18-crown-6 was treated for 0 h and 24 h, respectively (no $ZrCl_4$). "Glu" identifies glutamate; "*pyro*Glu" identifies pyroglutamate. The spectra were acquired in negative ion mode.

Table 2.1. HPLC-ESI-MS analysis of peptides observed after oxidized bovine insulin chain B was reacted in the presence of $ZrCl_4$ and 4,13-diaza-18-crown-6 (pH 7.0 and 60 °C)

Peak assignment	Elution time (min)	Relative abundance HPLC (%)		*m/z* singly charged peptide		*m/z* doubly charged		*m/z* triply charged	
		t = 4h	t = 8h	obsd	calcd	obsd	calcd	obsd	calcd
A: Phe1 to Ala30	33.82	100	100	*no*	3494.7	1747.8	1747.8	1165.5*	1165.6
B: Phe1 to Cys(SO_3H)$_7$	18.36	11	50	908.3*	908.4	454.6	454.7	*no*	303.5
B†(1): Gln4→Glu4	19.73	2	3	909.3*	909.4	455.1	455.2	*no*	303.8
B†(2): Asn3→Asp3, Gln4→Glu4	20.46	2	3	910.3*	910.4	455.6	455.7	*no*	304.1
C: Gly8 to Ala30	31.70	12	7	*no*	2605.3	1303.0	1303.1	869.1*	869.1
D: Phe1 to Gly8	18.50	11	50	965.5*	965.4	483.2*	483.2	322.7	322.5
D†(1): Gln4→Glu4	19.82	2	3	966.4*	966.4	483.6	483.7	*no*	322.5
D†(2): Asn3→Asp3, Gln4→Glu4	20.54	2	3	967.4*	967.4	484.2	484.2	*no*	323.1
E: Ser9 to Ala30	31.70	12	7	*no*	2548.3	1274.5	1274.6	850.0*	850.1
F: Phe1 to Ser9	18.74	11	50	1052.5*	1052.5	526.7	526.7	351.7	351.5
F†(1): Gln4→Glu4	19.99	2	3	1053.4*	1053.4	527.2	527.2	*no*	351.8
F†(2): Asn3→Asp3, Gln4→Glu4	20.67	2	3	1054.4*	1054.4	527.7	527.7	*no*	352.1
G: His10 to Ala30	31.70	12	7	*no*	2461.2	1231.0*	1231.1	821.0	821.1
H: Phe1 to Cys(SO_3H)19	33.79	5	5	*no*	2241.0	1121.0	1121.0	748.0	747.7
I: Gly20 to Ala30	23.54	9	44	1272.5	1272.6	636.8*	636.8	424.8	424.9
J: Phe1 to Gly20	33.79	5	5	2298.2	2298.1	1149.4	1149.5	766.7*	766.7
K: Glu21 to Ala30	23.54	9	44	1215.5	1215.6	608.3*	608.3	405.8	405.9
K‡: Glu21→*pyro*(Glu21)	26.48	3	16	1197.5*	1197.6	599.3*	599.3	400.1	399.9
L: Phe1 to Leu6	17.00	6	15	756.4*	757.4	378.6	379.2	*no*	253.1
M: Leu6 to Tyr16	28.11	1	4	*no*	1252.6	627.9	626.8	418.5	418.2

[a](oxidized bovine insulin chain B)$_0$ = 0.5 mM; [$ZrCl_4$]$_0$ = 10 mM; [4,13-diaza-18-crown-6]$_0$ = 20 mM. Data were acquired over multiple trials. Representative HPLC chromatograms are in Figure 2.4, 2.5, and 2.6. of the accompanying manuscript. Peak assignments highlighted in blue correspond to apparent major peptide hydrolysis products. Peak assignments in red correspond to apparent intermediate peptide hydrolysis products. Peak assignments in green correspond to apparent trace peptide hydrolysis products. Not observed = *no*. "*" indicates that peak assignments were confirmed by ESI-MS/MS sequencing. "†" indicates deamidation of peptide: Asn3 to Asp3 and/or Gln4 to Glu4. "‡" indicates lactamization of *N*-terminal Glu21 to pyroglutamate21 (*pyro*Glu21).

Continued Table 2.1.: HPLC-ESI-MS analysis of peptides observed after oxidized bovine insulin chain B was reacted in the presence of $ZrCl_4$ and 4,13-diaza-18-crown-6 (pH 7.0 and 60 °C)

Peak assignment	Elution time (min)	Relative abundance HPLC (%)		*m/z* singly charged peptide		*m/z* doubly charged		*m/z* triply charged	
		t = 4h	t = 8h	obsd	calcd	obsd	calcd	obsd	calcd
N: Gly8 to Cys(SO_3H)19	29.70	1	1	1351.8	1351.7	676.3*	676.3	*no*	451.2
O: Gly8 to Gly20	29.82	3	4	1408.6	1408.7	704.8	704.8	470.2	470.2
P: Ser9 to Cys(SO_3H)19	30.39	1	*no*	1294.5	1294.6	647.7	647.8	432.5	432.2
Q: Ser9 to Gly20	28.11	1	1	1351.8	1351.7	676.3*	676.3	451.5	451.2
R: His10 to Cys(SO_3H)19	33.40	2	2	1207.7	1207.6	604.73	604.3	403.5	403.2
S: His10 to Gly20	27.90	1	1	1264.5	1264.6	632.8	632.8	422.5	422.2
T: His10 to Lys29	29.61	1	1	*no*	2390.2	1195.4	1195.6	797.4	797.4
U: Val2 to Ala30	33.51	1	1	*no*	3347.6	1674.3	1674.3	1116.4	1116.5
V: Leu11 to Ala30	33.79	1	1	*no*	2324.2	1162.5*	1162.6	775.4	775.4
W: Gly23 to Ala30	25.82	6	25	930.5*	930.5	465.6	465.7	*no*	310.8
X: Phe24 to Ala30	24.19	3	13	873.3*	873.4	437.1	437.1	*no*	291.8

[a](oxidized bovine insulin chain B)$_0$ = 0.5 mM; $[ZrCl_4]_0$ = 10 mM; [4,13-diaza-18-crown-6]$_0$ = 20 mM. Data were acquired over multiple trials. Representative HPLC chromatograms are in Figure 2.4, 2.5, and 2.6 of the accompanying manuscript. Peak assignments highlighted in blue correspond to apparent major peptide hydrolysis products. Peak assignments in red correspond to apparent intermediate peptide hydrolysis products. Peak assignments in green correspond to apparent trace peptide hydrolysis products. Not observed = *no*. "*" indicates that peak assignments were confirmed by ESI-MS/MS sequencing. "†" indicates deamidation of peptide: Asn3 to Asp3 and/or Gln4 to Glu4. "‡" indicates lactamization of *N*-terminal Glu21 to pyroglutamate21 (*pyro*Glu21).

Table 2.2. MALDI-TOF MS analysis of peptides observed after oxidized bovine insulin chain B was reacted for 4.2 h in the presence of $ZrCl_4$ and 4,13-diaza-18-crown-6 (pH 7.2 and 60 °C)

Peak assignment	Relative abundance MS (%)	m/z singly charged peptide		m/z doubly charged peptide	
	t = 4.2 h	obsd	calcd	obsd	calcd
A: Phe1 to Ala30	22	3494.65	3494.65	1747.81	1747.83
C: Gly8 to Ala30	18	2605.21	2605.28	*no*	1303.14
E: Ser9 to Ala30	54	2548.16	2548.26	*no*	1274.63
G: His10 to Ala30	21	2461.13	2461.22	*no*	1231.11
I: Gly20 to Ala30	30	1272.63	1272.64	*no*	636.82
K‡: (Glu21→*pyro*Glu21)	100	1197.60*	1197.61	*no*	599.31
M: Leu6 to Tyr16	1	1252.68	1252.59	*no*	626.80
T: His10 to Lys29	1	2390.12	2390.19	*no*	1195.60
U: Val2 to Ala30	3	3347.48	3347.58	*no*	1674.29
V: Leu11 to Ala30	1	2324.08	2324.16	*no*	1162.58

[a][oxidized bovine insulin chain B]$_0$ = 1 mM; [$ZrCl_4$]$_0$ = 10 mM; [4,13-diaza-18-crown-6]$_0$ = 20 mM. Data were acquired over multiple trials. Representative MALDI-TOF mass spectra are in Figure 2.3 of the accompanying manuscript. Peak assignments highlighted in blue correspond to apparent major peptide hydrolysis products. Peak assignments in red correspond to apparent intermediate peptide hydrolysis products. Peak assignments in green correspond to apparent trace peptide hydrolysis products. Not observed = *no*. "*" indicates that peak assignments were confirmed by ESI-MS/MS sequencing. "‡" indicates lactamization of *N*-terminal Glu21 to pyroglutamate21 (*pyro*Glu21).

References.

1 (a) S. Capasso, L. Mazzarella, F. Sica and A. Zagari, *Peptide Res.*, 1989, 2, 195;

(b) S. Capasso, L. Mazzarella, F. Sica and A. Zagari, *J. Chem. Soc., Chem. Commun.*, 1991, 1667.

2 A.B. Robinson, C.J. Rudd, *Curr. Top. Cell Regul.*, 1974, 8, 247.

3 N.E. Robinson, A.B. Robinson, *Proc. Natl. Acad. Sci U.S.A.*, 2001, 98, 4367.

4 N.E. Robinson, Z.W. Robinson, B.R. Robinson, A.L. Robinson, J.A. Robinson, M.L. Robinson, A.B. Robinson, *J. Peptide Res.*, 2004, 63, 426.

Epilogue.

Deamidation of a dipeptide by Zr^{IV} metal.

Deamidation results in the formation of glutamate from glutamine residues or aspartate from asparagine residues by hydrolysis. The deamidated products may also include geometric isomers such as *iso*-Glu and *iso*-Asp.[1a-b] In addition to Zr^{IV}, a number of metal ions, including Ce^{III}, Ce^{IV}, La^{III}, and Th^{IV}, are known to promote deamidation of glutamine to glutamate and of asparagines to aspartate.[2] As mentioned previously, side reaction of zirconium hydrolysis in our data is deamidation of Asn3 and/or Gln4 residues in those hydrolysis products of insulin chain B which contained the two residues including the products Phe1-Cys(SO_3H)7 (*m/z* 906), Phe1-Gly8 (*m/z* 965), and Phe1-Ser9 (*m/z* 1052). (Figure 2.1, Table 2.1) which all showed minor +1 and +2 Da analogs which were chromatographically separable by HPLC. The MS/MS spectra also contained some Asn- and Gln-containing fragments which had a +1 and +2 Da shift.

In order to confirm that Zr^{IV} promotes deamidation of glutamine in the presence of 4,13-diaza-18-crown-6, a total of 2 mM of the dipeptide GlyGln was reacted in the presence of 20 mM azacrown ether, with and without 10 mM of $ZrCl_4$ as shown in Figure 2.9. A similar

experiment was performed with the single amino acid Gln (data now shown). After 36 h of treatment at pH 7.0 and 60 °C, significant amounts of the hydrolyzed glutamine (*m/z* 147.1) was converted to the deamidated glutamate (*m/z* 148.1) product as observed in the reaction containing Zr^{IV} / 4,13-diaza-18-crown-6 and not in the reaction where Zr^{IV} was omitted. The absence of deamidated glutamine from the single amino acid glutamine indicates that internal peptide cleavage produces the deamidated product. Glutamine presumably deamidates through a glutarimide intermediate while asparagine deamidates through a succinimide intermediate.

References.

1 (a) S. Capasso, L. Mazzarella, F. Sica and A. Zagari, *Peptide Res.*, 1989, 2, 195;

(b) S. Capasso, L. Mazzarella, F. Sica and A. Zagari, *J. Chem. Soc., Chem. Commun.*, 1991, 1667.

2 E. Bamann, H. Trapmann and H. Muenstermann, *Arch. Pharm.*, 1963, 296, 47

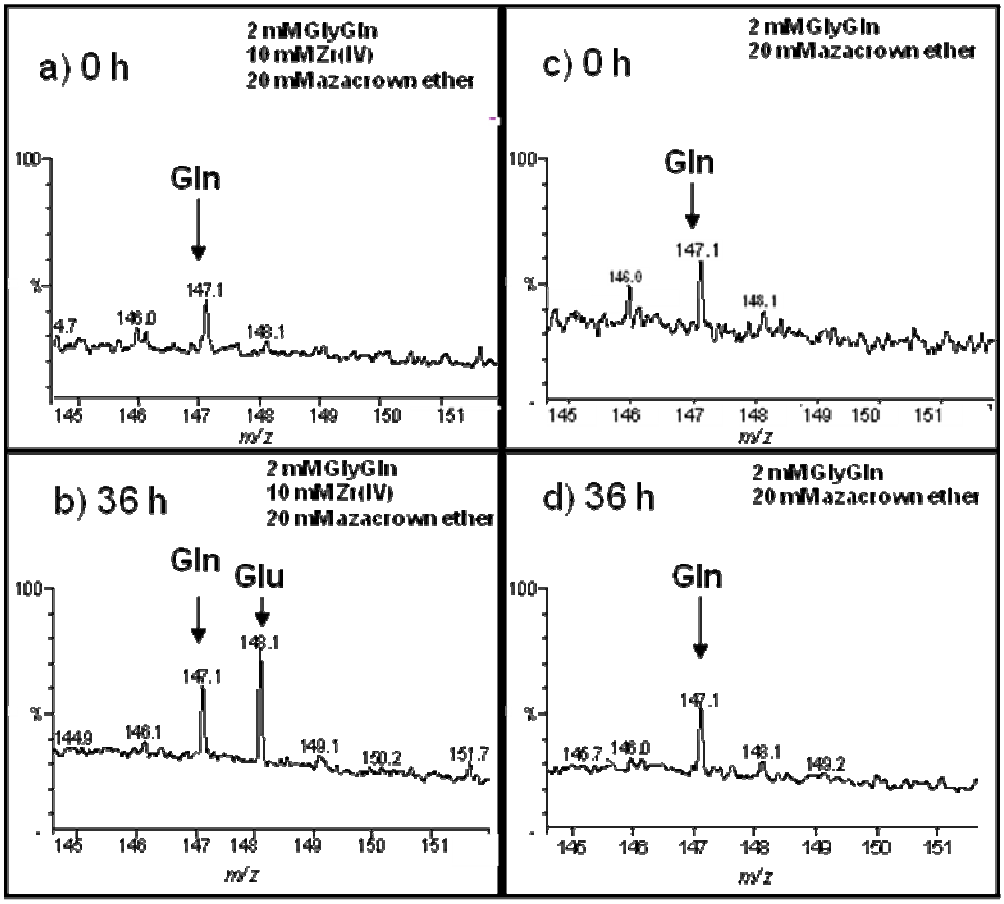

Figure 2.9. ESI mass spectra show deamidation of glutamine hydrolysis product to glutamate only in the presence of Zr^{IV} and azacrown ether (left). Spectra a) and b): 2 mM GlyGln was reacted with 10 mM Zr^{IV} and 20 mM azacrown ether for 0 h and 36 h, respectively (60 °C and pH 6.90). Spectra c) and d): 2 mM GlyGln was reacted with 20 mM azacrown ether (no metal) for 0 and 36 h, respectively (60 °C and pH 7.15). Spectra were acquired in positive ion mode.

CHAPTER III METAL-ASSISTED HYDROLYSIS OF SPHINGOMYELIN.

Abstract.

Niemann-Pick diseases types A and B are incurable lysosomal storage disorders caused by defective activity of the lysosomal enzyme acid sphingomyelinase, whose normal role is to hydrolyze the phospholipid sphingomyelin. In the severe phenotype A, there is a lethal build-up of sphingomyelin within the lysosomes of affected patients, with death by age 1 or 2 years.[1] We have demonstrated that Zr^{IV} complexes can hydrolyze the phosphate ester bond in sphingomyelin, and may possibly be developed as possible therapeutic tools in the treatment of Niemann-Pick disease, since Zr^{IV} complexes have the potential to mimic acid sphingomyelinase. Zr^{IV} hydrolysis of the phosphate ester bonds in sphingomyelin has been characterized by an assay that quantifies phosphocholine, which is the same proteolytic product produced by the active enzyme. Since the highest hydrolytic yields of DNA[2] and acetylated peptides[3] by Zr^{IV} is lysosomal pH 4.8 compared to cytosolic pH 7.0, we would like to develop phospholipid hydrolysis protocols to confirm that Zr^{IV} complexes hydrolyze sphingomyelin more efficiently at pH 4.8 and 37 °C than pH 7. We have found that Zr^{IV} in the presence of piperazine hydrolyzes sphingomyelin in good yields at 60 °C and pH 4.8 within 20 h. Since the amphiphilic sphingomyelin molecule exists physiologically in liposomes with bilayer structures, we have conducted Triton X-100 liposome-micelle transition studies and characterization protocols based on atomic force microscopy and UV-visible spectrophotometry to observe the effect of liposome solubilization. The effects of micelle formation by addition of Triton X-100 surfactant have been evaluated to increase the efficiency of metal-assisted phospholipid hydrolysis as a function of

temperature and pH. Also, the effect of membrane-bound cholesterol on hydrolysis yields has been investigated. We have demonstrated that zirconium hydrolyzes the phosphate ester bonds in two colorimetric assays which measure either free phosphate or phosphocholine/choline concentrations. Metals used by other researchers to hydrolyze unactivated amide and phosphate ester bonds [4-16] have been used to hydrolyze sphingomyelin for comparison to Zr^{IV}. These metals include Cu^{II}, Co^{II}, Ce^{IV}, Eu^{III}, Ni^{II}, Pd^{II}, La^{III}, Y^{III}, Yb^{III}, and Zn^{II}. For each metal, we have examined the increase in hydrolysis at lysosomal pH 4.8 compared to the cytosolic pH 7.0.

Introduction.

Metal-assisted hydrolysis of phospholipids.

Metals have been demonstrated to be effective reagents in the hydrolysis of the phosphate ester bond of substrates such as nucleic acids, synthetic phospholipids, and phosphorylated sugars. Metals, particularly lanthanide, actinides, rare earth, and tetravalent transition metals are excellent hydrolytic reagents because of their dual ability to neutralize the phosphate anionic charge and to provide a nucleophile using their deprotonated bound waters of hydration.[4-16] Figure 3.1 ranks the metals used in this study with their respective hydrolysis constants (pK_a) of the water-bound metal species. The tetravalent metal ions Ce^{IV}, Zr^{IV}, Hf^{IV}, and divalent Pd^{II} lower the pK_a of water from 15.7 to < 2 and, thereby, form metal-hydroxide species when dissolved in aqueous hydrolysis reactions at pH 4.8 or 7.[17-20] The metal ion zirconium(IV) has been found to efficiently hydrolyze amide bonds in peptides.[21] Zr^{IV} also hydrolyzes phosphate ester bonds in a synthetic *p*-nitrophenol activated phosphate ester.[7,9,10,11,13,15] According to these studies, cleavage levels were substantially increased when the reaction pH was changed from 7.0 to more acidic pH values in the range of 4.0-4.7, which is near the lysosomal pH of 4.8.

The metal-assisted hydrolysis of the phosphate ester bond of biological phospholipids involved in cell membrane structures is a novel approach to the development of therapeutic drugs for use in the incurable lysosomal storage disease of Niemann-Pick disease A and B. These disorders produce a lethal build-up of sphingomyelin in liver, spleen, and brain cells due to the defective lysosomal acid sphingomyelinase enzyme. Selected metals were used in the present study to represent a range of cellular toxicities, and selectivity toward the phosphate ester bond in synthetic phospholipids and human phospholipids.[7,11] The pH of the lysosomal interior is pH 4.8, and is thus considerably more acidic than the cytoplasm (pH 7.2). It is worthwhile to investigate the pH-dependent reactivities of metals to estimate the increase in metal-assisted hydrolytic cleavage of sphingomyelin in the lysosomes compared to cytosol. Zr^{IV} is of particular interest due to its low cellular toxicity and lack of natural metalloenzyme activity interference in humans.[22a-o] The optimal hydrolysis of DNA and acetylated peptides by Zr^{IV} has been shown to be higher at (lysosomal) pH 4.8 than (cytosolic) pH 7.0.[2-3] Table 3.1 shows various pH values which are relevant to optimal Zr^{IV} activity and lysosomal pH. The lysosomal pH is not only the optimal pH of the acid sphingomyelinase enzyme which is defective in Niemann-Pick patients, but is also approaching the optimal pH of $ZrCl_4$ activity in the hydrolysis of acetylated Gly-Gly.[2] There is strong motivation to use Zr^{IV} and similar metals as therapeutic agents to target disease-related, lysosomal phospholipids such as sphingomyelin.

Sphingomyelin.

Sphingomyelin is a major phospholipid in animal plasma membranes and predominates in the human brain, the myelin sheath of nerve cell axons, and in erythrocytes. It consists of a phosphate group, sphingosine, choline, and an N-acyl linked fatty acid. The fatty acid content of sphingosine and the N-acyl linked fatty acid varies, but palmitic (16:0), stearic (18:0) and

nervonic acids (24:1) are the most abundant in humans. Approximately 60 % of the fatty acids of of the sphingomyelin of the grey matter of the human brain consist of stearic acid (18:0) while 60 % of the corresponding sphingomyelin in the white brain matter consist of lignoceric (24:0) and nervonic (24:1) acids. Human sphingomyelin interdisperses with phosphatidylcholine and cholesterol in the exoplasmic layer of the plasma membrane lipid bilayer. The fatty acids which predominate in sphingomyelin of plasma membranes are more saturated than phosphatidylcholine. The sphingosine-bound fatty acid is typically longer than the N-acyl linked fatty acid moiety which introduces length assymetry.[23-24] Figure 3.2 shows the structure of sphingomyelin along with two possible hydrolysis products of phosphocholine and choline. Figure 3.3 shows the structures of piperazine and HEPES which are the buffers used in the hydrolysis reactions described in this dissertation since their pK_a values corresponded to lysosomal pH 4.8 or to cytosolic pH 7, respectively. Figure 3.4 shows the polar and nonpolar regions of sphingomyelin along with the two possible metal-assisted hydrolytic pathways which produce either phosphocholine or choline. Sphingomyelin is capable of both intra- and inter-molecular bonding. The amide group's nitrogen and the hydroxyl on the sphingosine moiety are hydrogen donor sites, while the amide carbonyl oxygen provides a hydrogen acceptor site. Intramolecular bonding occurs between the free hydroxyl on the sphingosine base and the phosphate ester oxygen. Intermolecular bonding arises from van der Waals forces between the hydrocarbon chains and cholesterol which associates with sphingomyelin in membranes. The intermolecular bonding is decreased in the case of the *trans* double bond in the nervonic acid fatty acid. The configuration of human sphingomyelin is the enantiomerically pure form of D-*erythro* with two chiral centers formed by the sphingosine free hydroxyl (C3) and the amide NH_2 (C2) groups in the 2S, 3R configuration.

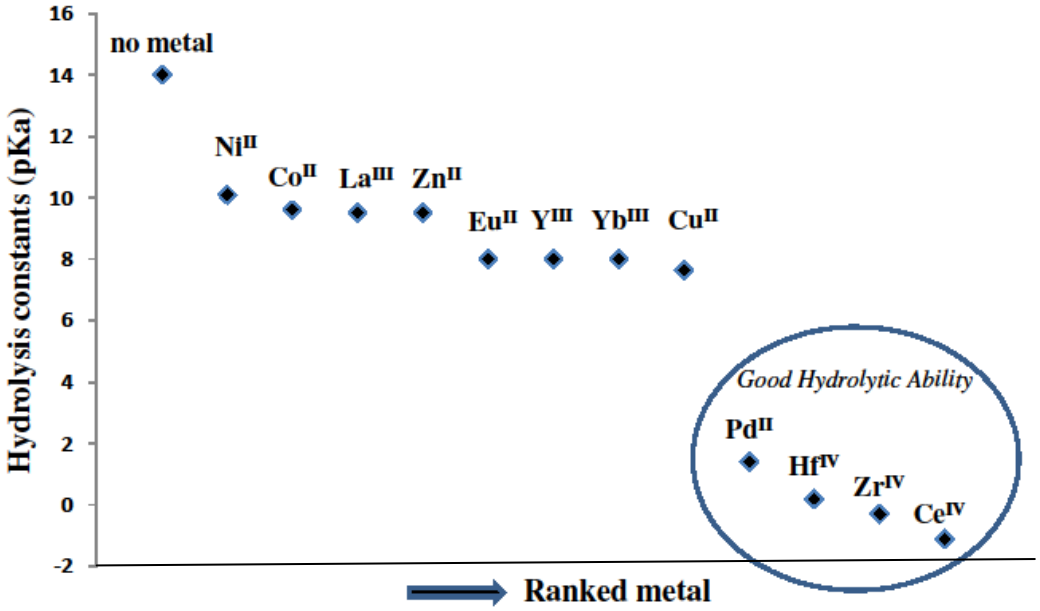

Figure 3.1. Deprotonation of the waters of hydration on selected metal ions. Encircled metals demonstrate the highest hydrolysis yields in metal-assisted hydrolysis of phospholipids as discussed in this chapter.The pK_a data were taken from *Metal Ions in Solution*, 1978, p. 356 by John Burgess.[17]

Table 3.1. The correlation of biological pH values to optimal pH of Zr^{IV}-assisted hydrolysis.

Cellular location or experiment	**Optimal pH**
Lysosome	pH 4.8
Cytosol	pH 7.2
Optimal activity of acid sphingomyelinase	pH 4.8 (inactive at pH 7.0)
Maximum reactivity of 20 mM $ZrCl_4$ hydrolysis of DNA at 20 °C [2]	pH 4.0
Optimal activity of Zr^{IV}-assisted hydrolysis of AcGG at 37 °C, 45 °C, and 60 °C [3]	pH 4.4

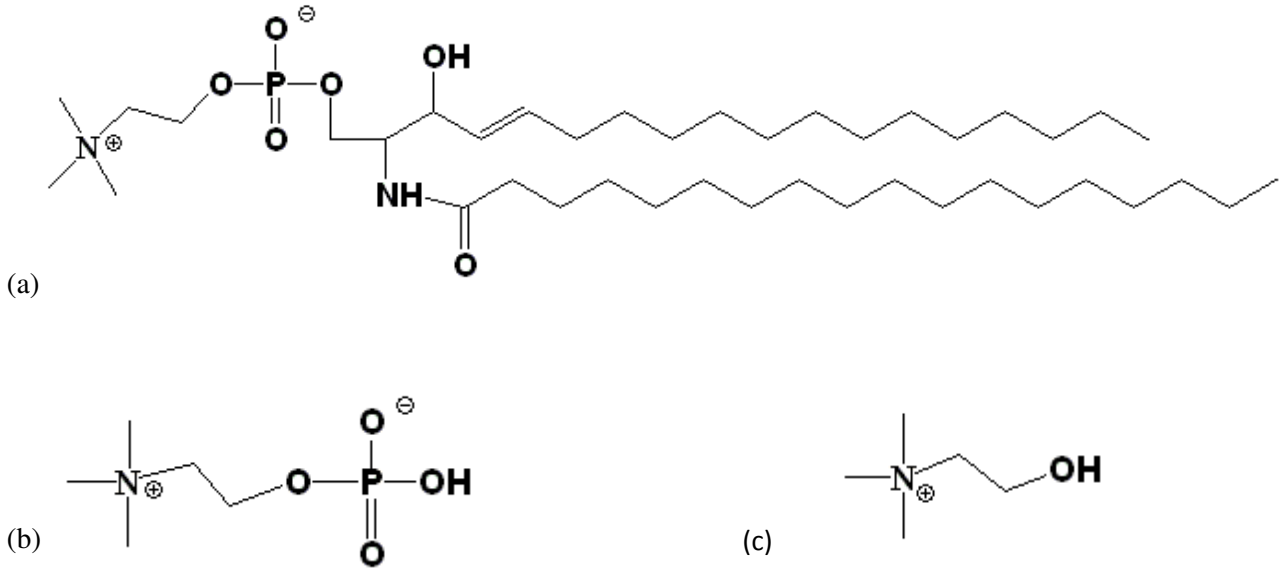

Figure 3.2. (a) Structure of sphingomyelin; (b) structure of phosphocholine; (c) structure of choline.

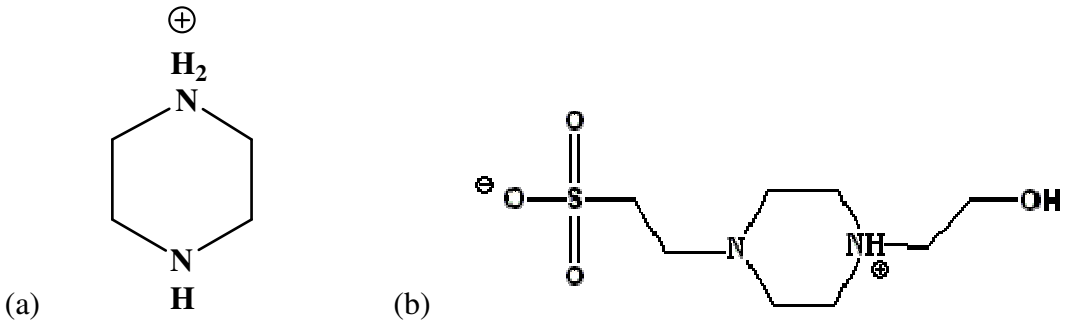

Figure 3.3. The molecular structures of the buffers used in our hydrolysis experiments: (a) piperazine (lysosomal pH 4.8); (b) HEPES (cytosolic pH 7). The piperazine and HEPES structures show the protonation site responsible for the pKa values.[40]

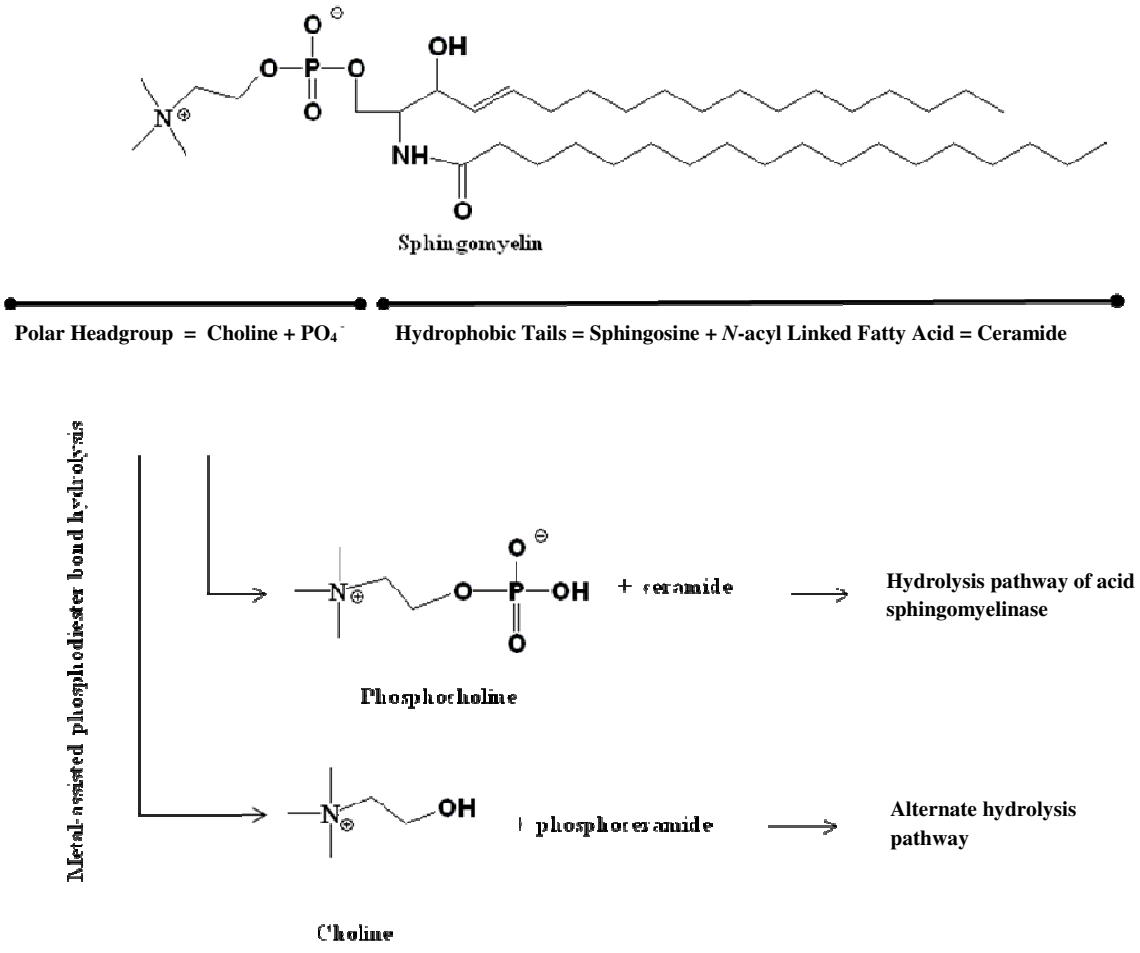

Figure 3.4. Diagram of the metal-assisted phosphate ester bond hydrolysis of sphingomyelin to either phosphocholine or choline products. The sphingomyelin structure contains a polar headgroup and a non-polar hydrophobic tail.

The acyl chain composition of sphingomyelin determines the gel to liquid-crystalline phase transition temperature and the enthalpy of transition. The gel to liquid-crystalline phase transition for pure sphingomyelin is the physiological temperature of 37 °C. The transition temperature is governed by phosphocholine head group repulsion and hydrocarbon chain packing. [23-31]

Cholesterol is closely associated with sphingomyelin in amounts up to 45 mol % in normal cell membranes, but accumulates to a much higher percentage in Niemann-Pick diseased cells. It controls membrane fluidity by restricting acyl chain motion and reduces permeability of the membrane. The cholesterol molecule consists of a polar hydroxyl group which hydrogen bonds with the polar head of sphingomyelin and a nonpolar sterol center and a hydrocarbon chain of 7 carbons which are embedded in the nonpolar fatty acid tails of the inner sphingomyelin bilayer.[23-24] The addition of 30 mol % of cholesterol to sphingomyelin eliminates the gel-to-liquid crystalline phase transition.[28] Cholesterol also increases the detergent resistance of sphingomyelin in plasma membranes.[27]

In normal cells, sphingomyelin exists physiologically as liposomes. However, the speciation of sphingomyelin in Niemann-Pick disease is unknown. Therefore, the incorporation of Triton X-100 to solubilize the normal vesicle structures was undertaken. Triton X-100 is a nonionic surfactant commonly used to solubilize phospholipid vesicles in many studies in order to induce a transition from vesicles to micelles with intermediate mixed populations.[*32a-k*] Figure 3.5 shows the transition envisioned by Lopez et al.[*32f*] with five stages: pure vesicles, enlarged vesicles with interdispersed Triton X-100, saturated bilayered vesicles plus detached micelles for a mixed population, a predominate micellar population with few saturated bilayers, and, finally, a population consisting of exclusively micelles with sphingomyelin interdispersed with Triton X-100.

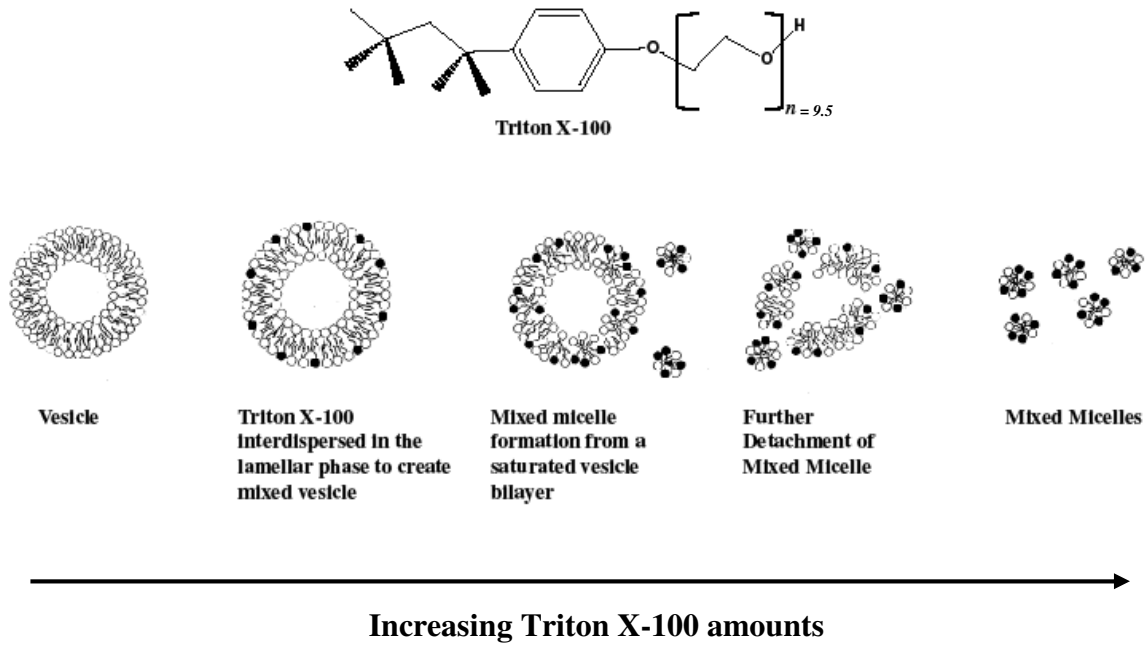

Figure 3.5. Schematic of Triton X-100 induced phospholipid vesicle to micelle transition, *Lopez et al, FEBS Letters, 1998*,[32f] shown along with the structure of Triton X-100. The ethylene oxide units have n = 9.5 according to manufacturer label.

In the *in vivo* enzymatic reaction of acid sphingomylinase, the hydrolysis of sphingomyelin occurs at the phosphate ester bond between the phosphocholine and sphingosine to release phosphocholine and a ceramide as shown in Figure 3.4. In order for metal-assisted hydrolysis to mimic the enzyme, the metal will be oxophilic and a hard Lewis acid in order toactivate the phosphate ester bond. Ideally as an enzyme mimic, the hydrolysis reaction should be regioselective and cleave only one side of the phosphate ester. Tetravalent metals such as Zr^{IV}, Ce^{IV}, and Hf^{IV} are oxophilic with high charge density and, as we show, are capable of hydrolyzing the phosphate ester bond of sphingomyelin to yield a phosphocholine and a ceramide. If the metals lack regioselectivity, the hydrolysis will produce a choline and phosphoceramide.

Niemann-Pick disease.

Niemann-Pick disease (NPD)[33a-i] is an incurable, autosomal recessive, lysosomal storage disorder with two phenotypes *A* and *B*. Type A primarily affects Ashkenazic Jews with infant mortality while type B affects other diverse ethnic groups with middle age mortality. The NPD forms A and B result from over 18 mutations on the acid sphingomyelinase gene in chromosome 11, and both types A and B are associated with very low acid sphingomyelinase activity compared to the wild type. Approximately 80 % of NPD patients are Type A. The majority of the Type A patients of European Jewish ancestry have a 1:90 type A gene carrier rate and 1:30,000 physical disease occurrence. The defective enzyme acid sphingomyelinase has only 1-3% normal activity in type A while type B has 10-60 % of normal enzyme activity, and both result in fatal accumulation of sphingomyelin in the lysosomes. Based on the autopsies of Niemann-Pick patients in several studies, sphingomyelin accumulated in the spleen is 15 - 99 μmol of sphingomyelin per g of wet tissue compared to the control spleens at 2 - 4 μmol per g of

wet tissue.[33a-b] The affected organs in type A are the spleen, lymph nodes' monocyte-macrophage system, liver, kidneys, brain, and lung, while type B has similar patterns except for a lack of accumulation in the brain. Cholesterol also builds up in the lysosomes, most probably due to the interdispersion of cholesterol with sphingomyelin in the periplasmic membrane. Enzyme replacement and chemical chaperones have had limited therapeutic success in treating Niemann-Pick patients.[33a-i] A novel therapeutic cure based on Zr^{IV}-assisted phospholipid hydrolysis is the concept developed in this dissertation. This approach would serve to decrease this fatal accumulation of sphingomyelin in NPD patients. Since Zr^{IV} is redox-inactive and possesses low cellular toxicity, a Zr^{IV} complex which efficiently hydrolyzes sphingomyelin at the same hydrolytic bonds and pH values as the acid sphingomyelinase enzyme may function as an enzymatic mimic.

Methods.

Purchases.

All metals were purchased from Sigma-Aldrich and all had a purity of 99.999% except for potassium tetrachloropalladate(II) (K_2PdCl_4) and europium(III) chloride hexahydrate ($EuCl_3$-$6H_2O$) (99.99%), hafnium(IV) tetrachloride ($HfCl_4$) (98%), and bis(cyclopentidienyl) zirconocene(IV) dichloride ($C_{10}H_{10}Cl_2Zr$) (>98%). Metal hydrolytic activity was assayed on vesicles composed of pure sphingomyelin without and with cholesterol. Porcine brain sphingomyelin was purchased from Avanti Polar Lipids (860062P) and was used without further purification. The sphingomyelin has a reported gel-liquid transition temperature at ca. 35 °C and is a heterogeneous mixture of 18:0 stearic acid (49%), 24:1 nervonic acid (20%), and 31% various (16:0, 20:0, 22:0, 24:0, and other) fatty acid composition.[34] Observed MALDI mass peaks of the sodium adducts at *m/z* 753 and *m/z* 835 correlate to the stearic and nervonic fatty

acid content. Triton X-100 solution (93443) was purchased from Fluka BioChemika. HEPES sodium salt (H7006) was purchased from Sigma-Aldrich, and piperazine anhydrous buffer (80621) was purchased from Fluka. Cholesterol (C8667) was purchased from Sigma in 99% purity.

Metal-assisted hydrolysis.

The sphingomyelin liposomes were prepared by sonication as follows. The sphingomyelin was dissolved in chloroform. This solution was evaporated overnight to produce a dry film followed by 2 h of drying under vacuum. For cholesterol experiments, the dried sphingomyelin and cholesterol were dissolved together in chloroform and the solution evaporated by the same protocol. The dried sphingomyelin was hydrated to a concentration of 100 mM in pre-heated doubly-deionized H_2O at 55 °C, a temperature that is above the gel-liquid crystal transition temperature of sphingomyelin. The aqueous suspension was placed in a water bath and sonicated for 30 min (45 min for cholesterol experiments) to produce a milky suspension with a high surface tension. These liposomes are assumed by definition to be small, unilamellar vesicles (SUVs) and were later examined by atomic force microscopy (AFM).

Hydrolysis reactions of liposomes prepared from the stock sphingomyelin solution in 1000 µl volumes contained a final concentration of 2 mM sphingomyelin, 10 mM metal and 20 mM piperazine (pH 4.8) or HEPES (pH 7) buffer. The metals included period 4, 5, and 6 metals $Ce(NH_4)_2(NO_3)_6$, $ZrCl_4$, $HfCl_4$, K_2PdCl_4, $CuCl_2$-$2H_2O$, $ZnCl_2$, $CoCl_2$-H_2O, $NiCl_2$-$6H_2O$, $EuCl_3$-$6H_2O$, $LaCl_3$-H_2O, YCl_3-$6H_2O$, and $YbCl_3$-$6H_2O$. The metal and the buffer were premixed and pH-adjusted to 4.8 or 7.0 with HCl or NaOH prior to adding to the final volume of the diluted aqueous sphingomyelin stock solution. For solutions containing surfactant, the Triton X-100 was vortexed with the aqueous sonicated sphingomyelin solution at 25 °C and pre-equilibrated for at

least 30 minutes prior to the dilution and metal/buffer addition. The final Triton X-100 concentrations were either 0, 2, or 16 mM. Individual reactions were placed on an Eppendorf Thermomixer R preheated to 60 °C or 37 °C for 20 h at 500 rpm.

Malachite green assay and turbidity.

A Quantichrom Phosphate Assay™ (Bioassay Systems, Inc.) was used to detect free inorganic phosphate. A Shimadzu UV-1601 UV-visible spectrophotometer was used to record the absorbance at 620 nm with total acquisition in the 1100-300 nm range.[39] The inorganic phosphate is released as a secondary cleavage product after sequential hydrolysis of both sphingomyelin phosphate ester bonds. This assay utilizes the complexation of molybdate and phosphate ions to form a heteropolyphosphomolybdate complex which is subsequently bound by the dye malachite green.[39] The malachite green assay utilized 25 μL for Zr^{IV} (3 μL for Ce^{IV} samples) samples, 142 μL for Zr^{IV} (164 μL for Ce^{IV}) H_2O, and 333 μL malachite green assay reagent for a total volume of 500 μL. The solutions were vortexed after each addition, and spectrally analyzed after 30 min. Positive controls of phosphocholine and choline that were prepared and reacted with similar metal/buffer concentrations at 60 °C for 20 h were used to determine statistical accuracy of the assay.

In order to correct for background levels of inorganic phosphate, the absorbance differences at both 0 h and 20 h for all of the metal reactions and for parallel control reaction ions run in the absence of metal were measured. Histograms were developed by subtracting the absorbance difference (20 h – 0 h) in the absence of metal from the absorbance difference (20 h – 0 h) in the presence of metal to yield a background-subtracted absorbance difference that represents phosphate released only from the metal-assisted reaction.

Standard curves.

A series of solutions of increasing phosphate concentration and a constant 10 mM metal and 20 mM buffer concentrations as the assayed hydrolysis samples were prepared in the absence of Triton X-100 in order to quantify the malachite green assay results and assess experimental metal interference with the molybdenum-phosphate-malachite green assay. Parallel non-metal control phosphate standards containing only 20 mM buffer were also measured. Solutions of 100 mM metal and 200 mM piperazine or HEPES buffer were prepared and mixed 1:1 v/v. The premixed 1:1 metal/buffer solution was pH-adjusted to either 4.8 or 7.0 with either HCl or NaOH and heated at 60 °C for 20 h. The dilution of 25 μL of a typical hydrolysis reaction sample to 500 μL total volume in a malachite green assay represents a 20-fold dilution of the sample so the diluted standards were prepared with similar metal/buffer concentrations as the diluted hydrolysis sample. The 30 μM phosphate stock solution was included in the Quantichrom Phosphate Assay™ kit from which a total of 9 different phosphate concentrations were prepared in the range of 0-11 μM at a total volume of 500 μL each. The amount of 30 μM phosphate stock solution, premixed 1:1 metal/buffer solution to give a final solution of 0.5 mM metal/1 mM buffer concentration, doubly-deionized water were mixed first followed by addition of 333 μl malachite green reagent. The total volume was mixed thoroughly and allowed to equilibrate for 30 minutes. In summary, the final concentrations of the standard solutions for all metals except cerium(IV) were 0, 1, 3, 5, 7, 8, 9, 10, 11 μM of inorganic phosphate in 0.5 mM metal, and 1 mM buffer in a total volume of 500 μL with two exceptions in the highest standards of 10 and 11 μM which each had 507 μL and 538 μL volumes. The two highest phosphate standards had a higher total volume (> 500 μL) in order to maintain the same malachite green reagent amount in all standard solutions. An example of a 5 μM phosphate standard would be prepared from 84 μL

of the 30 μM phosphate stock solution, 5 μL of the 1:1 metal/buffer solution, 78 μL doubly-deionized water, and 333 μL malachite green reagent for a total volume of 500 μL. The cerium standards were prepared with similar procedures except the 1:1 metal/buffer solutions were diluted 10-fold, i.e. 5 mM cerium(IV) metal ion concentration and 10 mM buffer concentration at this step, in water prior to addition to each standard because of the greater dilution of cerium reaction samples, e.g. 3 μL reaction sample instead of 25 μL diluted to 500 μL which is a 166.7-fold dilution. The final metal and buffer concentrations in the cerium(IV) samples were 60 μM cerium(IV) metal ion and 120 μM buffer. The standards prepared for the non-metal control samples were prepared with the 30 μL stock phosphate solution, 200 mM buffer (final buffer concentration in standard is 1 mM), doubly-deionized water, and malachite green reagent for a total volume of 500 μL. The standards were analyzed on a Shimadzu UV-1601 instrument in the 1100-300 nm range. The slope equations were determined from phosphate concentration plotted against absorbance at 620 nm and yielded linear slopes with correlation coefficients of $r = 0.999$.

Turbidity measurements were conducted on the liposomes to gain additional insight into the vesicle to micelle transition. Solubilization with Triton X-100 was measured as a decrease in turbidity of the sphingomyelin vesicle suspensions at 500 nm absorbance. Turbidity was measured on 2 mM sphingomyelin in piperazine buffer at pH 4.8 without metal with increasing amounts of Triton X-100 (0-100 mM) on a Shimadzu UV-1601 spectrophotometer with acquisition in the range of 1100-300 nm. Data absorbance at 500 nm was plotted.

Phosphocholine and choline quantification.

Phosphocholine and choline hydrolysis products were quantified with an Amplex® Red Sphingomyelinase Assay kit (Invitrogen-Molecular Probes™) which uses a multi-enzyme reaction series to produce H_2O_2 that reacts with the sensitive colorimetric Amplex® Red

reagent.[35] All enzymes were prepared according to the kit's instructions and the two-step sphingomyelinase assay described in the kit was used since the lysosomal pH samples were in the acidic pH range. Figure 3.6 illustrates the conversion of the phosphocholine and/or choline substrates to a detectable product. The alkaline phosphatase enzyme converts phosphocholine to choline which is subsequently converted by choline oxidase to betaine and H_2O_2. The H_2O_2 substrate in the presence of horseradish peroxidase reacts with Amplex® Red reagent to produce a red solution which was analyzed with a Shimadzu UV-1601 UV-visible spectrophotometer in the acquisition range 300-1100 nm with the absorbance at 570 nm recorded for quantification calculations. Since both phosphocholine and choline were possible hydrolytic products, the results yielded the total phosphocholine and choline products from the hydrolysis reactions. In order to distinguish the phosphocholine yields from the choline yields in the mixture, a novel adaptation of the assay was developed by preparation of a parallel, multi-enzymatic reaction series where the alkaline phosphatase enzyme was omitted to prevent any phosphocholine hydrolysis product from being enzymatically converted to choline.

Dual sets of phosphocholine or choline standards were prepared for quantification of the enzyme mixes with and without the alkaline phosphatase, respectively. The stock solutions of phosphocholine and choline from which the standards were directly prepared were 100 mM concentration serially diluted in 100 mM Tris buffer, pH 8, to a substock concentration of 1 mM phosphocholine or choline in 100 mM Tris buffer with no metal or hydrolysis reaction buffer. Many reaction samples were diluted 10-fold for the Amplex® Red assay so the phosphocholine and choline standards were prepared with 1 mM metal and 2 mM buffer final concentrations. The metal and piperazine or HEPES stock solution was prepared with a concentration of 100 mM and 200 mM, respectively, and premixed in a 1:1 v/v solution with pH adjustment to pH 4.8

or 7 depending on the experiment. The 1:1 premixed metal/buffer solutions were heated at 60 °C for 20 h. Amounts of the 1 mM phosphocholine or choline substock solution, 20 μL of the 1:1 metal/buffer mix, and 100 mM Tris buffer, pH 8, were mixed for final phosphocholine or choline concentrations of 0.005, 0.01, 0.02, 0.05, 0.08, 0.1, and 0.2 mM with a final metal/buffer concentration of 1 mM metal and 2 mM buffer in a total volume of 1000 μL for each standard. Each set included seven standards in the concentration range of 0 - 0.2 mM substrate and produced slope equations with correlation coefficients of ≥ 0.99 in the 0 - 0.1 mM linear range of the slope. Amounts of these phosphocholine and choline standard sets were later mixed with the enzyme mix which is described below.

The enzyme mix stock solution components were prepared according to the kit's protocols. The final enzyme mix for the total phosphocholine plus choline quantification included 100 μL horseradish peroxidase solution, 100 μL choline oxidase solution, 200 μL alkaline phosphatase solution, 100 μL Amplex® Red reagent solution, and 9.5 mL of 100 mM Tris-HCl, pH 8.0. For the final enzyme mix for the choline-only assay, the amount of alkaline phosphatase was substituted with an equivalent volume of 100 mM Tris-HCl, pH 8. The enzyme mixes were used immediately without storage of the remaining, unused enzyme mix.

For the final assay sample preparations prior to the 37 °C incubation step, the following protocol was performed. The hydrolysis reaction samples were diluted between 10 to 50-fold with 100 mM Tris buffer, pH 8, in order to have absorbances in the linear standard range. For the final, enzymatic sample preparation using the Amplex® Red enzyme mixture, 50 μL of diluted reaction sample or standard solution was mixed with 100 μL of either of the two enzyme mixes described above containing horseradish peroxidase, choline oxidase, and alkaline phosphatase, and the Amplex® Red reagent. A second set of samples were prepared with the non-alkaline

phosphatase enzyme mix for the choline-only quantification. Enzyme controls were prepared with an equivalent amount of doubly-deionized water plus enzyme mix. The solutions were gently stirred and placed in a 37 °C incubator for one hour. After one hour, the vials were placed in the freezer to quench the enzymatic reactions. Immediately prior to analysis, 400 µL of doubly-deionized water was added to each 150 µL sample, vortexed, and placed in a cuvette for spectral acquisition. All data was acquired within hours of the sample preparation. All assays were performed on the same day as the completion of the 20 h hydrolysis reactions.

Positive controls of phosphocholine and choline were prepared in a similar procedure as the metal-assisted sphingomyelin reaction samples. Stock solutions of 55.82 mM phosphocholine or 75.08 mM choline were prepared along with 100 mM metal and 200 mM piperazine or HEPES buffer solutions. The metal and buffer were premixed in a 1:1 v/v solution, and the pH was adjusted to pH 4.8 or 7 with HCl or NaOH. All positive control samples were prepared with no Triton X-100 addition. The final concentrations of the metal-assisted phosphocholine or choline reaction samples were 1.12 mM and 1.49 mM, respectively, in 10 mM metal and 20 mM buffer concentrations. Positive controls of phosphocholine and choline were heated at 60 °C for 20 h similar to the hydrolyzed sphingomyelin reactions. The hydrolyzed samples were diluted 50-fold in 100 mM Tris buffer, pH 8 prior to the Amplex® Red assay to a final concentration of 22.4 µM original phosphocholine or 29.8 µM original choline in 100 mM Tris buffer, pH 8 with diluted metal and buffer concentrations of 200 µM metal and 400 µM buffer. A total of 50 µL of each of the diluted positive control reaction samples was added to 100 µL of either of the two enzyme mixes containing the Amplex® Red reagent and treated as described in the previous paragraph.

For the phosphate determinations, the positive control samples of phosphocholine and choline were prepared according to the metal used in the hydrolysis reaction. If the sample was hydrolyzed with zirconium(IV) metal, then 25 μL volumes of the 1.12 mM phosphocholine or 1.49 mM choline metal-assisted samples were added to 142 μL of doubly-deionized water and vortexed. If the sample was hydrolyzed with cerium(IV) metal, then 3 μL of the 1.12 mM phosphocholine or 1.49 mM choline metal-assisted samples were added to 164 μL doubly-deionized water and vortexed. Next, 333 μL of the malachite green reagent was added to the diluted sample mix (all metals) and vortexed. The green colorimetric solution developed for 30 minutes. Afterwards, the entire 500 μL volume was pipetted into a cuvette and spectrally analyzed over the wavelength range of 300-1100 nm and the absorbances at 620 nm were recorded.

Hydrogen peroxide positive controls were provided in the kit with the specific concentration on the label which was ~ 3 %. Only new, unopened vials were used for the controls since the hydrogen peroxide degrades quickly. Based on the precise concentration indicated on the vial, e.g., precisely 3.3%, a 20 mM working solution of H_2O_2 was prepared by dilution in doubly-deionized water. A second serial 10-fold dilution of this 20 mM H_2O_2 was prepared by dilution with doubly-deionized water for a final substock solution of 0.22 mM H_2O_2. From this substock solution, three different concentrations of 0.02, 0.04, and 0.06 mM were prepared and analyzed by either the total phosphocholine plus choline or the modified choline-only protocols described above with 50 μL hydrogen peroxide samples and 100 μL enzyme mix with 1 h incubation at 37 °C.

Atomic force microscopy.

Atomic force microscopy (AFM) was used to study the liposome preparations with various amounts of Triton X-100 to determine the size and shape of the pure and solubilized vesicles. Sphingomyelin vesicle suspensions equilibrated with 0, 2, or 16 mM Triton X-100 were imaged by AFM as follows. Aliquots of 10 μL were dried on mica substrates overnight and imaged by a Veeco Multi Mode V instrumentation at a rate of 2.5 μM/s. Imaged data was reviewed with Thermomicroscope SPMLab NT Ver. 5.01 software. The data included the image, histograms, and cross-sectional views from selected areas of the image. The histograms recorded the number of Z-heights from the probe to the nm-μm height range.

Results and discussion.

Liposome solubilization and turbidity.

Solubilization of liposomes by a detergent such as Triton X-100 provides a good model for the solubilization of cell membranes. Triton X-100 is a nonionic detergent that has been used to study the ability of surfactants to alter phospholipid bilayer structures with subsequent conversion from vesicle to mixed micelle or pure micelle populations. Triton X-100 causes a surfactant-dependent increase in phospholipid vesicle size as confirmed directly by light scattering and indirectly by an increase in turbidity of sphingomyelin preparations.[32f] A gradual increase in size with increasing Triton X-100 concentration and incorporation or interdigitation as noted by electron micrographs was observed parallel to the increase in turbidity in several studies.[32a,c] In these studies, turbidity was measured by recording the absorbance at 500 nm. The turbidity curve in Figure 3.7 shows the millimolar concentrations of Triton X-100 and the sphingomyelin lipid : Triton X-100 molar ratio as plotted against the absorbance at 500 nm. The liposomal sizes affect the transmittance of the beam as reflected an increase or reduction in

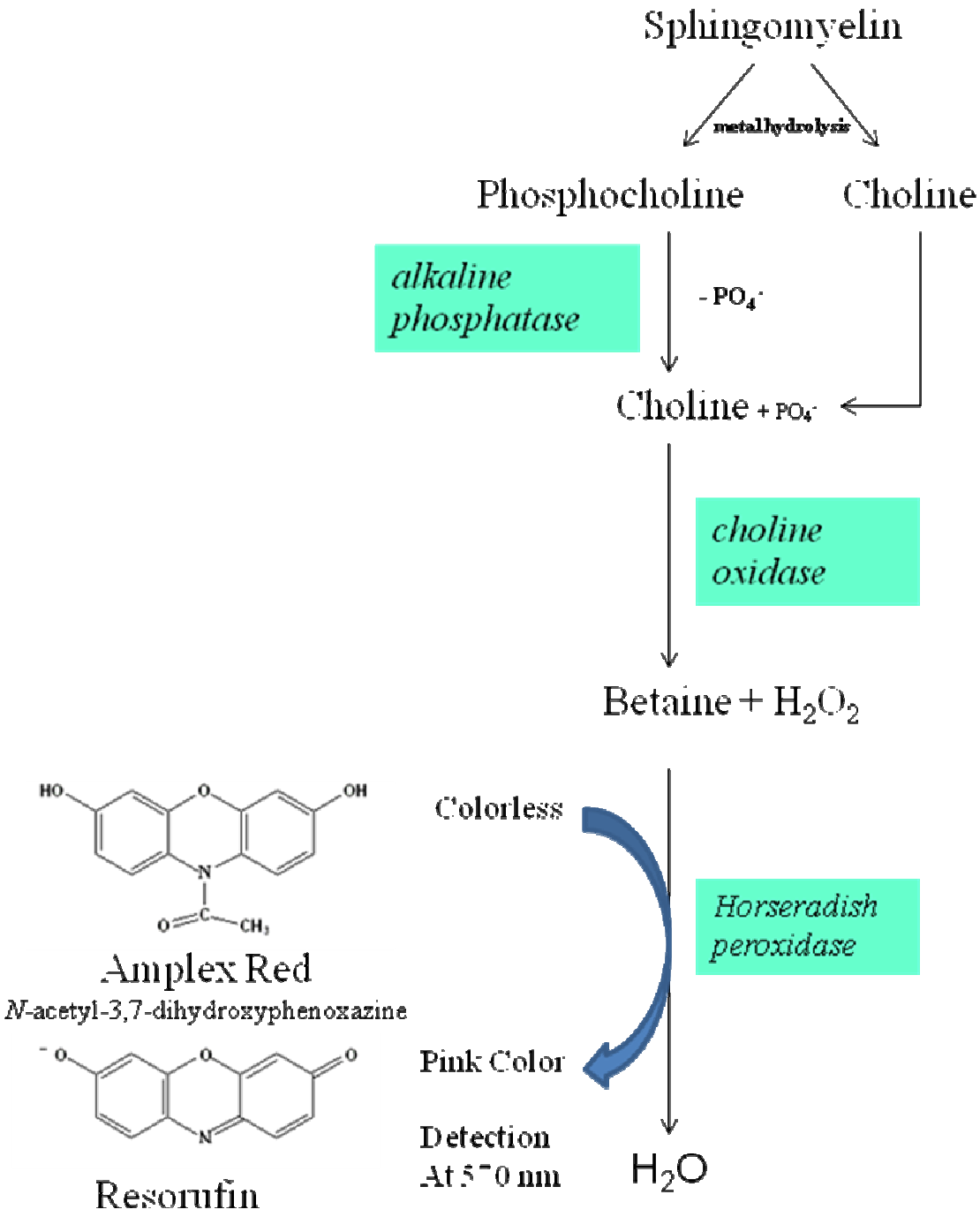

Figure 3.6. Molecular Probes™ Amplex® Red sphingomyelinase assay: detection of choline and phosphocholine products released upon metal-assisted hydrolysis of sphingomyelin.[35]

absorbance at 500 nm. The graphs show an increase in turbidity in the Triton X-100 range of 1-3 mM (less than 1: 2 phospholipid: Triton X-100 ratio) with a sharp decline in the turbidity with higher (> 3 mM) Triton X-100 concentrations. The sample appearance correspondingly changed from cloudy to transparent over this concentration range.

These trends are postulated to correspond to the incorporation of Triton X-100 into the vesicle structures with a resulting increase in size, and thus turbidity (1-3 mM Triton X-100 range of the curve) while the regionof negligible absorbance levels correspond to micelle formation (≥ 5 mM Triton X-100).According to Figure 3.5, the incorporation of Triton X-100 involves several stages of vesicle incorporation of Triton X-100 with accompanying increase in size and turbidity until saturation followed by subsequent transformation into breakaway micelles with decreased size and turbidity. The Triton X-100 concentrations of 0, 2, and 16 mM used in the hydrolysis represent distinctly different liposomal populations with pure vesicles (0 mM), mixed vesicle/micelle (2 mM), and pure micelles (16 mM). When cholesterol is added in 50 mol % of sphingomyelin, the turbidity pattern in Figure 3.8 shows an initial increase in turbidity which increases slightly over the entire Triton X-100 concentration range of 5-100 mM. Cholesterol increases resistance of sphingomyelin to solubilization as evidenced by the increased turbidity even at very high Triton X-100 amounts.[32j] Tighter packing of sphingomyelin's fatty acid chains, which is induced by cholesterol, has been attributed to this resistance to detergent solubility.[27] Additionally, cholesterol is hydrophobic and will aggregate in solution. The persistent increase in turbidity of the sphingomyelin liposomes prepared with 50 mol % cholesterol over the entire Triton X-100 concentration range is consistent with the observed solution cloudy appearance compared to solutions without cholesterol which become clear (decrease in turbidity) with Triton X-100 concentrations ≥ 5 mM.

Table 3.2. shows a summary of vesicle categories from various literature sources [23,24,34] where vesicle size ranges are provided for each category. The small unilamellar vesicles category (SUV) has a range of 15-30 nm and is typical of sonicated vesicle preparations; the rarely-used intermediate unilamellar vesicle category ranges from 100-200 nm; the large unilamellar vesicle category (LUV) ranges from 60-500 nm and is used frequently to describe extruded liposome preparations. These ranges will be used to compare with the Z-heights (approximation of the actual vesicle diameters) obtained by AFM images of the sphingomyelin preparation vesicles.

Atomic force microscopy imagery.

AFM measures surface topography of soft solids including phospholipid vesicle bilayers at nanomolar resolution. In this technique, the piezoelectric force between the probe tip and the surface is quantitated and processed to display an image.[36a-d] Figure 3.9 shows a representative image of a pure sphingomyelin vesicle preparation (0 mM Triton X-100). In Figure 3.9 (a), the 1D image shows distinct, round particles which can correspond to small, unilamellar vesicles with a mean Z-height of 40 ± 12 nm. From this Z-height, the diameter of 40 nm is classified as SUV. The histogram for this image shows a medium distribution. For comparison, Figure 3.9 (b) shows pure phosphatidylcholine vesicles prepared by aqueous sonication from a dried lipid film prepared by Leonenko et al.[36b] to demonstrate the similarity in vesicle shape for two phospholipids. The average diameter in that study was 22 ± 2 nm. Vesicles prepared by bath sonication typically produce SUVs.[34]

The vesicles prepared with 2 mM and 16 mM Triton X-100 revealed anomalous images (data not shown). The 2 mM Triton X-100 solubilized vesicles featured two distinct image types which may explain the larger standard deviations in the hydrolysis yield data associated with this

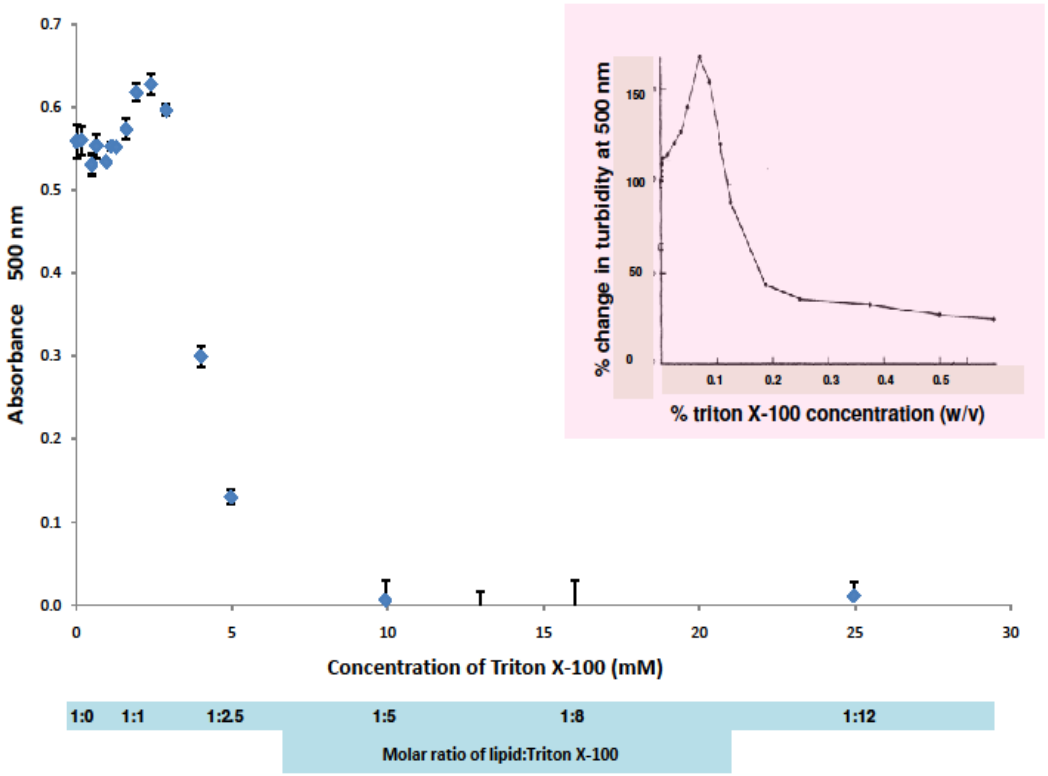

Figure 3.7. Graph shows the turbidity measurements of the vesicle to micelle transition of 2 mM sphingomyelin in 20 mM piperazine buffer with 0 - 25 mM Triton X-100. The x-axis is the concentration of Triton X-100 and the lower axis shows the molar ratio of lipid: Triton X-100. The y-axis is the absorbance at 500 nm. The inset shows similar results with egg yolk lecithin-dicetylphosphate vesicles taken from Alonso, Villena, Goñi, *FEBS Lett*., 1981.[32c] The number of trials = 4.

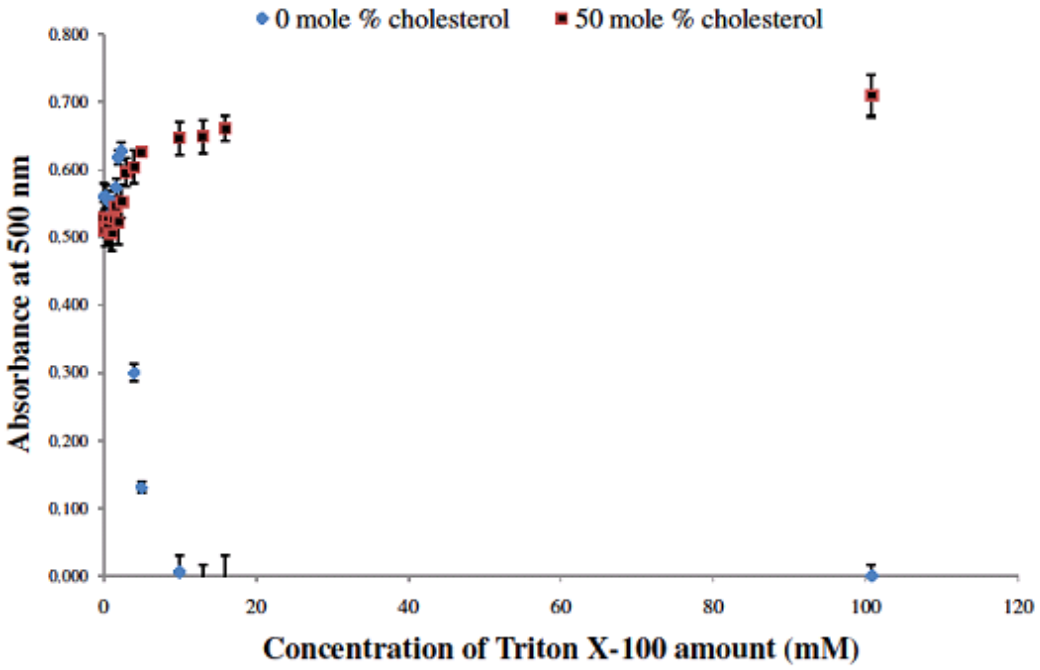

Figure 3.8. Comparison of turbidity for sphingomyelin without and with (0, 50 mole %) cholesterol. Graph shows a comparison of the data shown in Figure 3.7 with the turbidity measurements of 2 mM sphingomyelin in 20 mM piperazine buffer and 1 mM cholesterol with 0 - 100 mM Triton X-100 addition.

Table 3.2. Summary of vesicle size categories from literature sources.*

Liposome Category	**Diameter size range** [24]	**Diameter size range** [23]	**Diameter size range** [34]
Small unilamellar vesicles (SUV)	25 nm	22 - 50 nm	15 - 30 nm
Intermediate-sized unilamellar vesicle (IUV)	100 - 200 nm	*nd*	*nd*
Large unilamellar vesicle (LUV)	500 nm	>60 nm	100 - 200

**nd = not determined*

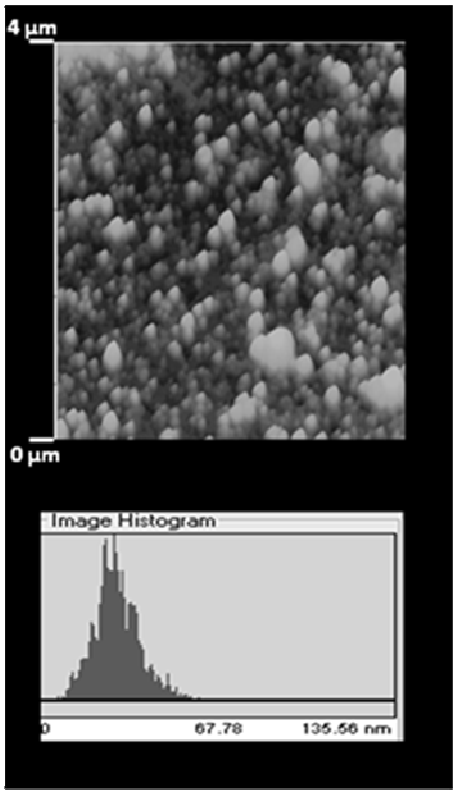

Pure SUV sphingomyelin vesicles

Z-height (avg ± SD, n) : 40 ± 12 nm, 12

(a)

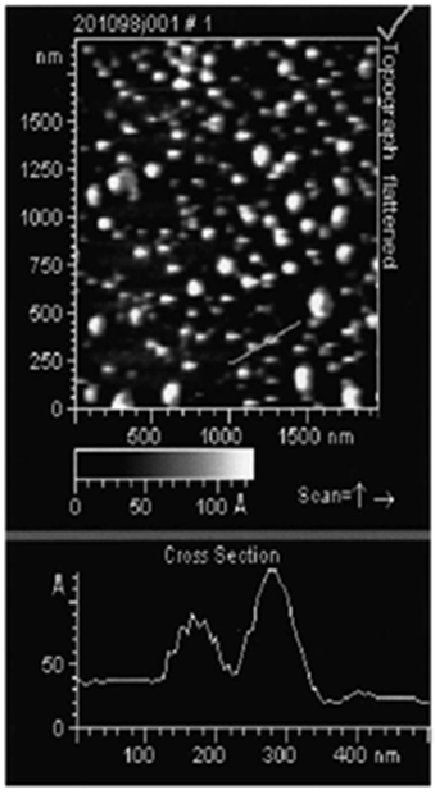

Pure phosphatidylcholine vesicles

Diameter (avg ± SD, n) : 22 ± 2 nm, 12

Z.V. Leonenko et al., Biochimica et Biophysica Acta, 2000.

(b)

Figure 3.9. Comparison of the AFM images of (a) the pure sphingomyelin from this study compared to (b) an image of pure phosphatidylcholine vesicles taken from Z.V. Leonenko, A. Cornini, D.T.Cramb, *Biochimica et Biophysica Acta* (2000).[36b] Both vesicles were prepared by sonication technique from dry film. The Z-height in (a) is approximated as the vesicle diameter.

detergent concentration. The vesicle preparation with 16 mM Triton X-100 amount produced an image with a regular clustered molecular array of non-rounded particles. Close observation of the image revealed stacked round particles which may correspond to clustered micelles.

The Triton X-100 evidently solubilizes the vesicles to produce non-uniform and uniform shape distributions. The images of vesicles prepared with experimental levels of metal and buffer are unavailable due to the difficulty in acquiring data on AFM samples with high salt content, e.g., cerium(IV) ammonium nitrate.

Phosphate determination of metal-assisted hydrolysis of pure sphingomyelin at 60 °C.

A panel of twelve, bi-, tri-, and tetravalent metals metals were each tested for their comparative abilities to hydrolyze the phosphate ester bond of pure and Triton X-100 solubilized sphingomyelin vesicles to release phosphocholine and/or choline products. Following this hydrolytic cleavage, the released product may undergo secondary cleavage of the remaining mono-phosphate bond which occurs at a much lower rate as evidenced by the low hydrolysis percentages quantified by the inorganic phosphate assay. The multiple trials of the metal-assisted hydrolysis of sphingomyelin preparations at 60 °C were assayed for inorganic phosphate concentrations at μmolar levels. The data for each metal is plotted in Figure 3.10 as a 3D histogram and listed in Table 3.3. The histogram shows a comparison of the percent hydrolysis by each metal at pH 4.8 and pH 7 (x-axis) as a function of increasing amounts of Triton X-100 (z-axis), and the percent of phosphate released by metal-assisted hydrolysis (y-axis). The inset in Figure 3.10 shows the results obtained with Ce^{IV} since the percentage of phosphate released was significantly higher in comparison to the other metals.

The ranked metals according to their hydrolytic ability are $Ce^{IV} > > Zr^{IV} > Hf^{IV} \geq Pd^{II} >$ all other divalent and trivalent metals. This ranking correlates with the order of hydrolysis

constants in Figure 3.1 especially for Ce^{IV}, Zr^{IV}, Hf^{IV}, and Pd^{II} where the ability to form a metal-OH nucleophile is best facilitated at low pH values. The pH 4.8 data for Zr^{IV} and Hf^{IV} show similar trends with 0 mM < 2 mM < 16 mM Triton X-100 which may indicate a Triton X-100-solubilization dependency. The solubilization of a vesicle which has ~40 % of its headgroups inside the vesicle would expose a larger amount in the micelle structure where all polar headgroups are exposed. The phosphate concentration data at pH 4.8 for Ce^{IV} show a different order of 0 mM < 16 mM < 2 mM. A 2 mM Triton X-100-solubilized vesicle has more exposed headgroups because of reduced Columbic repulsion from Triton X-100 interdigitation than the pure sphingomyelin vesicle where the polar headgroups are closer. For Ce^{IV}, Zr^{IV}, and Hf^{IV}, hydrolysis is considerably enhanced at pH 4.8 compared to pH 7. Pd^{II}-assisted hydrolysis is the exception with favorable hydrolysis at pH 7 compared to pH 4.8. Metal speciation may be a factor affecting the Pd^{II} data. For the Ce^{IV}, Zr^{IV}, and Hf^{IV} metals, the phosphate yields at pH 7 shows less Triton X-100 dependency, with the hydrolysis percentages at 2 mM and 16 mM having similar yields. The phosphate hydrolysis yields as percentages of the twelve metals are listed in Table 3.3. The highest yields per metal are 70.7 ± 7.1% for Ce^{IV} (2 mM Triton X-100, pH 4.72) > 11.3 ± 2.2% for Zr^{IV} (16 mM Triton X-100, pH 4.87) > 2.21 ± 0.25% for Hf^{IV} (16 mM, pH 4.85), and 2.49 ± 0.55% for Pd^{II} (2 mM, pH 6.98). Because the highest yields are from Zr^{IV}, Ce^{IV}, and Hf^{IV}, these metal ions would be used in further hydrolysis reactions to be analyzed by the Amplex® Red assay which quantitates the hydrolysis products of phosphocholine and choline. Notwithstanding, the malachite green data showed that Ce^{IV} produced the highest hydrolysis yields of the 12 tested metals. For Ce^{IV}, hydrolysis yields at pH 4.8 were statistically higher than hydrolysis yields at pH 7.0, at all Triton X-100 concentrations,

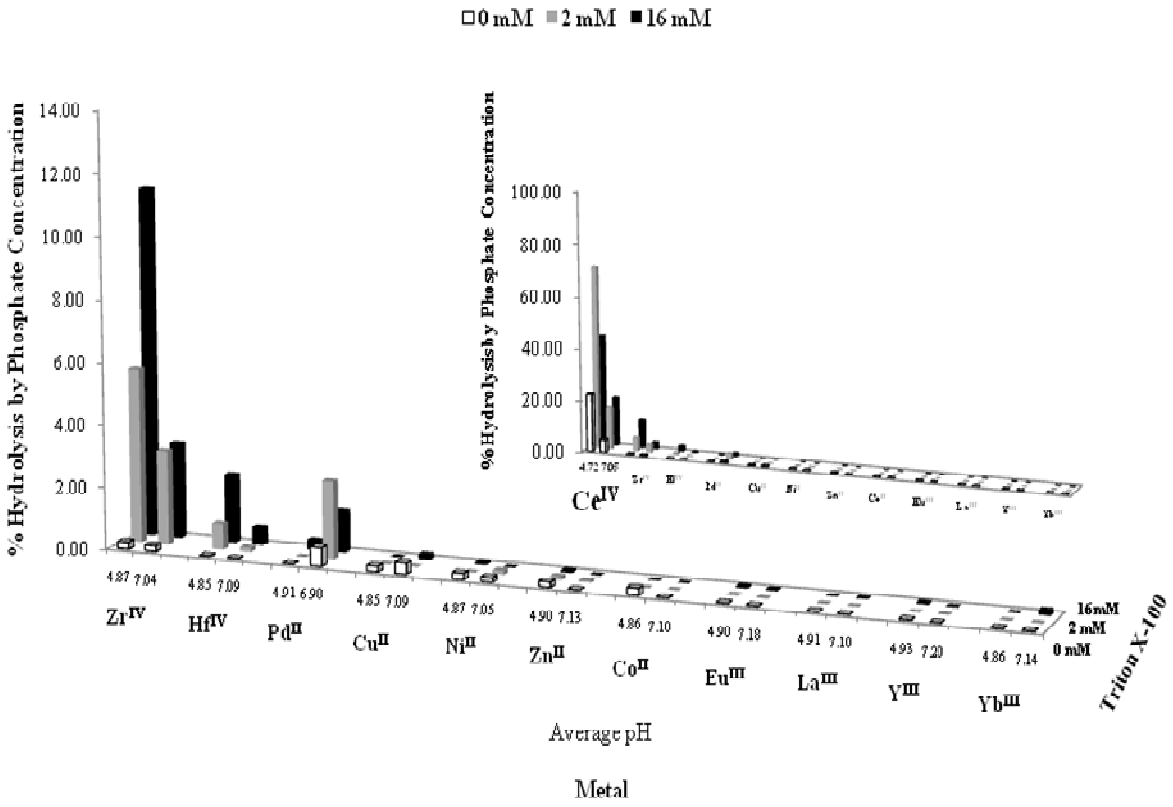

Figure 3.10. The 3D graph with inset ranks the percentage of hydrolysis by various metals as measured by the inorganic phosphate release. Solutions were prepared from 2 mM sphingomyelin, 10 mM metal, 20 mM piperazine (pH 4.8) or HEPES (pH 7.0), and reacted for 20 h, at 60 °C. Phosphate levels were determined by the malachite green assay. The inset shows the Ce^{IV} data with the other metals since the Ce^{IV} hydrolysis percentages were much higher.

Table 3.3. Summary of the twelve metals according to the inorganic phosphate quantification (μM) for 2 mM sphingomyelin reacted with 10 mM metal at pH 4.8 or pH 7 and 60 °C for 20 h.

Metal	Avg. pH	Avg. phosphate concentration (μM) ± SD (% hydrolysis ± SD)			*n*
		0 mM Triton X-100	**2 mM Triton X-100**	**16 mM Triton X-100**	
Ce^{IV}	4.72	444 ± 100 (22.2 ± 5.4)	1413 ±140 (70.7 ± 7.1)	861 ± 130 (43.0 ± 6.8)	13-15
	7.05	102 ± 39 (5.08 ± 1.9)	332 ± 91 (16.6 ± 4.6)	380 ± 70 (19.0 ± 3.5)	11-12
Zr^{IV}	4.87	4.36 ± 4.4 (0.22 ± 0.20)	112 ± 44 (5.62 ± 2.2)	226 ± 43.1 (11.3 ± 2.2)	18-19
	7.04	3.68 ± 4.2 (0.18 ± 0.2)	60.5 ± 28 (3.03± 1.4)	61.8 ± 25 (3.09 ± 1.2)	15-18
Hf^{IV}	4.85	0.21 ± 1.3 (0.01 ± 0.05)	16.9 ± 3.7 (0.85 ± 0.2)	44.1 ± 5.0 (2.21± 0.3)	6
	7.09	0.13 ± 0.8 (0.01 ± 0.05)	2.74 ± 2.9 (0.14± 0.2)	11.6 ± 3.8 (0.58 ± 0.2)	5-7
Pd^{II}	4.91	-1.05 ± 2.6 (-0.05 ± 0.1)	-3.16 ± 5.0 (-0.16 ± 0.2)	6.32 ± 3.7 (0.32 ± 0.2)	2
	6.98	12.0 ± 1.2 (0.60 ± 0.05)	50.0 ± 11 (2.49 ± 0.6)	27.2 ± 4.7 (1.36 ± 0.2)	2
Cu^{II}	4.85	3.41 ± 1.2 (0.17 ± 0.05)	0.24 ± 2.7 (0.01 ± 0.1)	-0.24 ± 0.7 (-0.01 ± 0.05)	2
	7.09	7.16 ± 9.1 (0.36±0.5)	-0.25 ± 5.7 (-0.01± 0.3)	3.46 ± 2.2 (0.17 ± 0.1)	2
Ni^{II}	4.87	3.86 ± 4.6 (0.19±0.2)	-0.48 ± 2.6 (-0.02 ± 0.1)	1.69 ± 1.0 (0.08 ± 0.05)	2
	7.05	2.65 ± 6.0 (0.13± 0.3)	2.65 ± 1.0 (0.13 ± 0.05)	-0.96 ± 2.7 (-0.05 ± 0.13)	2
Zn^{II}	4.90	3.40 ± 3.4 (0.17± 0.2)	2.20 ± 5.2 (0.11 ± 0.3)	1.40 ± 2.2 (0.07 ± 0.10)	2
	7.13	-0.20 ± 0.8 (-0.01± 0.05)	1.22 ± 4.3 (0.06 ± 0.2)	-1.22 ± 0.82 (-0.06 ± 0.04)	2
Co^{II}	4.86	4.42 ± 1.5 (0.22 ± 0.1)	-0.42 ± 3.6 (-0.02 ± 0.2)	-1.89 ± 0.84 (-0.09 ± 0.04)	2
	7.10	-2.71 ± 0.6 (-0.14 ± 0.05)	0.00 ± 1.5 (0.00 ± 0.1)	-0.21 ± 0.21 (-0.01 ± 0.01)	2
Eu^{III}	4.90	-1.56 ± 1.8 (-0.08 ± 0.1)	0.44 ± 4.7 (0.02 ± 0.2)	1.33 ± 0.9 (0.07 ± 0.04)	2
	7.18	-3.83 ± 0.9 (-0.19 ± 0.05)	-4.04 ±1.3 (-0.20 ± 0.05)	0.85 ± 1.9 (0.04 ± 0.1)	2

n = number of trials for both pH values

Continued Table 3.3.: Summary of the twelve metals according to the inorganic phosphate quantification (μM) for 2 mM sphingomyelin reacted with 10 mM metal at pH 4.8 or pH 7 and 60 °C for 20 h.

Metal	**Avg. pH**	**Avg. phosphate concentration (μM) ± SD (% hydrolysis ± SD)**			***n***
		0 mM Triton X-100	**2 mM Triton X-100**	**16 mM Triton X-100**	
La^{III}	4.91	-7.16 ± 0.0 (-0.36 ± 0.0)	-1.26 ± 0.8 (-0.06 ± 0.05)	-1.05 ± 1.5 (-0.05 ± 0.07)	2
	7.10	-4.01 ±1.5 (-0.20 ± 0.07)	-1.69 ± 1.1 (-0.08 ± 0.05)	0.42 ± 1.3 (0.02 ± 0.06)	2
Y^{III}	4.93	-1.01 ± 0.0 (-0.05 ± 0.0)	-0.20 ± 1.6 (-0.01 ± 0.08)	1.01 ± 0.0 (0.05 ± 0.0)	2
	7.20	-6.21 ± 0.8 (-0.31 ± 0.04)	-2.00 ± 1.8 (-0.10 ± 0.1)	0.20 ± 2.2 (0.01 ± 0.1)	2
Yb^{III}	4.86	-3.96 ± 1.7 (-0.20 ± 0.08)	-0.42 ± 0.2 (-0.02 ± 0.01)	-0.42 ± 0.4 (-0.02 ± 0.02)	2
	7.14	-2.13 ± 2.3 (-0.11 ± 0.1)	-2.13 ± 1.7 (-0.11± 0.1)	3.19 ± 0.85 (0.16 ± 0.04)	2

n = number of trials for both pH values

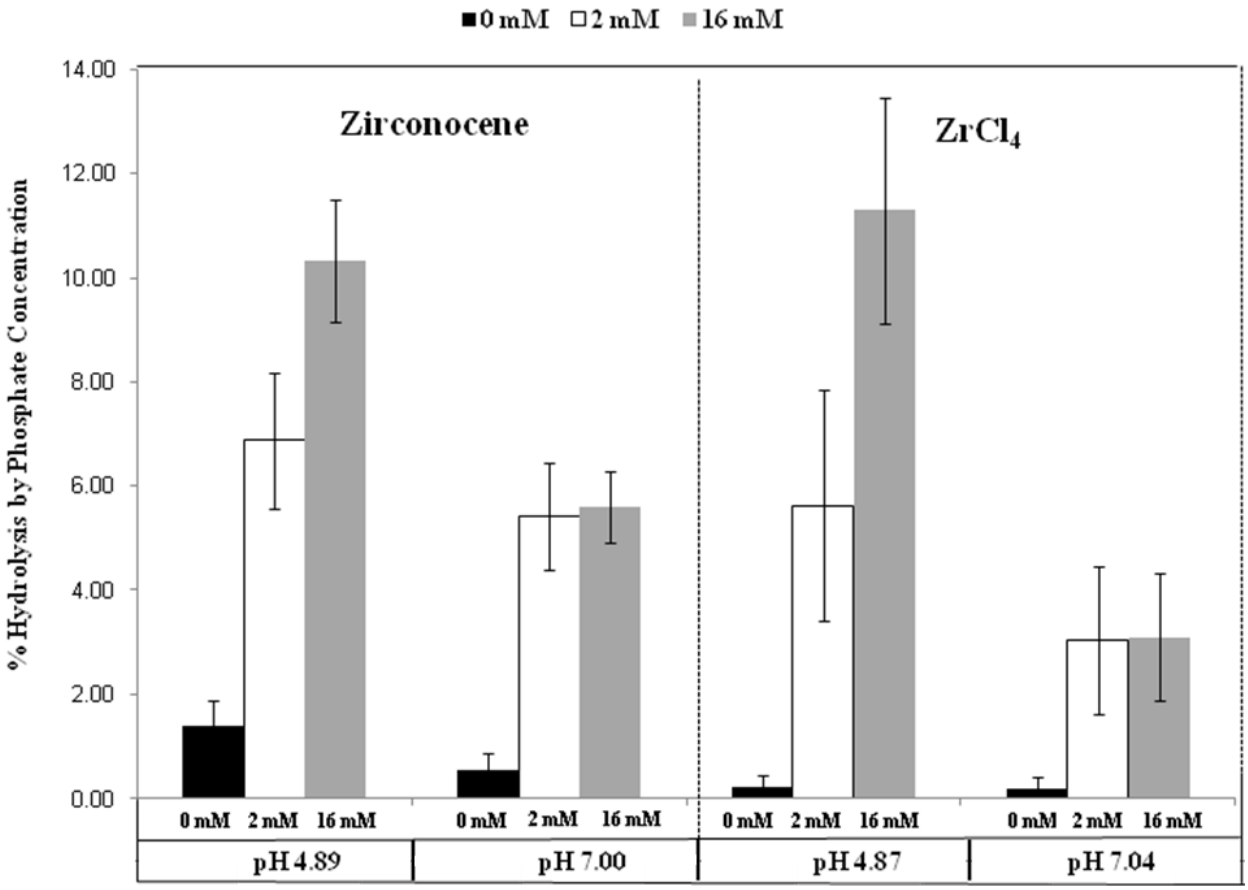

Figure 3.11. The histogram of zirconocene dichloride and $ZrCl_4$-assisted hydrolysis of sphingomyelin at pH 4.8 and pH 7 with the hydrolysis yields calculated from phosphate concentrations. Samples were prepared with 2 mM sphingomyelin, 10 mM metal, and 20 mM buffer at pH 4.8 or 7 and reacted at 60 °C for 20 h. The zirconocene dichloride experiments were conducted over 5 trials. The $ZrCl_4$ experiments were conducted over 15-19 trials.

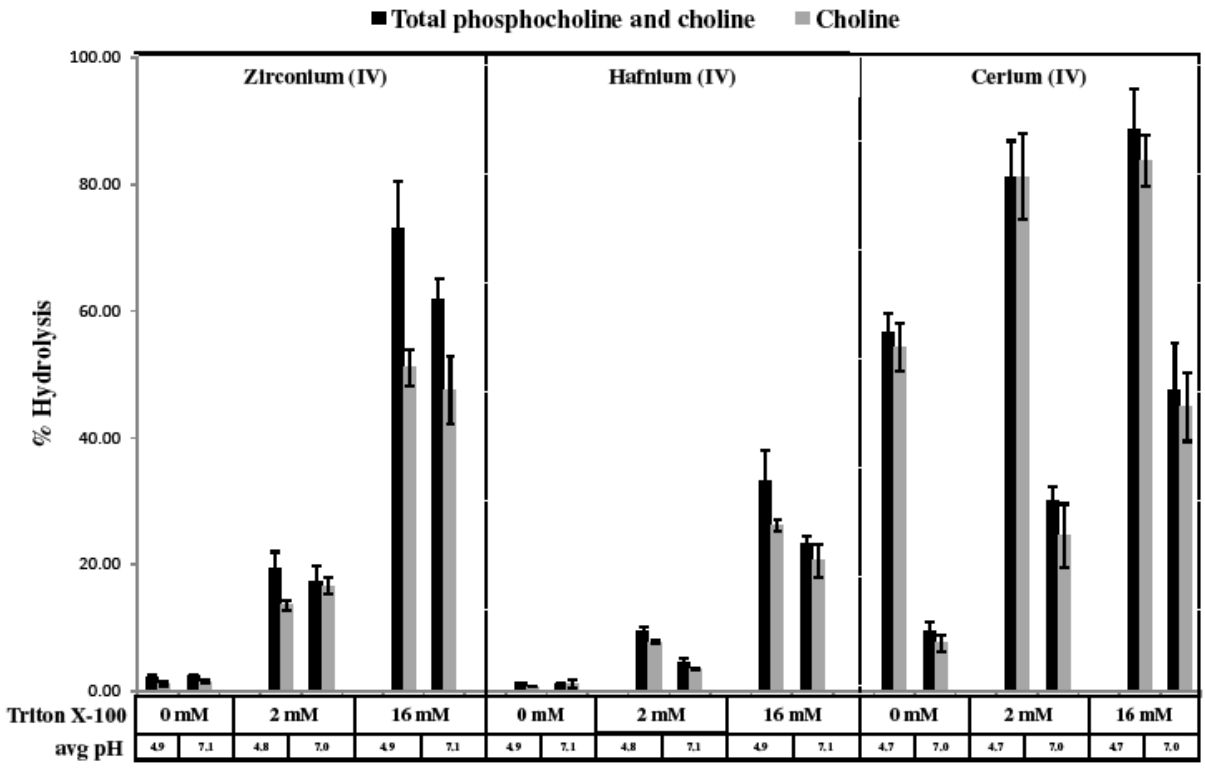

Figure 3.12. Graph shows the comparison of sphingomyelin hydrolysis yields produced by three metals as measured by total phosphocholine plus choline and total choline. Hydrolysis percentages are for 2 mM sphingomyelin, 10 mM metal, 20 mM piperazine buffer (pH 4.8) or HEPES buffer (pH 7.0) and 0, 2, or 16 mM Triton X-100 treated at 60 °C for 20 h. For Zr^{IV} and Ce^{IV}, n = 7, for Hf^{IV}, n = 3, where n = number of trials.

Table 3.4. Summary of the percentage hydrolysis from total phosphocholine plus choline concentrations and the choline-only concentrations for Zr^{IV}, Hf^{IV}, and Ce^{IV} metal-assisted hydrolysis for 2 mM sphingomyelin reacted with 10 mM metal at pH 4.8 or pH 7 and 60 °C for 20 h. The results are shown in Figure 3.12.

Metal	**pH**	**Percentage Hydrolysis for Total Phosphocholine plus Choline Concentrations, Avg ± SD (Percentage Hydrolysis for Choline-only Concentrations, Avg ± SD)**			***n***
		0 mM Triton X-100	**2 mM Triton X-100**	**16 mM Triton X-100**	
Zr^{IV}	4.8	2.33 ± 0.27 (1.17 ± 0.33)	19.3 ± 2.8 (13.6 ± 0.69)	73.0 ± 7.6 (51.1 ± 2.9)	7
	7	2.50 ± 0.26 (1.58 ± 0.27)	17.4 ± 2.3 (16.6 ± 1.3)	61.9 ± 3.3 (47.6 ± 5.4)	7
Hf^{IV}	4.8	1.38 ± 0.04 (0.74 ± 0.05)	9.40 ± 0.71 (7.75 ± 0.28)	33.2 ± 4.8 (26.2 ± 0.87)	3
	7	1.13 ± 0.18 (1.20 ± 0.57)	4.53 ± 0.71 (3.60 ± 0.14)	23.3 ± 1.3 (20.6 ± 2.5)	3
Ce^{IV}	4.8	56.8 ± 3.1 (54.4 ± 3.8)	81.2 ± 5.8 (81.3 ± 6.8)	88.7 ± 6.4 (83.8 ± 4.1)	7
	7	9.43 ± 1.6 (7.58 ± 1.3)	30.0 ± 2.2 (24.6 ± 5.0)	47.6 ± 7.3 (44.8 ± 5.4)	7

with the highest cleavage levels being produced at pH 4.8 in the presence of 2 mM Triton X-100, a concentration of surfactant which would be expected to produce mixed sphingomyelin vesicles.

The histogram in Figure 3.11 compares the percent hydrolysis as determined by phosphate assay results for zirconocene dichloride and $ZrCl_4$ in order to compare two Zr^{IV} complexes. Zirconocene dichloride is a non-toxic metallocene which has been used safely in clinical trials.[37] The data at pH 4.8 for both metals show a similar Triton X-100-solubilization dependencies as the percentage hydrolysis for 0 mM < 2 mM < 16 mM Triton X-100 amounts and are statistically similar. Both data sets at pH 7 shows that 0 mM < 2 mM ≈ 16 mM, and the zirconocene dichloride yields are slightly higher than $ZrCl_4$. For $ZrCl_4$ and zirconocene dichloride, reactivity is greater at lysosomal pH (4.8) than at cytosolic (7.0) pH only at 16 mM Triton X-100, with $ZrCl_4$ showing the highest differential cleavage at pH 4.8.

Quantification of phosphocholine and choline in metal-assisted hydrolysis reactions at 60 °C using an Amplex® Red method.

The hydrolysis of the phosphate ester bonds of sphingomyelin generates phosphocholine and choline. The phosphocholine and choline products produced in metal-assisted hydrolysis reactions were quantified by Amplex® Red assay. A novel adaptation of the assay's enzyme mix, whereby only the choline product is measureable, allowed differential quantification of the total phosphocholine plus choline products vs. the choline product (and thus phosphocholine concentrations indirectly by difference). Figure 3.12 shows the compilation of results of multiple sphingomyelin hydrolysis reaction trials at 60 °C for the three metals, Zr^{IV}, Hf^{IV}, and Ce^{IV} since these tetravalent metals produced the highest hydrolysis yields in the malachite green phosphate detection assay (Figure 3.10). The Amplex® Red data show that the order of metal reactivity for the hydrolysis of 2 mM sphingomyelin in the presence of 10 mM metal and 20 mM

buffer at 60 °C for 20 h is $Ce^{IV} > Zr^{IV} > Hf^{IV}$ (Figure 3.12). This trend correlates with the pK_a order of metals and their ability to form a hydroxide-bound metal complex which serves as a nucleophile in the phosphate ester hydrolysis reaction (Figure 3.1).

The pure sphingomyelin vesicles were solubilized by increasing amounts (0, 2, and 16 mM) of Triton X-100. For all three metals, the increased Triton X-100 levels were correlated to higher yields presumably due to the bilayer to monolayer transition with increased phosphate ester bond exposure on the exovesicular layer of the liposome. Also, the increased Triton X-100 interdigitation within the vesicle bilayer reduces columbic repulsion so that the metal-OH nucleophile may react in a more facile fashion.

The experiments at each Triton X-100 were performed at two different pH values which simulate the lysosomal pH 4.8 and the cytosolic pH 7.0 at 60 °C. The maximum hydrolysis yields per metal and per Triton X-100 amount as measured by the total phosphocholine and choline assay are 73.0 ± 7.55% for Zr^{IV} (16 mM Triton X-100 , pH 4.8), 33.2 ± 4.77% for Hf^{IV} (16 mM Triton X-100, pH 4.8), and 88.7 ± 6.40% for Ce^{IV} (16 mM Triton X-100, pH 4.8).

The data in Figure 3.12 for Zr^{IV} and Hf^{IV} show that the hydrolysis yields at 60 °C are not significantly enhanced at lysosomal pH since the ratios of yields pH 4.8: pH 7.0 for Zr^{IV} are 0.93 (0 mM), 1.11 (2 mM), 1.18 (16 mM); and for Hf^{IV} are 1.21 (0 mM), 2.07 (2 mM), 1.42 (16 mM). A value < 1 signifies no pH enhancement of hydrolysis in lysosome compared to cytosol, while a value > 1 shows reactivity that is has greater yields in the lysosome. In contrast, Ce^{IV} shows a significant enhancement in yields at lysosomal pH compared to cytosolic pH at 60 °C, with ratio of yields (pH 4.8: pH 7) of 6.02 (0 mM), 2.70 (2 mM), and 1.86 (16 mM).

The novel, modified choline-only assay is plotted alongside the total phosphocholine and choline results. Choline differentiation from the phosphocholine yields is important factor in the

determination of the regioselectivity of a metal-hydrolytic agent and its ability to mimic the acid sphingomyelinase enzyme although this neglects the dephosphorylation of the phosphocholine product which could occur as a secondary metal-assisted hydrolysis reaction. The choline product produced is approximately the same at pH 4.8 and pH 7 for Zr^{IV} and Hf^{IV} while Ce^{IV} shows much more choline produced much more at pH 4.8 than at pH 7. For Zr^{IV}, Hf^{IV}, and Ce^{IV} metals, the choline at pH 4.8 is less than the total phosphocholine plus choline amounts and ranges from 50-70 % for Zr^{IV}, 54-82% for Hf^{IV}, and 95-100 % for Ce^{IV} of the total phosphocholine plus choline yields. The choline at pH 7 is also less than the total phosphocholine plus choline amounts and ranges from 63-95% for Zr^{IV}, 79-106% for Hf^{IV}, and 80-94% for Ce^{IV} of the total phosphocholine plus choline yields. The predominance of choline product may originate from two pathways: 1) the metal preferentially hydrolyzes the choline side of the phosphate ester bond of sphingomyelin due to steric effects, or 2) phosphocholine hydrolysis product is hydrolyzed to choline and inorganic phosphate due to a labile phosphate, although the inorganic phosphate levels determined in the malachite green assay do not account for the differences between phosphocholine and choline. For Ce^{IV}, the choline yields are approximately the same yields as the total which indicates either very little phosphocholine product or an advanced degree of dephosphorylation of the phosphocholine product.

Cholesterol effects on sphingomyelin vesicles at 37 °C and at 60 °C.

Cholesterol plays a key role in phospholipid membranes because it modulates the structure, dynamics, and function of the bilayer. Cholesterol increases the cross-sectional packing of the phospholipid bilayer with denser packing. Since cholesterol induces tighter packing within the bilayer and thus higher columbic repulsion within the polar headgroup region of sphingomyelin vesicles, the predicted result is less metal-polar headgroup interaction and,

consequently, reduced hydrolysis.[23,24,28,32j-k] Niemann-Pick cells show elevated cholesterol in the liver and spleen cells that cause a characteristic foamy appearance. Lipid compositional analysis of a Niemann-Pick Type A patient's cerebral cortex showed 27.6 μmol/g wet wt. cholesterol with 31.9 μmol/g sphingomyelin compared to the control patient's cerebral cortex which had 24 μmol/g wet wt. cholesterol and 4.1 μmol/g wet wt. sphingomyelin. The cerebral white matter show 37 μmol/g wet wt. cholesterol and 28.3 μmol/g wet wt. sphingomyelin compared to the control patient's cerebral white matter which had 118.5 μmol/g wet wt. cholesterol and 112.1 μmol/g wet wt. sphingomyelin.[38,33b] Given these elevated cholesterol levels, sphingomyelin vesicles with 50 mole % cholesterol were hydrolyzed in the presence of 10 mM metal and 20 mM buffer to represent a balance between normal physiological cholesterol levels and high levels observed in Niemann-Pick Type A patients.

Figure 3.13 shows several trends for Zr^{IV} including a large reduction in hydrolytic yields when cholesterol is present, the similar yields for both pH 4.8 and 7.0 as observed in the use of pure sphingomyelin without cholesterol (Figure 3.12), and the total phosphocholine plus choline amounts are slightly greater than the choline. In Figure 3.13, vesicles with sphingomyelin and 50 mol % cholesterol were hydrolyzed with Zr^{IV} at both 60 °C and 37 °C for 20 h. The overall yields have decreased by half compared to the reactions without cholesterol. In addition, yield percentages as a function of Triton X-100 concentration follow the general trends of the non-cholesterol data for both pH 4.8 and 7 with 0 mM < 2 mM < < 16 mM. The Figure 3.13 (a) shows the maximum Zr^{IV}-assisted yields at 60 °C: 31.4 ± 1.3% (16 mM Triton X-100, pH 4.8) and 28.6 ± 1.1% (16 mM Triton X-100, pH 7) compared to 73.0 ± 7.6% (16 mM) at pH 4.8 and 61.9 ± 3.3% (16 mM) at pH 7 without cholesterol. (Figure 3.12 and Table 3.4*)* For the 60 °C data, cholesterol reduces the hydrolytic yields by 2-4 times. The hydrolysis yields at 37 °C are

much lower than the 60 °C. The overall yields at 37 °C in Figure 3.13 (b) show a maximum at 1.13 ± 0.49% (16 mM Triton X-100, pH 4.8) and at 1.02 ± 0.09% (16 mM Triton X-100, pH 7). The trends for the hydrolysis yield ratios at lysosomal pH 4.8 to cytosolic pH 7.0 are similar to the pure sphingomyelin vesicles without cholesterol at 60 °C where no pH advantage at pH 4.8 or 7 occurs in hydrolysis (Figure 3.12 and Figure 3.13).

The trends in hydrolytic yields as determined by phosphate concentrations are similar to the total phosphocholine plus choline yields except at 16 mM, pH 7 which shows a slightly lower phosphate yield than expected (Figure 3.13).

The cholesterol sphingomyelin reactions were then repeated for Ce^{IV}. Figure 3.14 (a-d) plots the hydrolysis yields for Ce^{IV}-assisted sphingomyelin vesicles that contain 50 mol % cholesterol. Figure 3.14 (a-d) shows several new trends: the addition of cholesterol reduces the hydrolysis yields to a lesser degree than Zr^{IV} (Figure 3.13), yields at pH 4.8 are reduced to a greater extent than at 7.0, and the maximum 60 ° C hydrolysis yields are highest at 2 mM Triton X-100. Unlike the Zr^{IV} data (37 °C and 60 °C; Figure 3.13), the maximum yields at 60 °C shown in Figure 3.14 (a) occur at 2 mM Triton X-100 for both pH 4.8 and 7 with 69.4 ± 6.7 % (2 mM, pH 4.8) and 37.4 ± 9.2% (2 mM, pH 7) compared to the non-cholesterol hydrolysis percentages of 81.2 ± 5.8% (2 mM, pH 4.8) and 30.0 ± 2.2% (2 mM, pH 7). The overall Triton X-100 rankings at 60 °C show that pH 4.8 and pH 7.0 trends are very different: 0 mM < 16 mM < 2 mM (pH 4.8) and 0 mM ~ 2 mM ~ 16 mM (pH 7.0). The pH 7 hydrolysis yields are elevated compared to Figure 3.12 where there was a dramatic difference between pH 4.8 and pH 7 in the non-cholesterol data. As seen in Table 3.5 for Ce^{IV} metal, the 0 and 2 mM Triton X-100 hydrolysis yields at pH 7 show reversed trends with the 50 mol % cholesterol reactions producing higher yields with cholesterol than without. Overall, the majority of the 60 °C data

shows between 1-2 times lower hydrolytic yields with cholesterol except for the two pH 7 reactions which are 1 and 3.5 times greater. The 37 °C hydrolysis yields in Figure 3.14 (b) show maxima at 16 mM Triton X-100 for both pH 4.8 and 7.0 with 21.3 ± 1.4% (16 mM Triton X-100, pH 4.8) and 11.3 ± 0.51% (16 mM Triton X-100, pH 7). The phosphate assay shows similar trends in Figure 3.14 (c-d) with 60 °C hydrolysis reactions producing maximum yields at 2 mM Triton X-100, and 37 °C hydrolysis reactions producing maximum yields at 16 mM Triton X-100. The pH 4.8 yields show a slight increase over the pH 7.0 yields at both 37 °C and 60 °C.

The comparison of 60 °C hydrolysis yields for sphingomyelin vesicles with 0 % (Figure 3.12) and 50 mol % cholesterol (Figures 3.13 and 3.14 and Table 3.5) shows less attenuation in hydrolytic yields for Ce^{IV} than for Zr^{IV}. For the majority of the Ce^{IV} data, the presence of the cholesterol reduces yields by 1.17 - 1.82 times excluding the above mentioned pH 7.0 reactions.

Time course studies of the metal-assisted hydrolysis reactions of sphingomyelin.

A major emphasis of this study is to investigate differential levels of hydrolysis at pH 4.8 versus pH 7 to assess the physiological differences that may occur between the lysosomal and the cytosolic pH for a potential metal-based therapeutic drug. Figure 3.15 (a-b) plots the ratio of Zr^{IV} and Ce^{IV} hydrolysis yields (pH 4.8/pH 7.0) from the total phosphocholine plus choline assay results at pH 4.8 and pH 7. A ratio greater than one indicates that hydrolysis is favored at pH 4.8 over pH 7 which may predict higher reactivity in the lysosome compared to the cytosol in a cellular environment. The majority of the Zr^{IV} plots in Figure 3.15 show that at 37 °C and 60 °C, the maximum ratio, and thus enzyme mimicry, occurs at 4 h and decreases slightly to a constant level.

For Zr^{IV} at 0 mM Triton X-100 and 37 °C, this pH 4.8 advantage is most dramatic since the ratio at t = 4 h approaches five (Figure 3.15). The results illustrate that Zr^{IV} hydrolysis of

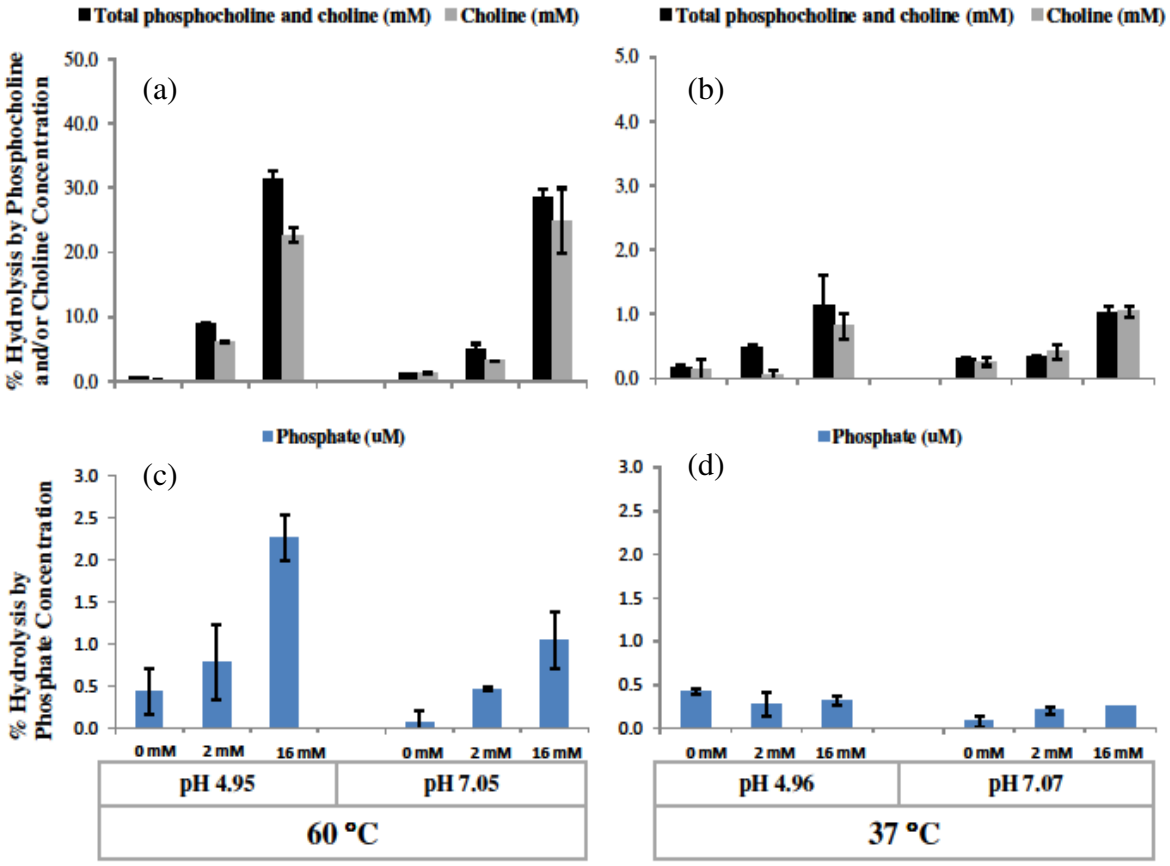

Figure 3.13. Yields produced by Zr^{IV} hydrolysis of sphingomyelin with 50 mole % cholesterol at 60 °C and 37 °C. The percentage hydrolysis of total phosphocholine plus choline or the modified choline-only assays are shown in (a-b) while the percentage hydrolysis as calculated from free inorganic phosphate are shown in (c-d). Samples prepared with 2 mM sphingomyelin, 10 mM $ZrCl_4$, 20 mM piperazine (pH 4.8) or HEPES (pH 7.0), and 1 mM cholesterol were reacted at 60 °C and 37 °C for 20 h. The number of trials = 3.

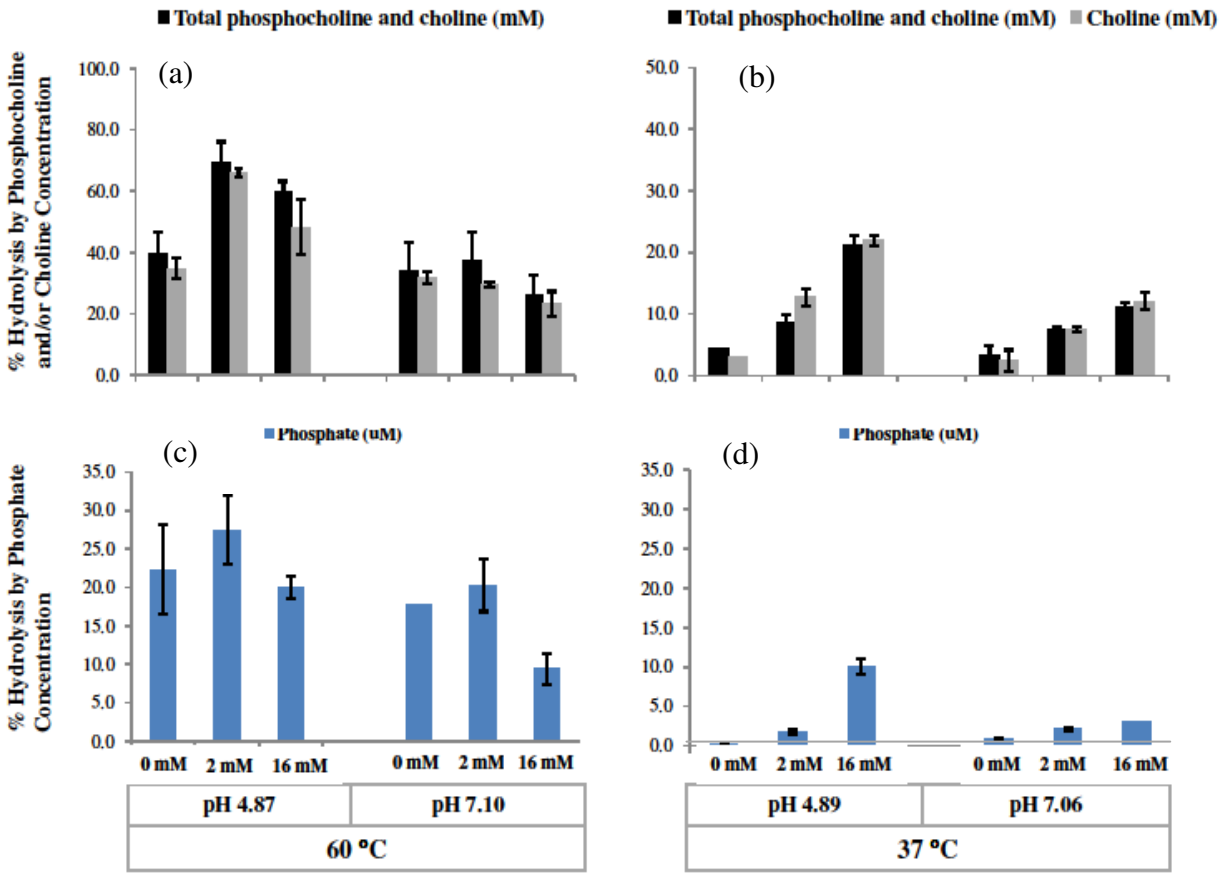

Figure 3.14. Yields produced by Ce^{IV} hydrolysis of sphingomyelin with 50 mole % cholesterol at 60 °C and 37 °C. The percentage hydrolysis of total phosphocholine plus choline or the modified choline-only assays are shown in (a-b) while the percentage hydrolysis as calculated from free inorganic phosphate are shown in (c-d). Samples prepared with 2 mM sphingomyelin, 10 mM Ce^{IV} ammonium nitrate, 20 mM piperazine (pH 4.8) or HEPES (pH 7.0), and 1 mM cholesterol were reacted at 60 °C and 37 °C for 20 h. The number of trials = 3.

Table 3.5. Percent hydrolysis yields of total phosphocholine plus choline for sphingomyelin reacted at 60 °C with 0 and 50 mol % cholesterol for Zr^{IV} and Ce^{IV}.

			Hydrolysis percentage average ± SD %	
Metal	**Triton X-100 (mM)**	**pH**	**0 mol % cholesterol**	**50 mol % cholesterol**
Zr^{IV}	0	4.8	2.33 ± 0.27	0.57 ± 0.01
		7	2.50 ± 0.26	1.2 ± 0.03
	2	4.8	19.3 ± 2.8	8.8 ± 0.2
		7	17.4 ± 2.3	5.1 ± 0.7
	16	4.8	73.0 ± 7.6	31.4 ±1.3
		7	61.9 ± 3.3	28.6 ± 1.1
Ce^{IV}	0	4.8	56.8 ± 3.1	39.9 ± 7.0
		7	9.43 ± 1.6	33.8 ± 9.4
	2	4.8	81.2 ± 5.8	69.4 ± 6.7
		7	30.0 ± 2.2	37.4 ± 9.2
	16	4.8	88.7 ± 6.4	59.7 ± 3.6
		7	47.6 ± 7.3	26.1 ± 6.6

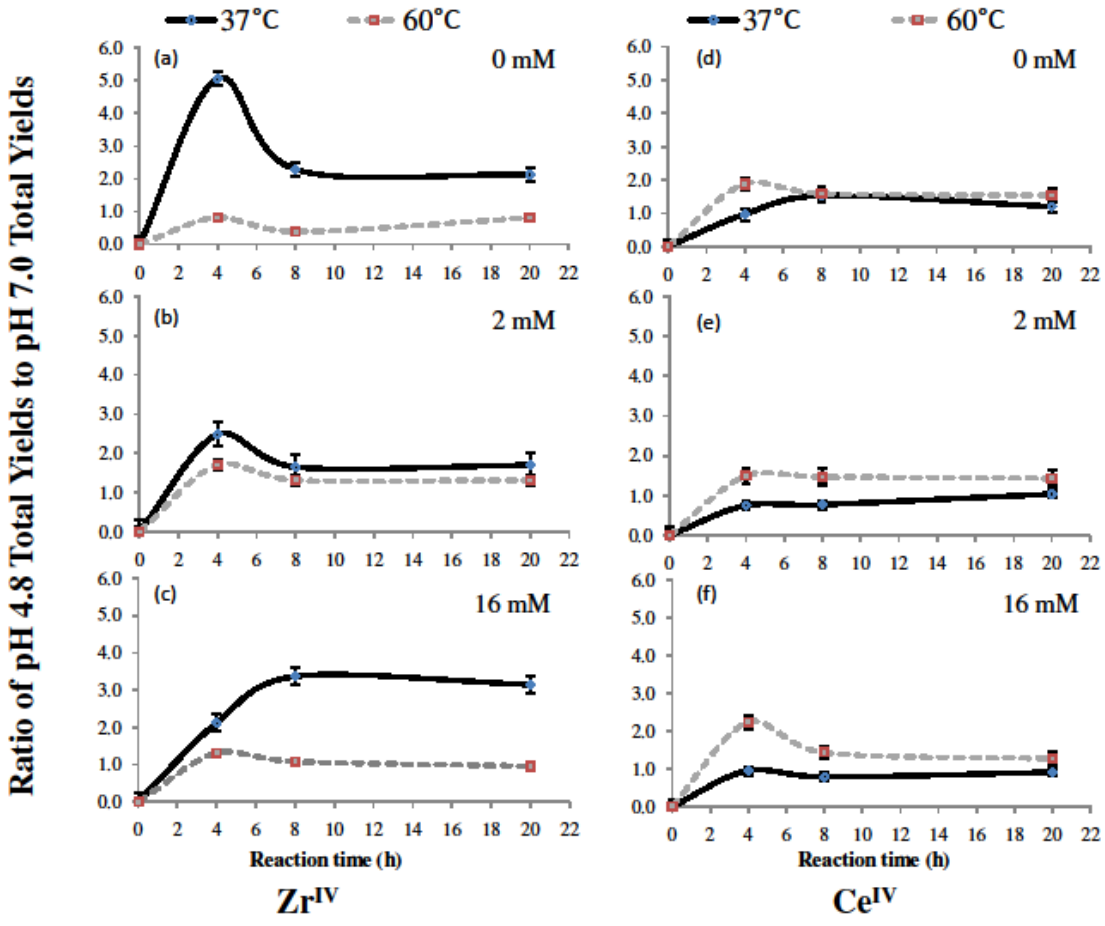

Figure 3.15. Time course experiments showing ratios of pH 4.8 total phosphocholine plus choline yields to pH 7.0 total phosphocholine plus choline yields at 37 °C and 60 °C as a function of Triton X-100 concentration. Samples were prepared with 2 mM sphingomyelin, 10 mM metal $ZrCl_4$ (shown in (a)) or $Ce(NH_4)_2(NO_3)_6$ (shown in (b)), 20 mM piperazine or HEPES were reacted at 37 °C and 60 °C for 20 h. Ratios were taken from the total phosphocholine and choline results of the Amplex® Red-based assay.The number of trials = 4. Ce^{IV} and Zr^{IV} yields are plotted in Figures 3.17 and 3.20.

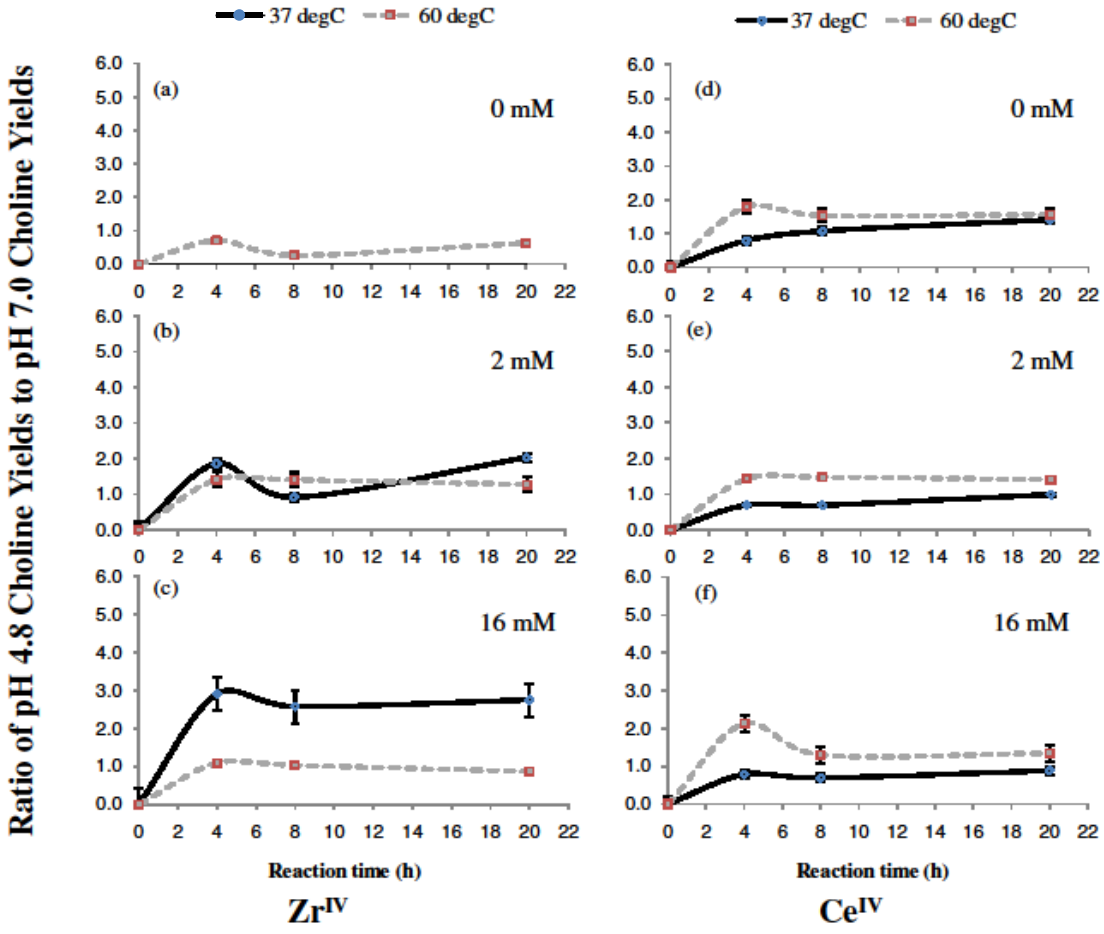

(a) (b)

Figure 3.16. Time course experiments showing ratios of pH 4.8 choline yields to pH 7.0 choline yields at 37 °C and 60 °C as a function of Triton X-100 concentration. Samples prepared with 2 mM sphingomyelin, 10 mM metal ($ZrCl_4$ shown in (a)) or ($Ce(NH_4)_2(NO_3)_6$ shown in (b)), 20 mM piperazine or HEPES were reacted at 37 °C and 60 °C for 20 h. Ratios were taken from the choline results of the Amplex® Red-based assay. The plot in (a) only shows the 60 °C data since the 37 °C data is below detection. The number of trials = 4. Ce^{IV} and Zr^{IV} yields are in Figures 3.18 and 3.21.

pure sphingomyelin vesicles is significantly enhanced at lysosomal pH at physiological termperature. The ratios at 2 and 16 mM Triton X-100 for 37 °C are also greater than one. At the higher temperature of 60 °C, the ratios at 0, 2, and 16 mM Triton X-100 for Zr^{IV} hydrolysis are approximately one which indicates no pH preference.

While the overall yields of Ce^{IV} are higher than Zr^{IV} for 0, 2, and 16 mM Triton X-100, the pH advantage at lysosomal pH 4.8 is not significant. At 60 °C, the pH ratio of yields shows a slight advantage especially at 4 h, but levels off to a ratio of one at longer reaction times. The 37 °C data show that the pH ratio of yields at 0, 2 and 16 mM are approximately one.

Figure 3.16 shows a corollary graph to the previous Figure 3.15 where the pH ratio of the modified choline-only assay yields are plotted. Similar trends in the Zr^{IV} data are observed compared to the previous figure except that the 37 °C, 0 mM Triton X-100 data is negligible. For the Ce^{IV} plots, only the 60 °C shows a pH 4.8 advantage with ratios slightly greater than 1, while the 37 °C shows no pH advantage since the ratios are approximately equal to unity.

Percentage hydrolysis by total phosphocholine plus choline, modified choline-only, and phosphate assays at 37 °C and 60 °C.

Ce^{IV}-assisted and Zr^{IV}-assisted hydrolysis. The hydrolysis yields used to produce ratios shown in Figures 3.15 and 3.16 are shown in Figures 3.17, 3.18, 3.19, 3.20, 3.21, and 3.22. The percentage of hydrolysis at 37 °C and 60 °C as calculated by the total phosphocholine plus choline assay is on the y- axis of each figure (Figure 3.17 and 3.20) or the modified choline-only assay is on the y-axis of each figure (Figure 3.18 and 3.21). Figures 3.17 and 3.18 show the progression of hydrolysis reactions of 2 mM of pure sphingomyelin vesicles as well as sphingomyelin solubilized by 0, 2, or 16 mM amounts of Triton X-100 detergent in the presence

of 10 mM cerium(IV) ammonium nitrate and 20 mM piperazine (pH 4.8) or HEPES (pH 7). The pH differences between the hydrolysis percentages at 37 °C and 60 °C at 20 h are fully discussed in a later section and presented in Table 3.11. At 37 °C, the pH 4.8 and 7 data almost overlapped with differences < 10 % for the total phosphocholine plus choline assay (Figure 3.17). The 60 °C data show that at pH 4.8, the hydrolysis is higher than at pH 7 by ~25 - 30% at all timpoints. Thus, the extreme pH-dependence (pH 4.8 > pH 7.0) in hydrolytic yields demonstrated at 60 °C disappears at 37 °C. The early timepoints of 4 h and 8 h show slower kinetics in the presence of 0 mM Triton X-100 (pure vesicle) compared to the 16 mM (micelles). Figure 3.19 shows the phosphate release during the reaction.

Figure 3.20 and 3.21 show the progression of the hydrolysis reactions of 2 mM pure sphingomyelin vesicles at 0, 2, and 16 mM amounts of Triton X-100 detergent in the presence of 10 mM $ZrCl_4$ and 20 mM piperazine (pH 4.8) or HEPES (pH 7). At 37 °C (Figure 3.20 (a) and Figure 3.21 (b)), the percentage of hydrolysis at 0 and 2 mM is barely detectable while 16 mM Triton X-100 levels show pH 4.8 > pH 7. At 60 °C (Figure 3.20 (b) and 3.21 (b), the pH 4.8 and 7 slopes almost overlap. The phosphate amounts in Figure 3.22 are approximately 10 % of the total phosphocholine plus choline results.

This data demonstrate that the regioselective hydrolysis by metals at the phosphate ester bond to release phosphocholine is not favored in this cleavage reaction since the high choline percentages indicate that the metals hydrolyze the polar side of the molecule to release choline. The choline side of the phosphate ester bond also represents less steric hindrance. The acid sphingomyelinase enzyme solely releases phosphocholine in the lysosomes. However, the metal-assisted hydrolysis of the primary product of phosphocholine to release inorganic phosphate and a secondary product of choline is a very likely possibility due to the phosphate and choline levels

detected in the hydrolysis of the phosphocholine positive control. This being said, the MALDI mass spectra in Figure 3.23 show the increase of choline in a metal-assisted hydrolysis of phosphocholine.

Estimated half-lives of Zr^{IV}- and Ce^{IV}-assisted reactions at 60 °C and 37 °C. Table 3.10 shows the estimated half lives ($t_{½}$) in units of hours for the reactions shown in Figures 3.17 - 3.22 according to the total phosphocholine plus choline assay and the choline assay results. The assays contained the four datapoints from t = 0, 4, 8, and 20 h from which the data was approximated. For each of the Ce^{IV} or Zr^{IV} reactions, the half-lives were estimated from multiple time course experiments with linear plots of the natural log of the remaining unreacted sphingomyelin ($\ln P_0 - P_{time}$) as a function of time according to a slope equation criteria that correlation coefficient of R be ≥ 0.98. Plots which produced correlation coefficients less than 0.98 or whose reaction was too slow and produced extremely long half-lives were listed in the table as "*nd*" for "*not determined*". According to the linear fit slope equations from each experiment's plots, the (-) slope = k and $t_{1/2} = 0.693/k$ values were calculated to obtain the half-life.

The half-life is the inverval required for the quantity to decay to half of its initial value. Since the total experimental times were 20 h, only the 60 °C data for Ce^{IV} (0, 2, and 16 mM Triton X-100) and Zr^{IV} data (16 mM only) have half-lives less than the 20 h time cut-off. Table 3.10. shows that at 60 °C data, Ce^{IV} had the shortest half-lives with a range of 5 h ± 0.5 (total phosphocholine plus choline assay, 2 mM Triton X-100, pH 4.86) to 19 h ± 1 (total phosphocholine plus choline assay, 0 mM Triton X-100, pH 6.95). Also at 60 °C, the half-lives for Zr^{IV} ranged from 7 h ± 0.5 (total phosphocholine plus choline assay, 16 mM, pH 7.07) to 300 h ± 1 (total phosphocholine plus choline assay, 0 mM Triton X-100, pH 4.84). For Ce^{IV}, the

shortest half-life of 5 h (total phosphocholine plus choline assay, 2 mM Triton X-100, pH 4.86, 60 °C) represents four half-lives in a total 20 h reaction time where 93.8 % of the sphingomyelin is reacted. For Zr^{IV}, the shortest half-life of 7 h (total phosphocholine plus choline assay, 16 mM Triton X-100, pH 7.07, 60 °C) represents approximately three half-lives in a 20 h reaction time where 87.5% of the sphingomyelin is reacted. At 37 °C, the Ce^{IV} had the shortest half-lives of 20 h ± 0.5 (total phosphocholine plus choline assay, 16 mM Triton X-100, pH 7.06) to 80 h ± 1 (total phosphocholine plus choline assay, 0 mM Triton X-100, pH 4.78 and pH 7.02). The estimated half-lives for Zr^{IV} at 37 °C range from 100 h ± 1 (total phosphocholine plus choline assay, 16 mM Triton X-100, pH 4.90) to 7000 h ± 2 (0 mM Triton X-100, pH 7.04). The plots from the choline assay produced half-lives which lagged the half-lives calculated from the total phosphocholine plus choline assay.

MALDI spectra for phosphocholine.

Figure 3.23 shows the MALDI mass spectra of the Zr^{IV}-assisted hydrolysis of phosphocholine used as a positive control. A total of 2 mM phosphocholine was reacted with 10 mM $ZrCl_4$ at 0, 5, and 23 h timepoints at 60 °C, 20 mM Tris buffer, pH 4.8. The experiment was conducted to validate the dephosphorylation of the phosphocholine molecule to produce a choline product. Only the mass range of 90 - 140 Da is shown in order to reduce the complexity of the spectra with other unrelated mass peaks such as solvent cluster peaks. The Tris buffer mass peak at *m/z* 122 is present in a constant 20 mM concentration and serves as a reaction surrogate been subjected to the experimental conditions and treatments as the phosphocholine analyte. At 0 h, a small choline product appears at < 10%. Its presence may be attributed to either pre-reaction degradation of phosphocholine or a choline impurity. The choline mass peak intensifies from 35% (5 h) to 100% (23 h) of the spectra as a product of the phosphocholine

hydrolysis. While the MALDI analysis variability in peak heights prevents strict quantification, an approximation of the reaction progress of the metal-assisted dephosphorylation can be made.

pH drift of the metal-assisted experiments.

The piperazine and HEPES buffers used in the experiments were chosen because their pKa values indicated potential buffering in the pH regions that simulate lysosomal (pH 4.8) and cytosolic (pH 7.0). The pK_a of piperazine is 5.33 with a buffer range of 5 - 6. The pKa of HEPES is 7.5 with a buffer region of 6.8 to 8.2. Additionally, the piperazine buffer does not contain a carboxylate group, a reactive functional group to the oxophilic metals, like the majority of the buffers in the pH 3 - 5 range. Table 3.11 shows the average pH and the ΔpH values for all of the experiments combined in order to see the extent of the pH drifts within the 20 h experiments conducted in this study. The pH drift value was calculated from the difference in pH at t = 0 h and t = 20 h (0 h – 20 h) which is equal to the ΔpH values. The lysosomal pH 4.8 data in the table shows that Zr^{IV}- or Hf^{IV}-assisted experiments showed good pH control with pH drift from -0.02 to 0.03 from the original 0 h pH setpoint at 60 °C (Zr^{IV} and Hf^{IV}) and 0.01 to 0.1 at 37 °C (Zr^{IV} only). The zirconocene and non-metal controls showed similar pH drifts. The Ce^{IV} reaction pH showed higher pH drifts in the range of 0.42 to 0.48 at 60 °C and 0.17 to 0.37 at 37 °C. The phosphocholine hydrolysis experiments showed the highest pH drift, 0.53 at 60 °C. Since the pH drift in the piperazine-buffered experiments is approximately correlated with hydrolysis yields, i.e., the greater the hydrolysis, the greater the pH drift, the proton flux generated during the hydrolysis was greater than the buffering capacity.

The buffering at pH 7 showed less drift in pH during the reactions. For the cytosolic pH 7 experiments buffered by HEPES, the pH drift of Zr^{IV} or Hf^{IV} experiments ranged from -0.03 to 0.02 at 60 °C (Zr^{IV} and Hf^{IV}) and -0.05 to 0.03 at 37 °C (Zr^{IV} only).

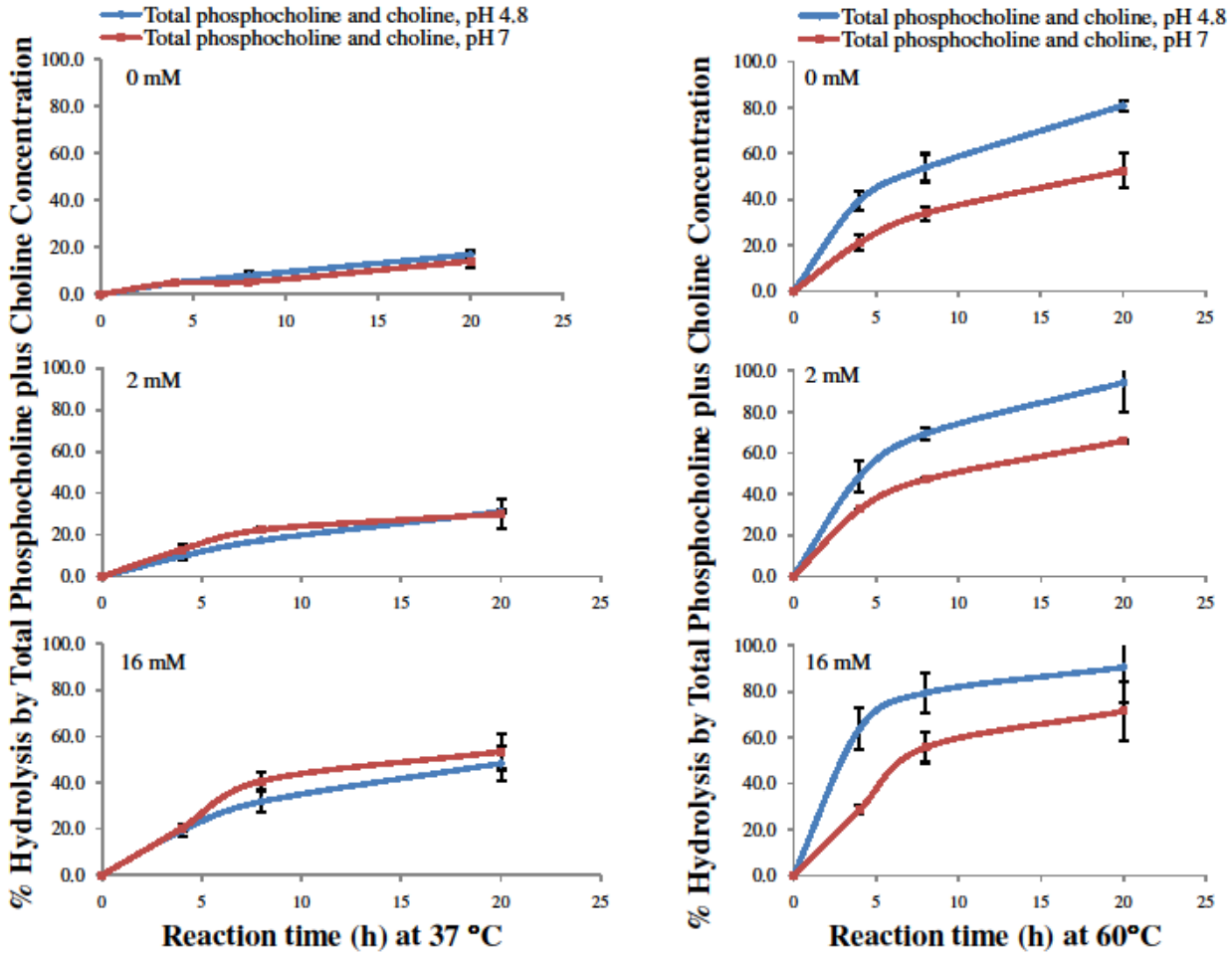

(a) (b)

Figure 3.17. The percentage of hydrolysis of 2 mM sphingomyelin with 10 mM Ce^{IV} ammonium nitrate at pH 4.8 or pH 7 and at 37 °C or 60 °C at 0, 4, 8, and 20 h timepoints as calculated by total phosphocholine plus choline concentrations. The graphs in column (a) are results at 37 °C and the graphs in column (b) are the results at 60 °C. For (a) and (b), the y-axis is the percentage of hydrolysis calculated from the Amplex® Red assay results of total phosphocholine and choline. Corresponding yield ratios are in Figure 3.15 (b).

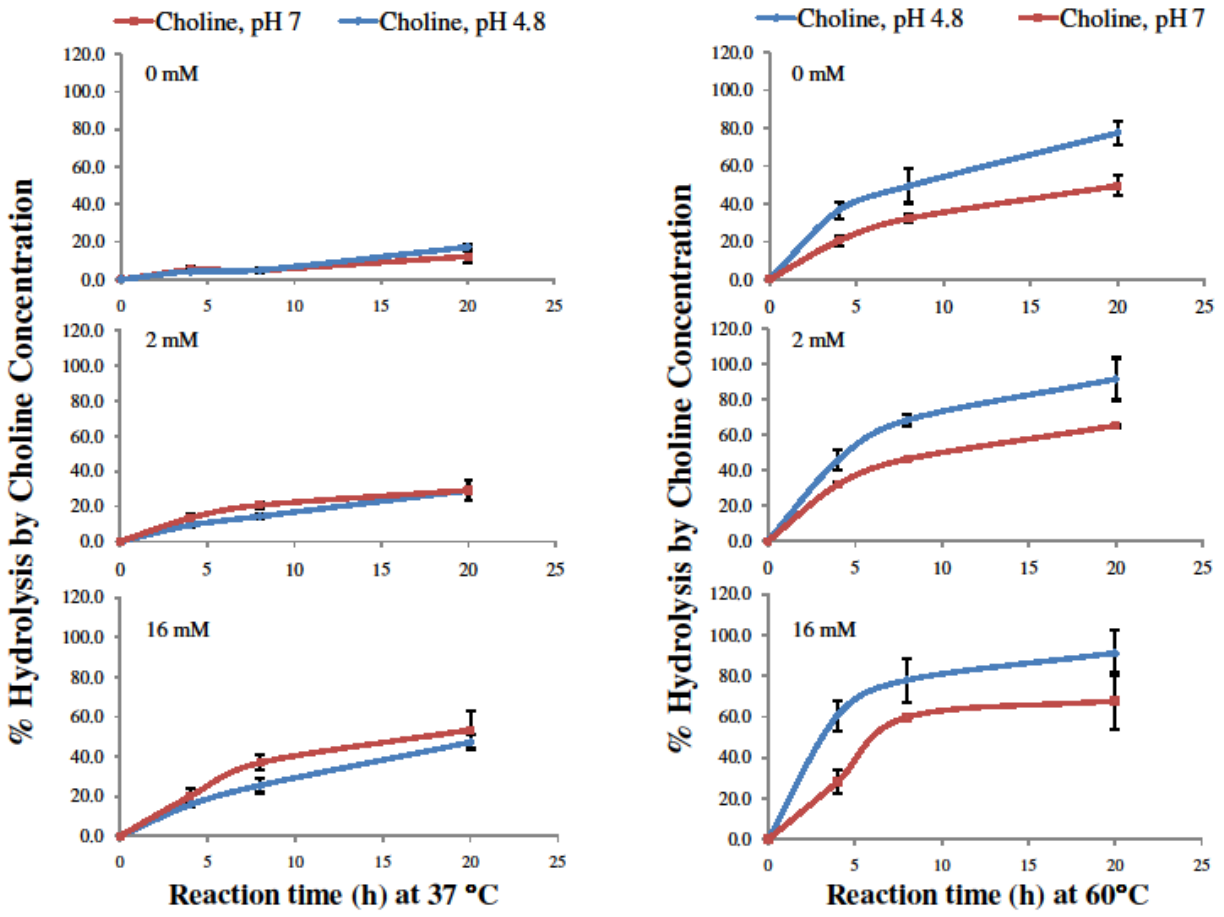

(a) (b)

Figure 3.18. The percentage of hydrolysis of 2 mM sphingomyelin with 10 mM Ce^{IV} ammonium nitrate at pH 4.8 or pH 7 and at 37 °C or 60 °C at 0, 4, 8, and 20 h timepoints as calculated by choline concentrations. The graphs in column (a) are results at 37 °C and the graphs in column (b) are the results at 60 °C. For (a) and (b), the y-axis is the percentage of hydrolysis calculated from the Amplex® Red assay results of choline. Corresponding yield ratios are in Figure 3.16 (b).

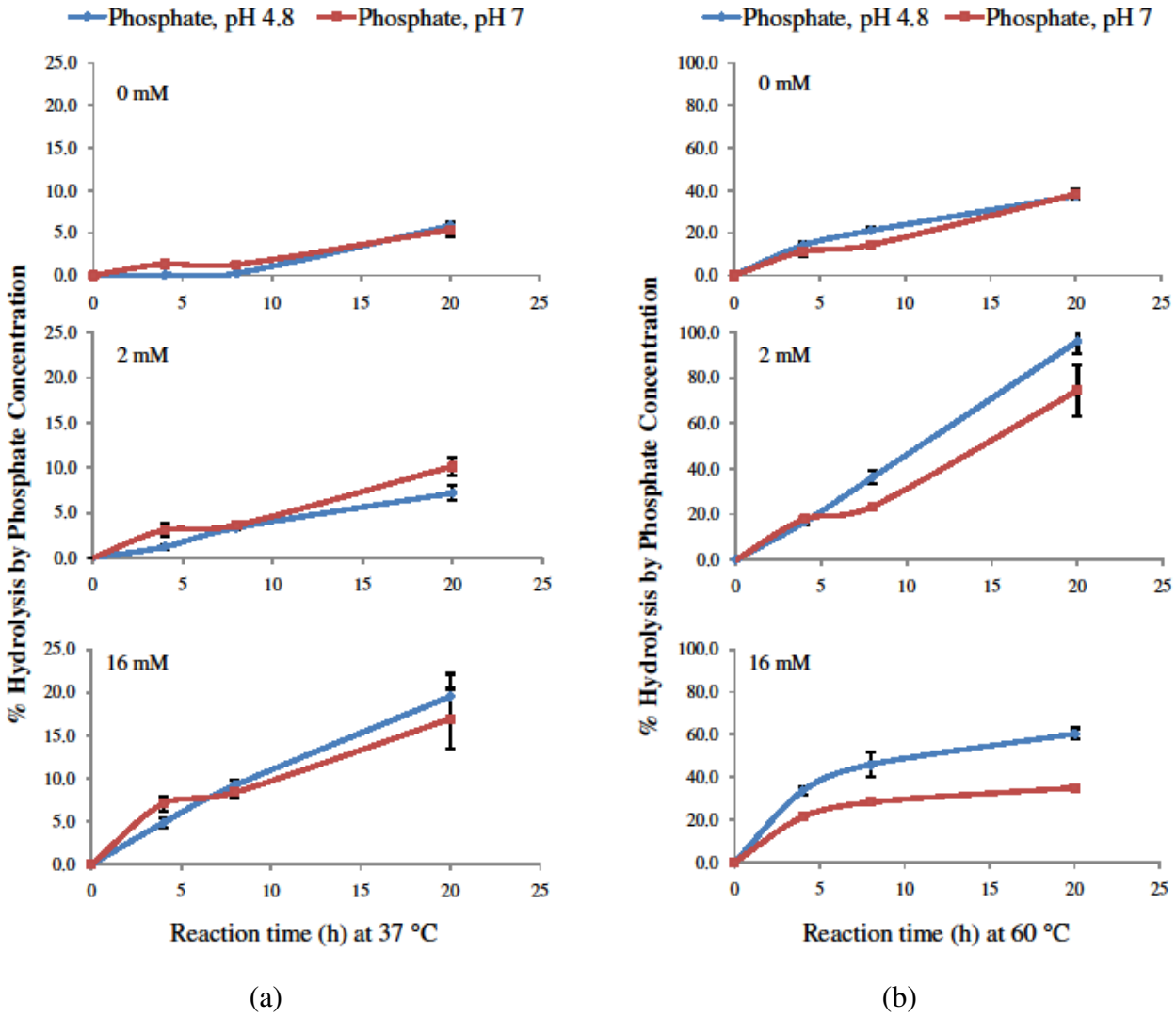

(a) (b)

Figure 3.19. The percentage of hydrolysis of 2 mM sphingomyelin with 10 mM Ce^{IV} ammonium nitrate at pH 4.8 or pH 7 and at 37 °C or 60 °C at 0, 4, 8, and 20 h timepoints as calculated by inorganic phosphate concentrations. The graphs in column (a) are results at 37 °C and the graphs in column (b) are the results at 60 °C. For (a) and (b), the y-axis is the percentage of hydrolysis calculated from the malachite green assay for phosphate.

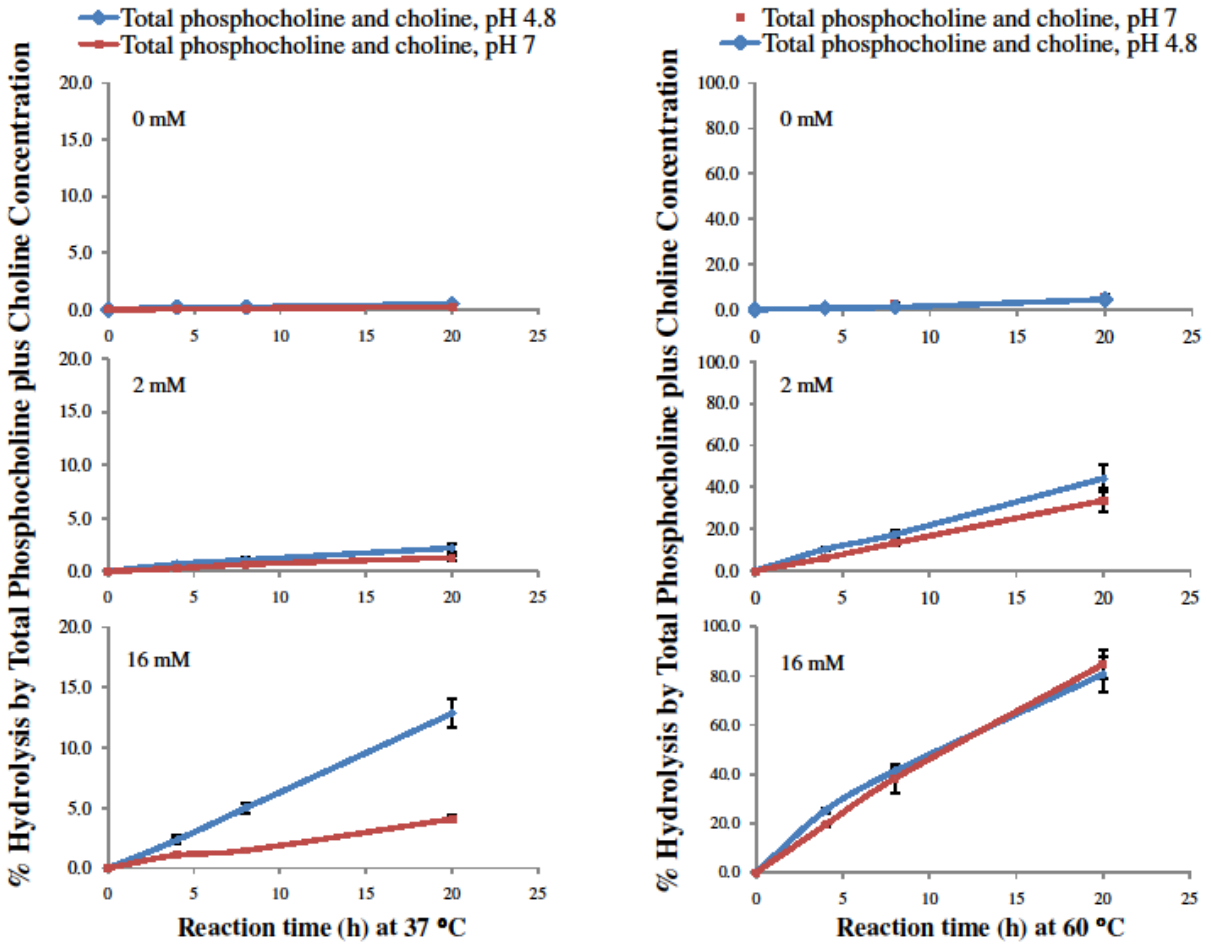

(a) (b)

Figure 3.20. The percentage of hydrolysis of 2 mM sphingomyelin with 10 mM $ZrCl_4$ at pH 4.8 or pH 7 and at 37 °C or 60 °C at 0, 4, 8, and 20 h timepoints as calculated by total phosphocholine plus choline concentrations. The graphs in column (a) are results at 37 °C and the graphs in column (b) are the results at 60 °C. For (a) and (b), the y-axis is the percentage of hydrolysis calculated from the Amplex® Red assay results of phosphocholine and choline. Corresponding yield ratios are in Figure 3.15 (a).

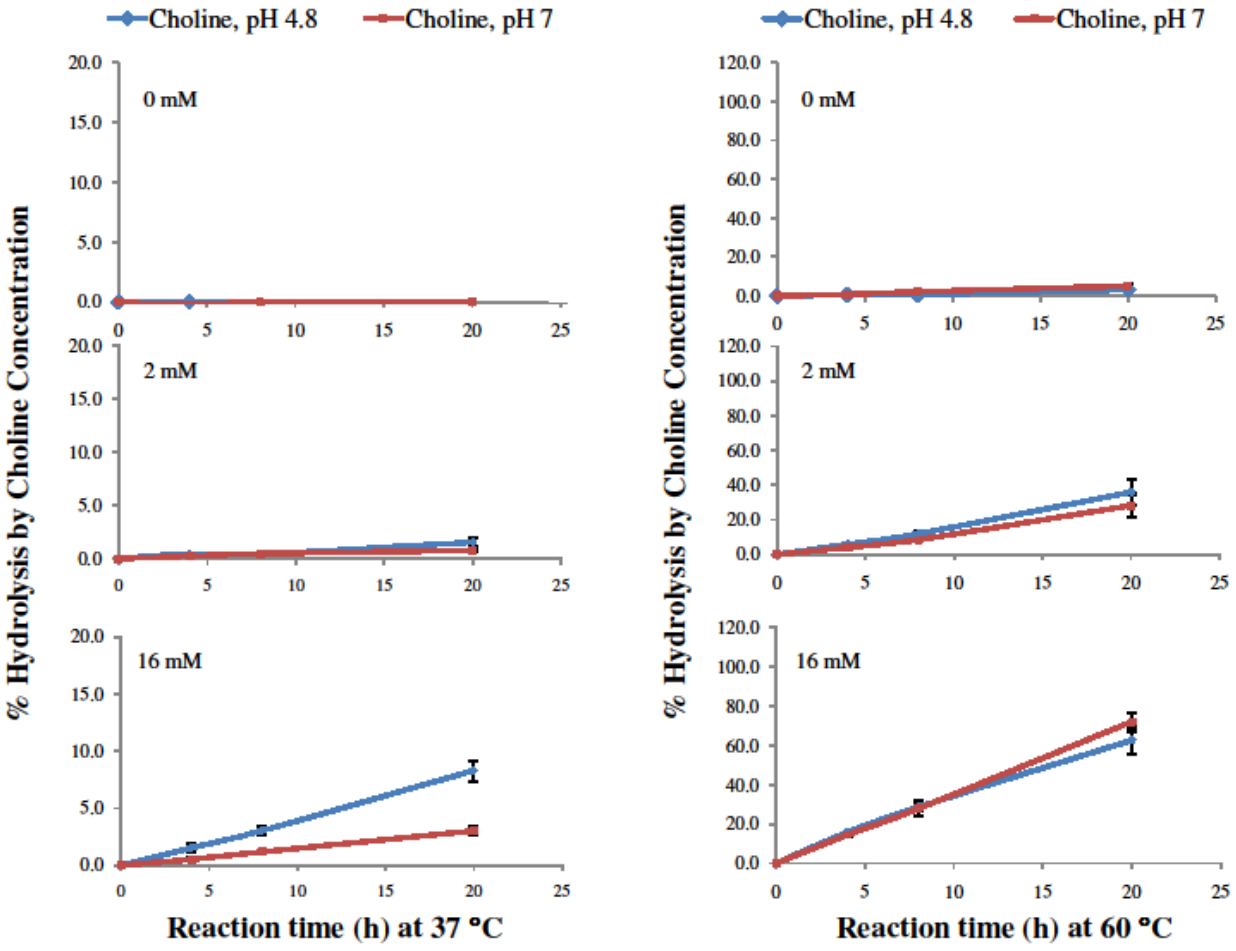

Figure 3.21. The percentage of hydrolysis of 2 mM sphingomyelin with 10 mM $ZrCl_4$ at pH 4.8 or pH 7 at 37 °C or 60 °C at 0, 4, 8, and 20 h timepoints as calculated by choline concentrations. The graphs in column (a) are results at 37 °C and the graphs in column (b) are the results at 60 °C. For (a) and (b), the y-axis is the percentage of hydrolysis calculated from the Amplex® Red assay results of choline. Corresponding yield ratios are in Figure 3.16 (a).

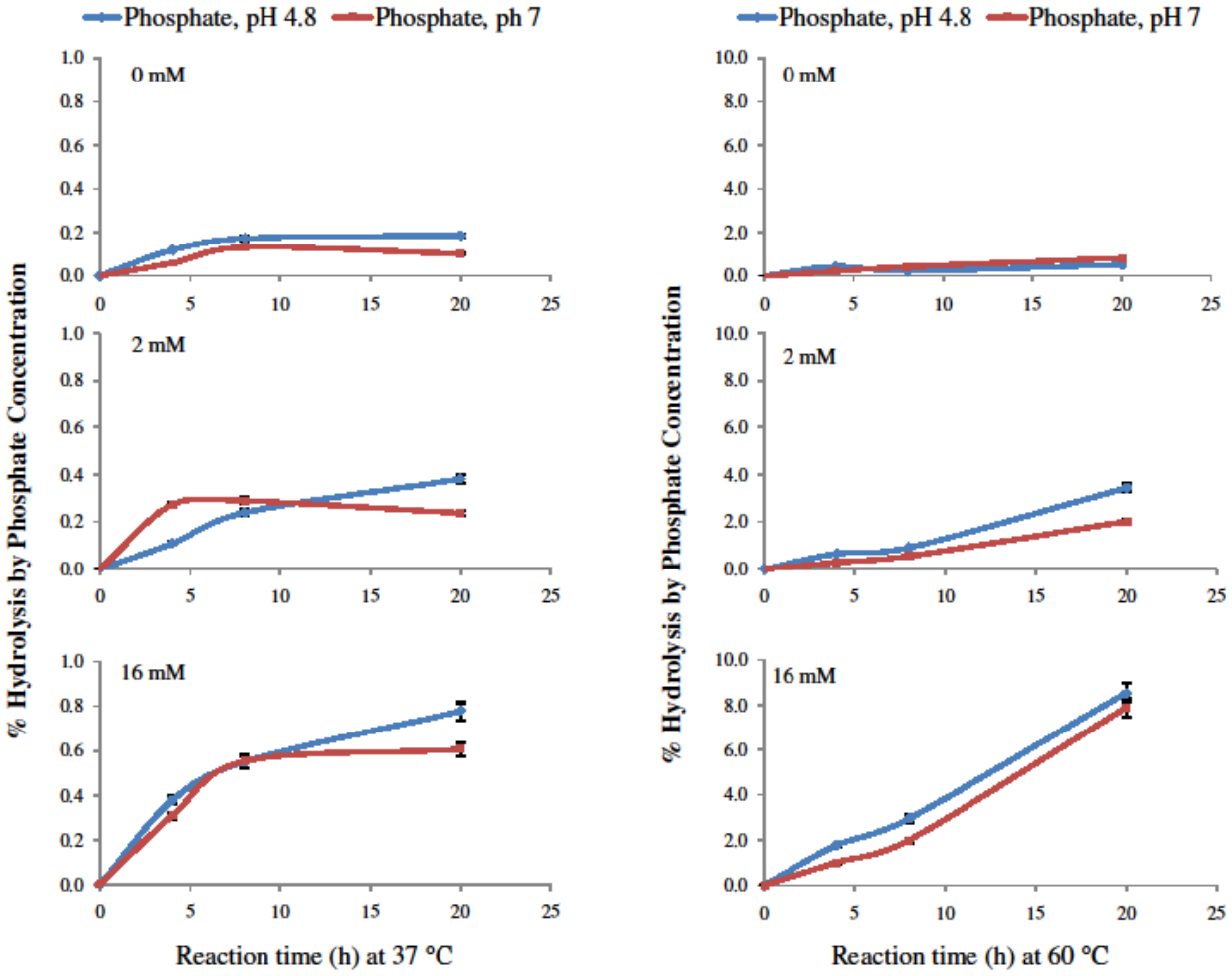

(a) (b)

Figure 3.22. The percentage of hydrolysis of 2 mM sphingomyelin with 10 mM $ZrCl_4$ at pH 4.8 or pH 7 and at 37 °C or 60 °C at 0, 4, 8, and 20 h timepoints as calculated by inorganic phosphate concentrations. The graphs in column (a) are results at 37 °C and the graphs in column (b) are the results at 60 °C. For (a) and (b), the y-axis is the percentage of hydrolysis calculated from the malachite green assay for phosphate.

Table 3.6. The percentage hydrolysis by total phosphocholine plus choline concentrations (or choline-only concentrations) for the reaction progress of the Zr^{IV} metal-assisted hydrolysis of sphingomyelin with four timepoints.

Metal ion	**Triton X-100 (mM)**	**Temp. (°C)**	**Time (h)**	**Percentage Hydrolysis at pH 4.8**	**Percentage Hydrolysis at pH 7**
				Avg. ± SD % of total phosphocholine plus choline (Avg. ± SD of choline only)	**Avg. ± SD % of total phosphocholine plus choline (Avg. ± SD of choline only)**
Zr^{IV}	0	37	0	0.00 ± 0.00 (0.00 ± 0.00)	0.00 ± 0.00 (0.00 ± 0.00)
			4	0.23 ± 0.04 (0.05 ± 0.00)	0.04 ± 0.05 (-0.20 ± 0.00)
			8	0.23 ± 0.11 (-0.10 ± 0.00)	0.10 ± 0.03 (0.00 ± 0.00)
			20	0.50 ± 0.21 (-0.10 ± 0.00)	0.23 ± 0.02 (0.00 ± 0.00)
		60	0	0.00 ± 0.00 (0.00 ± 0.00)	0.00 ± 0.00 (0.00 ± 0.00)
			4	0.71 ± 0.13 (0.46 ± 0.01)	0.87 ± 0.17 (0.65 ± 0.14)
			8	1.08 ± 0.07 (0.54 ±0.05)	2.80 ± 0.02 (2.05 ± 0.42)
			20	4.50 ± 0.23 (3.16 ± 0.54)	5.60 ±0.71 (5.03 ±1.2)
	2	37	0	0.00 ± 0.00 (0.00 ± 0.00)	0.00 ± 0.00 (0.00 ±0.00)
			4	0.71 ± 0.06 (0.46 ± 0.00)	0.28 ± 0.05 (0.25 ± 0.00)
			8	1.07 ±0.30 (0.42 ± 0.03)	0.65 ± 0.05 (0.46 ± 0.02)
			20	2.20 ± 0.40 (1.55 ± 0.39)	1.29 ± 0.22 (0.76 ± 0.05)
		60	0	0.00 ± 0.00 (0.00 ± 0.00)	0.00 ± 0.00 (0.00 ±0.00)
			4	10.4 ± 0.55 (5.91 ± 0.12)	6.07 ±0.04 (4.18 ± 0.80)
			8	17.4 ± 2.1 (12.1 ± 1.5)	13.2 ± 1.1 (8.62 ± 1.3)
			20	44.3 ± 6.6 (36.0 ± 7.6)	33.6 ± 5.6 (28.2 ± 6.7)

Continued Table 3.6.: The percentage hydrolysis by total phosphocholine plus choline concentrations or choline-only concentrations for the reaction progress of the Zr^{IV} metal-assisted hydrolysis of sphingomyelin with four timepoints.

Metal ion	**Triton X-100 (mM)**	**Temp. (°C)**	**Time (h)**	**Percentage Hydrolysis at pH 4.8** **Avg. ± SD % of total phosphocholine plus choline (Avg. ± SD of choline only)**	**Percentage Hydrolysis at pH 7** **Avg. ± SD % of total phosphocholine plus choline (Avg. ± SD of choline only)**
Zr^{IV}	16	37	0	0.00 ± 0.00 (0.00 ± 0.00)	0.00 ± 0.00 (0.00 ± 0.00)
			4	2.35 ± 0.34 (1.53 ± 0.36)	1.11 ± 0.09 (0.53 ± 0.13)
			8	5.00 ± 0.45 (3.04 ± 0.36)	1.49 ± 0.04 (1.18 ± 0.12)
			20	12.9 ± 1.2 (8.30 ± 0.90)	4.09 ± 0.27 (3.02 ± 0.35)
		60	0	0.00 ± 0.00 (0.00 ± 0.00)	0.00 ± 0.0 (0.00 ± 0.0)
			4	25.3 ± 0.92 (15.8 ± 0.54)	19.3 ± 0.6 (14.5 ± 0.6)
			8	41.3 ± 1.1 (28.6 ± 1.3)	38.3 ± 5.8 (27.8 ± 3.8)
			20	80.7 ±7.4 (62.6 ± 7.061)	84.7 ± 6.0 (72.1 ± 4.7)

Table 3.7. The percentage hydrolysis by total phosphocholine plus choline concentrations or choline-only concentrations for the reaction progress of the Ce^{IV} metal-assisted hydrolysis of sphingomyelin with four timepoints.

Metal	**Triton X-100 (mM)**	**Temp. (°C)**	**Time (h)**	**Percentage Hydrolysis at pH 4.8** **Avg. ± SD of total phosphocholine plus choline (Avg. ± SD of choline only)**	**Percentage Hydrolysis at pH 7** **Avg. ± SD of total phosphocholine plus choline (Avg. ± SD of choline only)**
Ce^{IV}	0	37	0	0.00 ± 0.00 (0.00 ± 0.00)	0.00 ± 0.0 (0.00 ± 0.0)
			4	4.88 ± 0.11 (4.36 ± 0.55)	5.04 ± 1.0 (5.50 ± 1.3)
			8	8.06 ± 1.8 (5.08 ± 1.2)	5.26 ± 0.34 (4.71 ± 0.37)
			20	17.0 ± 2.1 (17.3 ± 1.6)	14.18 ± 2.9 (12.3 ± 3.0)
		60	0	0.00 ± 0.0 (0.00 ± 0.0)	0.00 ± 0.0 (0.00 ± 0.0)
			4	39.6 ± 4.2 (36.7 ± 4.5)	21.1 ± 3.4 (20.5 ± 3.0)
			8	53.9 ± 6.1 (49.5 ± 9.0)	34.0 ± 3.2 (32.3 ± 2.0)
			20	80.9 ± 2.5 (77.6 ± 6.0)	52.5 ± 7.6 (49.6 ± 5.3)
	2	37	0	0.00 ± 0.0 (0.00 ± 0.0)	0.00 ± 0.0 (0.00 ± 0.0)
			4	9.75 ± 1.5 (9.28 ± 1.2)	13.0 ± 2.9 (13.3 ± 2.8)
			8	17.4 ± 0.32 (14.3 ± 1.6)	22.5 ± 1.1 (20.7 ± 2.0)
			20	31.2 ± 0.66 (28.9 ± 2.0)	30.1 ± 7.4 (29.2 ± 6.0)
		60	0	0.00 ± 0.0 (0.00 ± 0.0)	0.00 ± 0.00 (0.00 ± 0.00)
			4	48.7 ± 7.6 (45.6 ± 5.8)	32.5 ± 0.14 (31.8 ± 1.2)
			8	69.3 ± 3.3 (68.5 ± 3.1)	47.1 ± 0.58 (46.3 ± 0.03)
			20	94.2 ± 14.1 (91.6 ± 11.9)	65.8 ± 0.63 (65.2 ± 1.1)

Continued Table 3.7.: The percentage hydrolysis by total phosphocholine plus choline concentrations or choline-only concentrations for the reaction progress of the Ce^{IV} metal-assisted hydrolysis of sphingomyelin with four timepoints.

Metal	**Triton X-100 (mM)**	**Temp. (°C)**	**Time (h)**	**Percentage Hydrolysis at pH 4.8** **Avg. ± SD of total phosphocholine plus choline (Avg. ± SD of choline only)**	**Percentage Hydrolysis at pH 7** **Avg. ± SD of total phosphocholine plus choline (Avg. ± SD of choline only)**
Ce^{IV}	16	37	0	0.00 ± 0.0 (0.00 ± 0.0)	0.00 ± 0.0 (0.00 ± 0.0)
			4	19.3 ± 2.7 (15.6 ± 0.90)	20.2 ± 1.5 (19.9 ± 4.4)
			8	31.8 ± 4.4 (25.5 ± 3.7)	40.7 ± 3.78 (36.9 ±3.8)
			20	48.2 ± 7.6 (47.1 ± 3.9)	53.3 ± 7.8 (53.3 ± 9.4)
		60	0	0.00 ± 0.0 (0.00 ± 0.0)	0.00 ± 0.0 (0.00 ± 0.0)
			4	63.9 ± 9.2 (60.5 ±7.6)	28.6 ± 1.9 (28.3 ± 5.7)
			8	79.5 ± 8.8 (77.9 ± 11)	55.7 ± 6.6 (59.8 ± 0.22)
			20	90.5 ± 16 (91.2 ± 11)	71.5 ± 13.0 (67.8 ± 14)

Table 3.8. The percentage hydrolysis by phosphate concentrations for the reaction progress of the Zr^{IV} metal-assisted hydrolysis of sphingomyelin with four timepoints.

Metal	Triton X-100 (mM)	Temp. (°C)	Time (h)	Percentage Hydrolysis at pH 4.8 Avg. ± SD %	Percentage Hydrolysis at pH 7 Avg. ± SD %
Zr^{IV}	0	37	0	0.00 ± 0.00	0.00 ± 0.00
			4	0.12 ± 0.01	0.06 ± 0.00
			8	0.17 ± 0.01	0.13 ± 0.01
			20	0.19 ± 0.01	0.10 ± 0.01
		60	0	0.00 ± 0.00	0.00 ± 0.00
			4	0.43 ± 0.02	0.21 ± 0.01
			8	0.23 ± 0.01	0.42 ± 0.02
			20	0.51 ± 0.03	0.81 ± 0.04
	2	37	0	0.00 ± 0.00	0.00 ± 0.00
			4	0.11 ± 0.01	0.27 ± 0.01
			8	0.24 ± 0.01	0.29 ± 0.01
			20	0.38 ± 0.02	0.24 ± 0.01
		60	0	0.00 ± 0.00	0.00 ± 0.00
			4	0.65 ± 0.03	0.28 ± 0.01
			8	0.91 ± 0.05	0.55 ± 0.03
			20	3.44 ± 0.17	2.02 ± 0.10
	16	37	0	0.00 ± 0.00	0.00 ± 0.00
			4	0.38 ± 0.02	0.31 ± 0.02
			8	0.55 ± 0.03	0.55 ± 0.03
			20	0.78 ± 0.04	0.61 ± 0.03
		60	0	0.00 ± 0.00	0.00 ± 0.00
			4	1.77 ± 0.09	1.01 ± 0.05
			8	2.95 ± 0.15	2.00 ± 0.10
			20	8.54 ± 0.43	7.89 ± 0.39

Table 3.9. The percentage hydrolysis by phosphate concentrations for the reaction progress of the Ce^{IV} metal-assisted hydrolysis of sphingomyelin with four timepoints.

Metal	**Triton X-100 (mM)**	**Temp. (°C)**	**Time (h)**	**Percentage Hydrolysis at pH 4.8**	**Percentage Hydrolysis at pH 7**
				Avg. ± SD %	**Avg. ± SD %**
Ce^{IV}	0	37	0	0.00 ± 0.0	0.00 ± 0.0
			4	0.07 ± 0.0	1.35 ± 0.21
			8	0.24 ± 0.66	1.26 ± 0.23
			20	5.84 ± 0.54	5.36 ± 0.86
		60	0	0.00 ± 0.0	0.00 ± 0.0
			4	14.1 ± 1.9	11.2 ± 2.0
			8	21.1 ± 1.5	14.4 ± 0.55
			20	37.6 ± 2.1	38.3 ± 1.8
	2	37	0	0.00 ± 0.0	0.00 ± 0.00
			4	1.22 ± 0.33	3.11 ± 0.77
			8	3.35 ± 0.29	3.64 ± 0.01
			20	7.18 ± 0.84	10.2 ± 1.0
		60	0	0.00 ± 0.0	0.00 ± 0.0
			4	16.5 ± 0.88	18.0 ± 1.3
			8	36.3 ± 3.0	23.5 ± 0.45
			20	96.2 ± 5.3	74.5 ± 11
	16	37	0	0.00 ± 0.0	0.00 ± 0.00
			4	4.85 ± 0.62	7.08 ± 0.87
			8	9.21 ± 0.59	8.39 ± 0.70
			20	19.6 ± 2.6	16.9 ± 3.5
		60	0	0.00 ± 0.0	0.00 ± 0.0
			4	33.5 ± 1.8	21.3 ± 1.5
			8	45.9 ± 5.6	28.2 ± 0.15
			20	60.4 ± 2.6	35.1 ± 0.28

Table 3.10. Estimated half-lives ($t_{1/2}$) calculated from Zr^{IV} and Ce^{IV} hydrolysis of sphingomyelin at 60 °C or 37 °C from the total phosphocholine plus choline hydrolysis yield percentage or the choline-only yield percentage. "*nd*" signifies "*not determined*".

				Estimated $t_{1/2}$ (h)	
Metal	**Triton X-100 (mM)**	**Temperature**	**Avg. pH**	**Total phosphocholine plus choline**	**Choline**
				Avg. ± SD	**Avg. ± SD**
Zr^{IV}	0	60 °C	4.84	300 ± 1	433 ± 1
			7.03	200 ± 1	267 ± 1
	2		4.89	24 ± 1	30 ± 1
			7.06	33 ± 1	41 ± 1
	16		4.89	8 ± 0.5	14 ± 1
			7.07	7 ± 0.5	11 ± 0.3
Ce^{IV}	0		4.72	9 ± 1	10 ± 0.2
			6.95	19 ± 1	21 ± 0.3
	2		4.86	5 ± 1	6 ± 0.1
			7.01	14 ± 1	14 ± 0.2
	16		4.75	6 ± 0.2	6 ± 0.2
			7.02	11 ± 0.2	13 ± 0.2
Zr^{IV}	0	37 °C	4.89	3500± 4	*nd*
			7.04	7000 ± 2	*nd*
	2		4.90	800 ± 2	800 ± 1
			7.06	1200 ± 1	*nd*
	16		4.90	100 ± 1	150 ± 1
			7.06	350 ± 1	400 ± 1
Ce^{IV}	0		4.78	80 ± 1	60± 1
			7.02	80 ± 1	100 ± 1
	2		4.80	40 ± 1	50 ± 1
			7.04	50 ± 1	40 ± 1
	16		4.86	26 ± 1	25 ± 1
			7.06	20 ± 1	20 ± 1

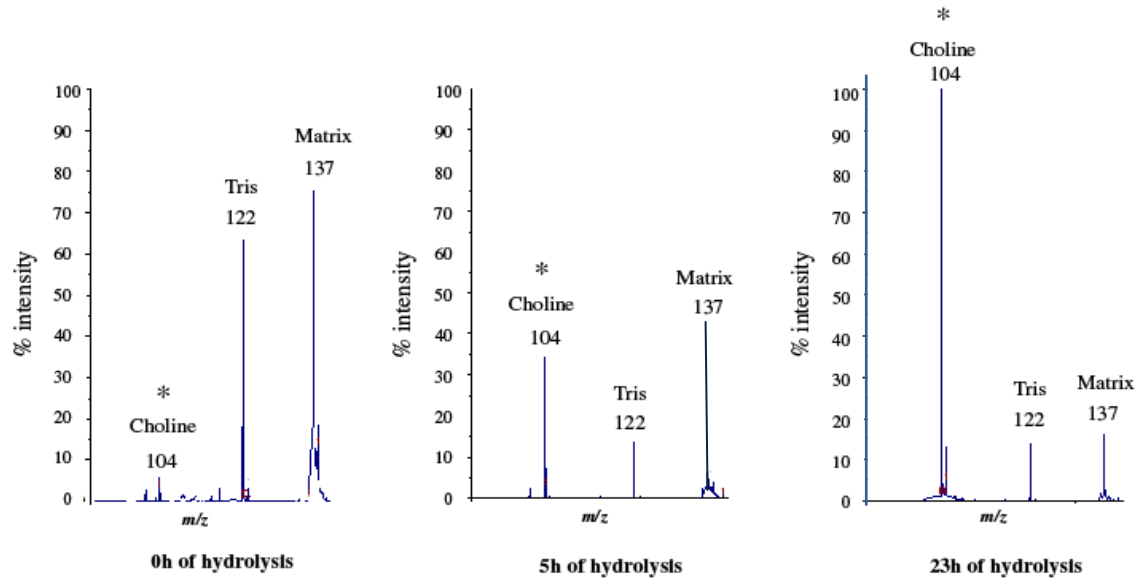

Figure 3.23. MALDI mass spectra showing the Zr^{IV}-assisted hydrolysis of phosphocholine with the increasing choline intensity at *m/z* 104. Spectra represent three different timepoints in the reaction at 0, 5, and 23 h. Samples prepared with 2 mM phosphocholine, 10 mM $ZrCl_4$, 20 mM TRIS, pH 4.8 were reacted at 60 °C, and then analyzed with MALDI-ToF instrumentation with DHB matrix in positive ion mode.

The zirconocene dichloride and non-metal experiments showed 0.05 to 0.12 pH drifts at 60 °C and -0.02 to 0.07 at 37 °C. The Ce^{IV} experiments showed pH drifts in the range of 0.08 to 0.10 at 60 °C and -0.01 to 0.03 at 37 °C which is considerably less than the corollary pH 4.8 experiments. The phosphocholine hydrolysis showed slight pH drifts at 0.05 pH units at 60 °C. The HEPES experiments demonstrate good pH control during the metal-assisted experiments.

Method validation.

Procedures using positive controls were performed to confirm that the experimental protocols are able to produce accurate results. The positive controls are compounds that are expected to give positive results because of their known reactivity with either the colorimetric reagents or the enzymatic reactions in the various assays. A known quantity of these compounds was used in similar hydrolysis reactions and/or assay quantification protocols as the hydrolysis samples, and their observed results were recorded as recovery percentages that were used for statistical assessment and not correction factors since the recoveries are vial-specific. The Amplex® Red assay quantification results of the positive controls of phosphocholine, choline, hydrogen peroxide, and the malachite green assay quantification results of inorganic phosphate levels are tabulated in Tables 3.12 and 3.13 for method validation. These results were evaluated to determine the validity and scientific significance of not only the established protocols of the Amplex® Red assay and the malachite green assay, but the novel modified choline-only assay using the Amplex® Red kit. The results for the 0 h and 20 h aliquots are shown separately to evaluate the effect of the experimental duration on the quantification. The positive controls were quantified by either the total phosphocholine plus choline assay where the enzyme mixture contained alkaline phosphatase or the choline-only assay where the enzyme mixture did not contain alkaline phosphatase.

The differences in metal, buffer, experimental time, and total phosphocholine plus choline yields vs. choline-only yields were noted. The recoveries of samples with zirconium(IV) metal were more accurate than the samples with cerium(IV) since the averages for zirconium(IV) were 98.4% (phosphocholine substrate, total phosphocholine plus choline analysis, 20 mM piperazine, 20h), 101.7% and 100.3% (choline substrate, total phosphocholine plus choline analysis, 20 mM piperazine, 0 and 20 h, respectively), 96.6% and 99.7% (choline substrate, choline-only analysis, 20 mM piperazine, 0 and 20 h, respectively). The recoveries for cerium(IV) metal were greater than the calculated value since the averages for cerium(IV) were 114.6% and 112.0% (phosphocholine substrate, total phosphocholine plus choline analysis, 20 mM piperazine, 0 and 20 h, respectively), 113.4% (phosphocholine substrate, total phosphocholine plus choline analysis, 20 mM HEPES, 20 h), 118.4% and 119.8% (choline substrate, total phosphocholine plus choline analysis, pH 4.8, 0 h and 20 h), 118.6% and 123.6 % (choline substrate, choline-only analysis, pH 4.8, 0 h and 20 h), and 123.4% and 127.4% (choline substrate, total phosphocholine and choline analysis, pH 7, 0 h and 20 h).

The hydrogen peroxide positive controls provided by the manufacturer with the assay were prepared in pure reaction buffer without the presence of experimental metal and buffer concentrations. The recovery percentages for three different amounts averaged 69.5 ± 1.8 % of the calculated value. Since the peroxide positive controls were prepared from new vials and fresh dilutions to optimize the recoveries, the poor recovery results indicate that the hydrogen peroxide positive controls are unacceptable for method validation purposes.

Table 3.13 shows the method validation statistics for the phosphate determinations from the malachite green assay. The expected phosphate concentration and the observed concentration calculated from the standard curves for each metal are shown with the recovery percentage. The

phosphate levels determined from the phosphocholine show 33.0% and 33.2% recoveries for Zr^{IV} and Ce^{IV}-assisted hydrolysis of 1.116 mM phosphocholine in the presence of 10 mM metal, 20 mM piperazine at 60 °C for 20 h which is substantially lower than the theoretical value. The choline which contains no hydrolysable phosphate shows the expected 0.00% recovery for the Ce^{IV}-assisted hydrolysis of 1.49 mM choline in the presence of 10 mM Ce^{IV} and 20 mM piperazine at 60 °C for 20 h. The hydrolysis percentages calculated from the phosphate concentrations were compared to the corresponding hydrolysis percentages calculated from the Amplex® Red assay. Two comparisons were taken from Table 3.3 and Table 3.4. For Ce^{IV} (2 mM Triton X-100, pH 4.8), the hydrolysis percentages were 70.7 ± 7.1% and 81.2 ± 5.8% for phosphate and total phosphocholine plus choline assays, respectively, which is in good agreement. However, for Zr^{IV} (16 mM, pH 4.8), the hydrolysis percentages were 11.3 ± 2.2% and 73.0 ± 7.6% for phosphate and total phosphocholine plus choline assays, respectively, which is not in good agreement. The recoveries of the positive controls can not be strictly correlated to the hydrolysis percentages of the sphingomyelin by phosphate concentration because of more than one dephosphorylation pathway, e.g. phosphate from released phosphocholine or phosphoceramide. Also, the phosphate used for the preparation of the standard curves did not undergo the same 20 h heat treatment at 37 °C or 60 °C as that the hydrolysis samples or the method validation positive controls.

Conclusions.

The ability of a select group of metals to hydrolyze the phosphate ester bond of sphingomyelin has been demonstrated at two pH values which represent lysosomal and cytosolic pH conditions and two temperatures of 37 °C and 60 °C which are at or above the gel-liquid transition of sphingomyelin. Out of the 12 metals salts tested, the metals with the highest

reactivity are the tetravalent metals Ce^{IV}, Zr^{IV}, and Hf^{IV}, and the divalent Pd^{II}. This can be predicted by the tetravalent metals' ability to substantially lower the pKa of water. A comparison of pH 4.8 and 7 yields at 60 °C show that hydrolysis by Ce^{IV} is strongly favored at pH 4.8 while Zr^{IV} and Hf^{IV} do not show a strong pH preference according to phosphocholine and choline product yields. However, the 37 °C data demonstrates that Zr^{IV} hydrolysis of the phosphate ester bond is enhanced at lysosomal pH compared to cytosolic pH, while the Ce^{IV} hydrolysis is not enhanced at lysosomal pH. This reversal of trends at the two temperatures most likely reflects a temperature dependence of metal solubilities, kinetics, and liposomal structure. The hydrolytic yield differences are much lower at 37 °C compared to 60 °C which reflects the effect of increasing temperature on reaction rates at 37 °C. Triton X-100 solubilization of sphingomyelin liposomes induces changes in the vesicle bilayer structure as evidenced by the turbidity and the altered hydrolytic yields for all metals.

In the presence of 0, 2, and 16 mM Triton X-100 concentrations, according to the turbidity, sphingomyelin corresponds to distinctly different structures which are attributed to vesicles (0 mM Triton X-100), mixed vesicle and mixed micelle (2 mM Triton X-100), and mixed micelle (16 mM Triton X-100) structures. Each of these sphingomyelin populations produced different metal-assisted hydrolytic yields. The additions of Triton X-100 and/or cholesterol had opposite effects on the pure sphingomyelin vesicles. The Triton X-100 incorporation increased hydrolytic yields possibly due to reduced Coloumbic repulsion of the charged headgroups due to Triton X-100 interdigitation with concomitant micelle formation. Cholesterol incorporation decreased hydrolytic yields possibly due to closer packing of the fatty acid chains in the inner sections of the bilayers which causes a denser outer vesicle shell and less penetration of metal ions.

Table 3.11. Summary of average pH and ΔpH values for all metal-assisted experiments.

Experimental Conditions	Triton X-100 (mM)	60 °C		37 °C	
		Avg pH ± SD	ΔpH ± SD, *n*	Avg pH ± SD	ΔpH ± SD, *n*
2mM sphingomyelin,	0	4.87 ± 0.03	0.03 ± 0.05, 28	4.88 ± 0.08	0.10 ± 0.09, 4
10 mM $ZrCl_4$,	2	4.86 ± 0.03	0.02 ± 0.03, 30	4.90 ± 0.04	0.04 ± 0.04, 4
20 mM piperazine	16	4.88 ± 0.03	-0.01 ± 0.03, 30	4.94 ± 0.08	0.01 ± 0.02, 4
2 mM sphingomyelin,	0	4.85 ± 0.01	0.01 ± 0.00, 10	*na*	*na*
10 mM $HfCl_4$	2	4.83 ± 0.01	-0.02 ± 0.01, 10	*na*	*na*
20 mM piperazine	16	4.88 ± 0.02	-0.01 ± 0.03, 10	*na*	*na*
2 mM sphingomyelin,	0	4.81 ± 0.19	0.48 ± 0.04, 25	4.71 ± 0.07	0.37 ± 0.13, 5
10 mM Ce^{IV} ammonium nitrate,	2	4.73 ± 0.02	0.42 ± 0.04, 27	4.86 ± 0.10	0.29 ± 0.07, 6
20 mM piperazine	16	4.74 ± 0.02	0.42 ± 0.03, 27	4.91 ± 0.09	0.17 ± 0.08, 5
2 mM sphingomyelin,	0	4.92 ± 0.03	-0.09 ± 0.09, 9	4.95 ± 0.16	-0.03 ± 0.13, 4
No metal,	2	4.91 ± 0.02	-0.06 ± 0.08, 9	4.93 ± 0.09	-0.05 ± 0.06, 4
20 mM piperazine	16	4.92 ± 0.05	-0.12 ± 0.06, 17	4.89 ± 0.13	-0.09 ± 0.14, 4
1.116 mM phosphocholine,	0	4.69 ± 0.06	0.53 ± 0.07, 18	*na*	*na*
10 mM Ce^{IV} ammonium nitrate,	2	*na*	*na*	*na*	*na*
20 mM piperazine	16	*na*	*na*	*na*	*na*
2 mM sphingomyelin,	0	4.86 ± 0.12	0.10 ± 0.10, 7	4.93 ± 0.06	-0.01 ± 0.08, 5
10 mM zirconocene dichloride,	2	4.88 ± 0.09	0.07 ± 0.08, 9	4.95 ± 0.04	0.03 ± 0.04, 6
20 mM piperazine	16	4.94 ± 0.08	0.10 ± 0.08, 9	5.01 ± 0.05	0.04 ± 0.05, 4
2 mM sphingomyelin,	0	7.05 ± 0.02	0.02 ± 0.01, 26	7.02 ± 0.05	0.03 ± 0.07, 5
10 mM $ZrCl_4$,	2	7.05 ± 0.01	0.01 ± 0.01, 28	7.07 ± 0.04	-0.05 ± 0.04, 5
20 mM HEPES	16	7.06 ± 0.03	-0.03 ± 0.03, 28	7.05 ± 0.07	-0.05 ± 0.09, 5
2 mM sphingomyelin,	0	7.10 ± 0.01	0.02 ± 0.01, 10	*na*	*na*
10 mM $HfCl_4$	2	7.07 ± 0.00	0.00 ± 0.00, 9	*na*	*na*
20 mM HEPES	16	7.10 ± 0.01	-0.03 ± 0.02, 10	*na*	*na*
2 mM sphingomyelin,	0	7.00 ± 0.05	0.10 ± 0.04, 24	7.05 ± 0.06	0.03 ± 0.11, 5
10 mM Ce^{IV} ammonium nitrate,	2	7.02 ± 0.03	0.10 ± 0.04, 26	7.08 ± 0.01	0.01 ± 0.08, 5
20 mM HEPES	16	7.03 ± 0.01	0.08 ± 0.04, 26	7.08 ± 0.12	-0.01 ± 0.09, 5
2 mM sphingomyelin,	0	7.08 ± 0.14	0.12 ± 0.01, 9	6.99 ± 0.10	0.06 ± 0.24, 4
No metal,	2	7.16 ± 0.12	0.07 ± 0.11, 10	7.05 ± 0.08	0.00 ± 0.1, 5
20 mM HEPES	16	7.07 ± 0.12	0.05 ± 0.10, 16	7.01 ± 0.08	-0.02 ± 0.09, 4
1.116 mM phosphocholine,	0	7.08 ± 0.08	0.05 ± 0.04, 14	*na*	*na*
10 mM Ce^{IV} ammonium nitrate,	2	*na*	*na*	*na*	*na*
20 mM HEPES	16	*na*	*na*	*na*	*na*
2 mM sphingomyelin,	0	7.03 ± 0.06	0.08 ± 0.14, 6	7.04 ± 0.05	0.07 ± 0.12, 5
10 mM zirconocene dichloride,	2	6.98 ± 0.07	0.06 ± 0.09, 9	7.01 ± 0.07	0.05 ± 0.12, 6
20 mM HEPES	16	6.99 ± 0.06	0.06 ± 0.09, 7	7.01 ± 0.11	0.05 ± 0.09, 4

ΔpH = initial reaction pH at t = 0 h minus final reaction pH at t = 20 h;
na = not available; *n* = number of trials

Table 3.12. Summary of the positive control results used in the Amplex® Red assay method validation.[c]

Positive Control	Sample	Parameters	Total phosphocholine and choline[a]		Choline[b]	
			t = 0 h	t = 20 h	t = 0 h	t = 20 h
Phosphocholine	1.116 mM phosphocholine, 10 mM $ZrCl_4$, 20 mM piperazine, pH 4.8, 60 °C, 20 h	Calculated concentration (mM)	1.12 mM	1.12 mM	0 mM	1.116 mM
		Observed concentration (mM) ± SD	0.980 ± 0.11	1.10 ± 0.29	0.039 ± 0.61	0.888
		n	3	4	3	2
		Recovery %	87.8%	98.4 %	3.50 %	79.6 %
Phosphocholine	1.116 mM phosphocholine, 10 mM Ce^{IV} ammonium nitrate, 20 mM piperazine, pH 4.8, 60 °C, 20 h	Calculated Concentration (mM)	1.12 mM	1.12 mM	1.12 mM	1.12 mM
		Observed concentration (mM) ± SD	1.28 ± 0.23	1.25 ± 0.25	0.213 ± 0.04	1.19 ± 0.26
		n	5	5	3	4
		Recovery %	114.6 %	112.0 %	19.09 %	106.5 %
Phosphocholine	1.116 mM phosphocholine, 10 mM Ce^{IV} ammonium nitrate, 20 mM HEPES, pH 7, 60 °C, 20 h	Calculated Concentration (mM)	1.12 mM	1.12 mM	1.12 mM	1.12 mM
		Observed concentration (mM) ± SD	1.15 ± 0.16	1.26 ± 0.18	0.290 ± 0.13	1.17 ± 0.06
		n	4	4	3	3
		Recovery %	103.4 %	113.4 %	26.0 %	105.0 %
Choline	1.116 mM phosphocholine, 10 mM $ZrCl_4$, 20 mM piperazine, pH 4.8, 60 °C, 20 h	Calculated Concentration (mM)	1.49 mM	1.49 mM	1.49 mM	1.49 mM
		Observed concentration (mM) ± SD	1.52	1.49	1.44 ± 0.08	1.49 ± 0.09
		n	2	2	3	4
		Recovery %	101.7 %	100.3 %	96.6 %	99.7 %
Choline	1.116 mM phosphocholine, 10 mM Ce^{IV} ammonium nitrate, 20 mM piperazine, pH 4.8, 60 °C, 20 h	Calculated Concentration (mM)	1.49 mM	1.49 mM	1.49 mM	1.49 mM
		Observed concentration (mM) ± SD	1.76 ± 0.17	1.79 ± 0.20	1.77 ± 0.31	1.84 ± 0.30
		n	5	5	4	4
		Recovery %	118.4 %	119.8 %	118.6 %	123.6 %

[a] The total phosphocholine and choline amount is calculated from the Amplex® Red assay where alkaline phosphatase enzyme was included in the reactive mix. Results include the phosphocholine and choline substrate present in the hydrolysis reaction. Metals included $ZrCl_4$ or cerium(IV) ammonium nitrate. Buffers included either piperazine, pH 4.8, or HEPES, pH 7.0.

[b] The choline amount is the amount calculated from the Amplex® Red assay where alkaline phosphatase enzyme was omitted in the reactive mix. Results include only the choline substrate present in the hydrolysis reaction.

[c] "*na*" = not available, *n* = number of samples

[d] The hydrogen peroxide samples were prepared immediately prior to the assay preparation and not a metal-assisted hydrolysis reaction.

Continued Table 3.12.: Summary of the positive control results used in the Amplex® Red assay method validation.[c]

Positive Control	**Sample**	**Parameters**	**Total phosphocholine and choline[a]**		**Choline[b]**	
			t = 0 h	t = 20 h	t = 0 h	t = 20 h
Choline	1.116 mM phosphocholine, 10 mM Ce^{IV} ammonium nitrate, 20 mM HEPES, pH 7, 60 °C, 20 h	Calculated Concentration (mM) Observed concentration (mM) ± SD *n* Recovery %	1.49 mM 1.84 ± 0.12 3 123.4 %	1.49 mM 1.90 ± 0.23 3 127.4 %	1.49 mM 1.68 2 112.6 %	1.49 mM 1.76 2 117.8 %
H_2O_2	Reaction buffer[d] (Tris, MgCl), 37 °C	Calculated Concentration (mM) Observed concentration (mM) *n* Recovery %	0.022 mM 0.015 2 68.2 %	*na*	*na*	*na*
H_2O_2	Reaction buffer[d] (Tris, MgCl) 37 °C	Calculated Concentration (mM) Observed concentration (mM) *n* Recovery %	0.044 mM 0.031 2 71.6 %	*na*	*na*	*na*
H_2O_2	Reaction buffer[d] (Tris, MgCl) 37 °C	Calculated Concentration (mM) Observed concentration (mM) *n* Recovery %	*na*	*na*	0.066 mM 0.045 2 68.8 %	*na*

[a] The total phosphocholine and choline amount is calculated from the Amplex® Red assay where alkaline phosphatase enzyme was included in the reactive mix. Results include the phosphocholine and choline substrate present in the hydrolysis reaction. Metals included $ZrCl_4$ or cerium(IV) ammonium nitrate. Buffers included either piperazine, pH 4.8, or HEPES, pH 7.0.

[b] The choline amount is the amount calculated from the Amplex® Red assay where alkaline phosphatase enzyme was omitted in the reactive mix. Results include only the choline substrate present in the hydrolysis reaction.

[c] "*na*" = not available, *n* = number of samples

[d] The hydrogen peroxide samples were prepared immediately prior to the assay preparation and not a metal-assisted hydrolysis reaction.

Table 3.13. Summary of the positive control results used in the malachite green assay method validation.

Positive Control	**Sample Description**	**Parameter**	**Inorganic Phosphate**
			t = 20 h - 0 h
Phosphocholine	1.116 mM phosphocholine, 10 mM $ZrCl_4$, 20 mM piperazine, pH 4.8, 60 °C, 20 h	Calculated concentration (μM) Observed concentration (μM) ± SD *n* Recovery %	1120 uM 370 uM 2 33.0 %
Phosphocholine	1.116 mM phosphocholine, 10 mM metal Ce^{IV} ammonium nitrate, 20 mM piperazine, pH 4.8, 60 °C, 20 h	Calculated concentration (μM) Observed concentration (μM) ± SD *n* Recovery %	1120 uM 372 uM ± 117 4 33.2 %
Phosphocholine	1.116 mM phosphocholine, 10 mM metal Ce^{IV} ammonium nitrate, 20 mM HEPES, pH 7, 60 °C, 20 h	Calculated concentration (μM) Observed concentration (μM) ± SD *n* Recovery %	1120 uM 447 uM ± 307 3 39.9 %
Choline	1.490 mM choline, 10 mM metal (Ce^{IV} ammonium nitrate), 20 mM piperazine, pH 4.8, 60 °C, 20 h	Calculated Concentration (μM) Observed concentration (μM) ± SD *n* Recovery %	0 uM -9.04 uM 2 < 0.00 %
Choline	1.490 mM choline, 10 mM metal (Ce^{IV} ammonium nitrate), 20 mM HEPES, pH 7, 60 °C, 20 h	Calculated Concentration (μM) Observed concentration (μM) ± SD *n* Recovery %	0 uM 16.02 uM 2 >0.00%

n = number of trials

The evaluation of Zr^{IV}-assisted metal hydrolysis of sphingomyelin as a possible therapeutic reagent in Niemann-Pick diseases Type A and B is confirmed because the hydrolysis is increased at lysosomal pH at physiological temperatures of 37 ℃. The cellular toxicity of metals which are used as therapeutic agents must be taken into account, and zirconium(IV) metal is non-toxic while cerium(IV) is toxic whose effects including liver damage may be better understood in terms of cerium(IV)'s ability to hydrolyze the phosphate ester bond in sphingomyelin.

References.

1 http://www.mssm.edu/niemann-pick/general_genetics.shtml and http://en.wikipedia.org/wiki/Niemann-Pick_disease

2 R. Ott, R. Kramer, *Angew. Chem. Int. Edit.*, 1998, 37, 1957.

3 Unpublished data by R.G. Ravi, M.Kassai, K.B. Grant.

4 K. Matsumara, M. Komiyama, *J. Inorg. Biochem.*, 1994, 55, 153.

5 H. Liu, J. Hu, X. Liu, R. Li, K. Wang, *Chinese Sci. Bull*., 2001, 46, 401.

6 R.F. Boyer, M.E. Wernette, S. Van Wylen, E. Faustman, R. Titus, *J. Inorg. Biochem.*, 1979, 10, 205.

7 P. Scrimin, S. Caruso, N. Paggiarin, P. Tecilla, *Langmuir*, 2000, 16, 203.

8 G. Ghirlanda, P. Scrimin, P. Tecilla, U. Tonellato, *J. Org. Chem*., 1993, 58, 3025.

9 R. A. Moss, W. Jiang, *Langmuir*, 2000, 16, 49.

10 R. A. Moss, B. D. Park, P. Scrimin, G. Ghirlanda, *J. Chem. Soc., Chem. Comm.*, 1995, 1627.

11 R. A. Moss, J. Zhang, K. G. Ragunathan, *Tetrahedron Lett.*, 1998, 39, 1529.

12 R.A. Moss, H. Morales-Rojas, *J. Am. Chem. Soc.*, 2001, 123, 7457.

13 K. Bracken, R.A. Moss, K.G. Ragunathan, *J.Am. Chem. Soc.,* 1997, 119, 9323.

14. N.W. Luedtke, A. Schepartz, *Chem. Comm.,* 2005, 5426.

15. B. Zhu, D. Xue, K. Wang, *BioMetals*, 2004, 17, 423.

16. P. Scrimin, P. Tecilla, R.A. Moss, K. Bracken, *J.Am. Chem. Soc.,* 1998, 120,1179.

17 J. Burgess, *Metal Ions in Solution*, Halsted Press (Wiley): New York, 1978, 356.

18 J. F. Pankow, *Aquatic Chemistry Concepts*, Lewis Publishers: Chelsea, Michigan. 1991.

19 D. Langmuir, *Aqueous Environmental Chemistry*, Prentice-Hall, Inc.: Upper Saddle River, N. J., 1997.

20 R.M.Smith; A.E.Martell, *Critical Stability Constants. Vol 4 Inorganic Complexes,* Plenum Press: New York**,** 1976.

21 M. Kassai, R.G. Ravi, S.J. Shealy, K.B. Grant, *Inorg. Chem.,* 2004, 43, 6130.

22 (a) W.E. Meijs, H.J.Haisma, R.P. Klok, F.B. Van Gog, E.Kievit, H.M. Pinedo, J. Herschied, D.M.Jacobus , *J. Nucl. Med.*, 1997, 38, 112.

(b) W.E.Meijs, H.J. Haisma, R. Van Der Schors, R. Wijbrandts, K. Van Den Oever, R.P. Klok, H.M. Pinedo, J.D.M. Herscheid, *Nucl.Med. Biol.*, 1996, 23, 439.

(c) R. Amano, S. Oishi, S. Enomoto, F. Ambe, *Riken Rev.,* 1996, 25.

(d) A. Ando, I. Ando, S. Sanada, T. Hiraki, T. Takeuchi, K. Hisada, N. Tonami, *Ann. Nucl. Med.*, 1999, 13, 83.

(e) L.R.Perk, O.J. Visser, M. Stigter-Van Walsum, M.Vosjan, Visser, W.M. Gerard, J. Zijlstra, P.C. Huijgens, G. Dongen, *Euro. J. Nucl. Med. Mol. Imaging*, 2006, 33,1337.

(f) K. Yo, J.E. Salvaggio, *Igaku no Ayumi*, 1976, 98, 665.

(g) K.-Y. Kang, D. Bice, E. Hoffmann, R. D'Amato, J. Salvaggio, *J. Allergy Clin. Immun.*, 1977, 59, 425.

(h) R.J. Price, D.N. Skilleter, *Toxicol. Lett.*, 1986, 30, 89.

(i) Y. Ukai, S. Shima, T. Yoshida, H. Kurita, K. Nagai, N. Mori, Murai, F. Narusawa, Y. Yamamoto, K. Morita, *Nippon Eiseigaku Zasshi*, 1990, 45, 648.

(j) N.Mori, S. Shima, K. Morita, H. Kurita, T. Yoshida, T. Arakawa, H. Taniwaki, *Rodo Kagaku*, 1990, 66, 493.

(k) N.J. Hallab, S. Anderson, M. Caiceo, J.J. Jacobs, *ASTM Special Tech. Pub., 2006, STP 1471, Titanium, Niobium, Zirconium, and Tantalum for Medical and Surgical Applications*, 248.

(l) M.G. Tikhaya, *Meditsinskaya Radiologiya*, 1959, 4, 62.

(m) A.D. Montemarano, P. Sau, F.B. Johnson, W.D. James, *J. Am. Acad. Dermatol.*, 1997, 37, 496.

(n) B. Liu, S. Enomoto, S. Ambe, R.G. Weginwar, F. Ambe, *Riken Rev.*, 1996, 13, 35.

(o) W.E. Meijs; H.J. Haisma; R.P. Klok; F.B. Van Gog; E. Kievit; H.M. Pinedo; J. D.M. Herschied, *J. Nucl. Med.,* 1997, 38, 112.

23 F. Szoka, D. Papahadjopoulos in *Liposomes: from physical structure to therapeutic applications*, Elsevier: New York, 1981, C.G. Knight, *editor*, ch. 3.

24 R.C.New in *Liposomes as tools in basic research and industry*, CRC Press: Boca Raton, 1995, J.R. Philippot and F. Schuber, *editor*, ch. 1.

25 B. Ramstedt, J.P.Slotte, *FEBS Lett.*, 2002, 531, 33.

26 A. Rietveld, K. Simons, *Biochim. Biophys. Acta*, 1998, 1376, 467.

27 D.A. Brown, E. London, *J. Biol. Chem.*, 2000, 275, 17221.

28 J.B. Massey, *Biochim. Biophys. Acta*, 2001, 1510, 167.

29 P.R. Maulik and G.G. Shipley, *Biochem.*, 1996, 35, 8025.

30 A. Rietveld, K. Simons, *Biochim. Biophys. Acta*, 1998, 1376, 467.

31 C.M. Talbott, I. Vorobyov, D. Borchman, K.G. Taylor, D.B. DuPre, M.C. Yappert, *Biochim. Biophys. Acta*, 2000, 1467, 326.

32 (a) M.-A. Urbaneja, F.M. Goñi, A. Alonso, *Euro. J. Biochem.,* 1988, 173, 585;

(b) S.K. Patra, A. Alonso, F.M. Goñi, *Biochim. Biophys. Acta,* 1998, 1373, 112;

(c) A. Alonso, A. Villena, F.M. Goñi, *FEBS Lett.,* 1981, 123, 200;

(d) M.-A. Urbaneja, F.M. Goni, A. Alonso, *Eur. J. Biochem*., 1988, 173, 585;

(e) K. Anzai, H. Utsumi, K. Inoue, S. Nojima, T. Kwan, *Chem. Pharm. Bull.*, 1980, 28, 1762;

(f) O. Lopez, A. de la Maza, L. Coderch, C. Lopez-Iglesias, E. Wehrli, J.L. Parra, *FEBS Lett.*, 1998, 426, 314;

(g) C.Arnulphi, J. Sot, M. Garcia-Pacios, J.-L. R. Arrondo, A. Alonso, F. M. Goñi, *Biophys. J.*, 2007, 93, 3504;

(h) A. de la Maza, J.L. Parra, *Biochem. J.,* 1994, 303, 907;

(i) A. Alonso, R. Saez, and F.M. Goni, *FEBS Lett.*, 1982, 137, 141;

(j) A. Moschetta, P.M. Frederik, P. Portincasa, G. P. van Berge-Henegouwen, K.J. van Erpecum, *J. Lipid Res.*, 2002, 43, 1046;

(k) E. Schnitzer, M.M. Kozlov, D. Lichtenberg, *Chem. Phys. Lipids*, 2005, 135, 69.

33 (a) G.T.N. Besley, M. Elleder, *J. Inher. Metab. Dis. 9,* 1986, 59;

(b) S.F. O'B. Donaghey, D.Noel Raine, and J.E. Crossley, *J. Inher. Metab. Dis. 6*, 1983, 190;

(c) S. Fowler, C. De Duve, *J. Biol. Chem.,* 1969*,* 244, 471;

(d) X. He, F. Chen, S. Gatt, E. H. Schuchman, *Anal.Biochem.*, 2001, 293, 204;

(e) M. Heller, B. Shapiro, *Biochem J.,*1966, 98, 763;

(f) T. Levade, M. Leruth, D. Graber, A. Moisand, S. Vermeersch, R. Salvayre, P. J. Courtoy, *J. Lipid Res.,*1996*,* 37, 2525;

(g) D. H. Nelson, D. K. Murray**,** *Proc. Natl. Acad. Sci. USA*.,1982, 79, 6690;

(h) P. B. Schneider,E. P. Kennedy, *J.Lipid Res.,*1967, 8, 202;

(i) C. –L. E. Yen, M.-H. Mar, S. H. Zeisel, *FASEB J.,* 1999*,*13, 135.

34 Avanti Polar Lipids website: http://www.avantilipids.com

35 M. Zhou, Z. Diwu, N. Panchuk-Voloshina, R.P. Haugland, *Anal. Biochem.*, 1997, 253, 162.

36 (a) S. Singh, D.J. Keller, *Biophys. J.*, 1991, 60, 1401;

(b) Z.V. Leonenko, A. Carnini, D.T. Cramb, *Biochim. Biophys. Acta*, 2000, 1509, 131;

(c) Z. V. Leonenko, D. Merkle, S.P. Lees-Miller, D.T. Cramb, *Langmuir*, 2002, 18, 4873;

(d) Z.V. Leonenko, E. Finot, H. Ma, T.E.S. Dahms, D.T. Cramb, *Biophys. J.*, 2004, 86, 3783.

37 P. Ghosh, O.J. D'Cruz, R.K. Narla, F. M. Uckun, *Clin. Canc. Res.*, 2000, 6, 1536.

38 C. Rodriguez-Lafrasse, M.T. Vanier, *Neurochem. Res.*,1999, 24, 199.

39 E. B. Cogan, G.B. Birrell, O.H. Griffith, *Anal. Biochem.*, 1999, 271, 29.

40. http://www.bmrb.wisc.edu website for the Biological Magnetic Resonance Data Bank.

CHAPTER IV CONCLUSIONS.

Peptide hydrolysis.

We have described in the first chapter the potential uses for metal-assisted hydrolysis of the peptide bond or the phosphate ester bond for potential therapeutic and proteolytic use. In the second chapter, we have described the unique application of Zr^{IV}-assisted hydrolysis of the peptide bond of a biologically-active protein using a metal-azacrown ether complex. By using HPLC-ESI-MS and MS/MS, and MALDI-TOF MS, we have demonstrated that Zr^{IV}/4, 13-diaza-18-crown-6 facilitates hydrolysis of the 30-mer oligopeptides oxidized bovine insulin chain B at pH 7.0 and 60 °C. The Zr^{IV}-assisted hydrolysis of insulin chain B demonstrated that not only does the Zr^{IV} have amino acid side chain specificity, but that it hydrolyzes in good yields. Using the extensive characterization of the hydrolysis products by Findpept software and MS/MS mass spectral techniques, we were able to discover that the Zr^{IV} in the presence of the azacrown ether hydrolyzes not only at oxophilic, negatively-charged amino acids as predicted by earlier dipeptide work, but also possesses an unprecedented specificity toward cysteine sulfonic acid which is a distinctive marker for protein oxidative stress. This may be a useful metalloprotease for proteolytic studies which focus on the effect of oxidative stress on proteins.

In our analysis of the hydrolysis products, apparent major levels of cleavage were produced at Gly8-Ser9, Gly20-Glu21, Ser9-His10, Cys(SO_3H)7-Gly8 and Cys(SO_3H)19-Gly20 sequences which indicates three hydrolytic specificities, namely, cysteine sulfonic acids, negatively-charged, sequential Gly-Glu, and a Gly-Ser-His motif which contains an oxygen-containing sidechain. Given the association of cysteine sulfonic acids in proteins that have

undergone oxidative stress such as those found in amyloid fibril formation, Parkinson's disease, and other physiological processes, the therapeutic potential in the hydrolysis of these irreversibly-oxidized amino acids to prevent possible misfolding is promising.Two minor side reactions were also characterized in order to monitor any peptide product modifications. It was found that the Zr^{IV}/4,13-diaza-18-crown-6 complex promotes lactamization of the *N*-terminal Glu21 and deamidation of Asn3 and Gln4.

Phospholipid hydrolysis.

The development of Zr^{IV} and other non-toxic metal complexes for therapeutic treatment of patients with Niemann-Pick Disease and other lysosomal storage disorders is a very novel, promising area of research. We first analyzed a group of metals, described in Chapter III, which included transition metals and lanthanides with demonstrated ability to hydrolyze the phosphate ester bond in synthetic compounds. While the Zr^{IV} does not have significant cellular toxicity and has potential therapeutic use, the toxic effects of Ce^{IV} through phosphate ester hydrolytic pathways may be elucidated through this study. Two different assays were chosen for quantification of yields including the malachite green assay which quantitates inorganic phosphate and the Amplex®-Red assay which measures the total phosphocholine plus choline yields. The novel adaptation of this Amplex®-Red assay by inclusion of a choline-specific enzymatic reaction using similar reagents with selective omission of the alkaline phosphatase enzyme produced corollary results that allowed quantification and comparison of both the phosphocholine and the choline yields. This differentiation between phosphocholine and choline yields allows direct assessment of the regioselectivity of the metal-assisted hydrolysis of the phosphate ester bond of sphingomyelin in order to compare with the physiological enzymatic hydrolysis by acid sphingomyelinase in the lysosomes which yields exclusively phosphocholine

product plus a ceramide that proceeds as a second messenger to downstream signal transduction cascades. The data show that tetravalent metals Zr^{IV}, Ce^{IV}, and Hf^{IV} and the divalent Pd^{II} hydrolyze the phosphate ester bond in sphingomyelin in high yields. The solubilization of pure sphingomyelin vesicles to mixed micelles and/or pure micelles by the addition of Triton X-100 surfactant increased hydrolysis rates. Estimated half-lives of Ce^{IV} and Zr^{IV} for pure sphingomyelin liposomes with Triton X-100 solubilization at 60 °C are 5.06 h and 6.50 h, respectively. All hydrolysis experiments were run in parallel at two pH values which represent lysosomal pH 4.8 and cytosolic pH 7 in order to assess the increase in hydrolysis of the phosphate ester bond, and thus enzymatic mimicry, at lysosomal pH relative to cytosolic pH. We have shown that Zr^{IV}-assisted hydrolysis of pure sphingomyelin liposomes at 37 °C is significantly enhanced at pH 4.8 compared to pH 7 in micellar form. Experiments with cholesterol effects on sphingomyelin liposomes demonstrate that the dense packing effects of cholesterol decrease the hydrolysis rates. Overall, we have demonstrated metal-assisted hydrolysis of a major, physiological phospholipid to yield non-cytotoxic products of phosphocholine and choline.